Biohybrid Electrodes Based on Photosystem I for Solar Energy Conversion

By

Gabriel LeBlanc

Dissertation

Submitted to the Faculty of the

Graduate School of Vanderbilt University

in partial fulfillment of the requirements

for the degree of

DOCTOR OF PHILOSOPHY

in

Chemistry

May, 2014

Nashville, Tennessee

Approved:

Janet Macdonald, PhD.

Sandra J. Rosenthal, PhD.

G. Kane Jennings, PhD.

David E. Cliffel, PhD.

For my family

ACKNOWLEDGEMENTS

Additionally, there are a great number of people that I would like to thank for their support of both this dissertation and me. I would first like to thank my advisor Professor David E. Cliffel for allowing me to work in his laboratory and for providing the guidance and support for this project. Working with Professor Cliffel has made me a

iv

better student, scientist, and mentor. Professor G. Kane Jennings has also been a mentor and advisor for me, and I thank him for this thoughts, ideas, support, and influence he has had on both this project and on me personally. Additionally, I would like to thank Professor Sandra J. Rosenthal and Professor Janet Macdonald for serving on my committee and offering their insight and assistance towards this project. I am especially lucky to have these four professors on my committee as they are all involved with solar energy projects and therefore provided a unique opportunity for me to learn from a panel of experts in this field.

During my time at Vanderbilt University I was fortunate enough to work with a number of great faculty, post-docs, graduate students, and undergraduate students. I would like to thank Professor Eva Harth and Dr. Artez Sims who mentored me during a Research Experience for Undergraduates (REU) the summer prior to my graduate studies. This experience not only introduced me to the world of graduate research, but also to the people of Vanderbilt University and the city of Nashville. After joining the Cliffel research group in 2010, I began my dissertation project that built off the work of several previous graduate students. In particular, I would like to thank Dr. Peter N. Ciesielski who introduced me to the project and performed the research that laid the framework for my own studies. While I worked on this project, I was assisted by several faculty, graduate students, and undergraduate students including Dr. Nsoki Phambu, Dr. Kirill Bolotin, Dr. Gongping Chen, Evan A. Gizzie, Darlene Gunther, Dhiraj Prasai, Jeremiah C. Beam, J. Scott Niezgoda, Toshia L. Wrenn, Kevin M. Winter, Siyaun (Leo) Yang, Danna Sharp, Jia Jia (Jamie) R. Zhang, Melinda J. Shearer, William B. Crosby, Karla Dumeng, Emily Darby, Alyssa E. Jaffe, and Jake Jordan. I would also like to recognize

the Vanderbilt Institute for Nanoscale Science and Engineering (VINSE), which provided both state-of-the-art instrumentation and a collaborative environment for performing world-class research. I would especially like to recognize Benjamin W. Schmidt, Dmitry Koktysh, and Anthony B. Hmelo. I also need to thank the rest of the Cliffel research group for their feed-back, support, and the wonderful environment they provided to perform this research. I would especially like to thank Dr. Danielle Kimmel, Dr. Jennifer McKenzie, and Dr. Leslie Hiatt for their mentorship. I also need to recognize Lyon College, which provided me with the educational foundation that led me to the field of chemistry. I am particularly indebted to my advisors, Dr. A. Kurt Grafton and Dr. Floyd Beckford, who introduced me to the wonders of chemistry and scientific research.

Finally, I need to thank my friends and family that have made my time in graduate school fun and exciting. To Alexis, Wes, Ramon, Ethan, Megan, Lauren, and Okey, thank you for the incredible friendship you all have shown me. To all of my friends I have met through soccer, thank you for the wonderful distraction. To my in-laws, John and Paula, thank you for making me a part of your family. To my parents, Gervais and Sharon, thank you for your incredible support and love. You truly convinced me that I could do whatever I wanted to with my life, and for that I can never thank you enough. To my brother, Marc-André, the most incredible companion through my childhood. You make me a better person and scientist. And finally to my wife, Leah, who has been supportive, loving, and kind. Thank you for going on this journey with me.

TABLE OF CONTENTS

LIST OF TABLES

LIST OF FIGURES

LIST OF ABBREVIATIONS

Abbreviation	Term
AFM	Atomic force microscopy
Ag/AgCl	Silver/silver chloride reference electrode
APTES	Aminopropyl triethoxysilane
AQS	Anthraquinone-2-sulfonate
BV	1,1'-dibenzyl-4,4'-bipyridinium
CB	Conduction band
CPCD	Confined plume chemical deposition
CV	Cyclic voltammetry
CVD	Chemical vapor deposition
Cyt C	Cytochrome C
DCPIP	2,6-dichlorophenolindophenol
DMSO	Dimethyl sulfoxide
DQ	1,1'-ethylene-2,2'-bipyridinium
DTMBP	4,4'-dimethyl-1,1'-trimethylene-2,2'-biyridinium
EDX	Energy dispersive X-ray spectroscopy
E_F	Fermi energy
EIS	Electrochemical impedance spectroscopy
F_B	Terminal iron-sulfur cluster of PSI
FcTMA	Ferrocenylmethyl-trimethylammonium hexaflorophosphate
$Fe(CN)_6^{3-}$	Ferricyanide
$Fe(CN)_6^{4-}$	Ferrocyanide
FET	Field-effect transistor
ff	Fill-factor

FTO .... Fluorine doped tin oxide

GO .... Graphene oxide

HNQ 2-Hydroxy-1,4-naphathoquinone

Hn-Silicon .... Heavily n-doped silicon

Hp-Silicon .... Heavily p-doped silicon

I^-/I_3^- .... Iodide/Triiodide

IR .... Infrared

I-V .... Current-voltage

J_{SC} .... Short-circuit current

KPFM .... Kelvin probe force microscopy

Kudzu .... *Pueraria lobata*

L-B .... Langmuir-Blodgett

Ln-Silicon .... Lightly n-doped silicon

Lp-Silicon .... Lightly p-doped silicon

MB .... Methylene blue

MV .... 1,1'-dimethyl-4,4'-bipyridinium

η .... external efficiency

NHE .... Normal hydrogen reference electrode

NMR .... Nuclear magnetic resonace

OCP .... Open-circuit potential

P700 .... Reaction Center of PSI

PDV .... Poly-decyl viologen

PMMA .... Poly(methyl methacrylate)

PPV .... Poly-propyl viologen

PSI .... Photosystem I

p-Si .... p-doped silicon

PXV .... Poly-p-xylene viologen

RAIR .... Reflection absorption infrared spectroscopy

RGO .... Reduced graphene oxide

RMS ....Root mean squared

$Ru(NH_3)_6^{3+}$ .... Hexaammineruthenium (III)

RuHex .... Hexaammineruthenium (III)

SAM...Self-assembled monolayer

SECM...Scanning electrochemical microscopy

SEM .... Scanning electron microscopy

TMBP..1,1'-trimethylene-2,2'-bipyridinium

UME.. Ultramicroelectrode

UV-vis..Ultraviolet-visible light

VB ....Valence band

V_{OC}..Open-circuit voltage

XPS .... X-ray photoelectron spectroscopy

XRD .... X-ray diffraction

CHAPTER I

INTRODUCTION TO PHOTOSYSTEM I AND ITS USE IN NON-BIOLOGICAL
SYSTEMS FOR SOLAR ENERGY CONVERSION[*]

Photosynthesis is the process by which plants, algae, and cyanobacteria convert our most abundant energy source (solar radiation from the sun) into stored energy in the form of reduced carbon.[1] This process has supported the energy demands of the earth since the beginning of life and continues to fuel our ever-increasing consumption through the use of fossil fuels derived from ancient organic matter. Unfortunately, the release of this stored energy has, in recent years, resulted in numerous problems such as climate change, environmental pollution, political unrest, and insufficient supply chains.[2] Thus, a tremendous research effort has been focused in the area of alternative energy in order to provide new avenues to convert and store energy. Of the many possible routes, solar energy appears promising due to its abundance, availability, and safety.[3] Since the discovery of the photoelectric effect in 1839,[4] researchers have attempted to efficiently capture and convert sunlight into useable and storable energy. Materials such as silicon, ruthenium dyes, zinc oxides, and other alloys have provided the bases for state-of-the-art devices. Until recently, nature's stunning photosynthetic process was neglected as a

research avenue to achieve solar cells and devices, despite the growing appreciation for its remarkable and highly efficient nanoscale, photoelectrochemical protein complexes.

One of these nanoscale protein complexes is Photosystem I (PSI). PSI is a ~500 kDa membrane protein complex found in most organisms that perform oxygenic photosynthesis.[5] In the process of photosynthesis, PSI operates as a photodiode, photoexciting electrons across the thylakoid membrane in roughly 1 μs with an internal quantum efficiency approaching unity.[6] The speed and efficiency of this charge transfer and separation is due to the protein's ability to move the excited electron down an internal electron transfer chain (**Figure 1.1**). The energy of each step is slightly lower than the proceeding step, thus thermodynamically favoring a unidirectional electron flow. Once the electron reaches the terminal iron-sulfur complex (F_B), it is ushered along to the next step of photosynthesis by the soluble redox protein ferredoxin. At the other side of the protein, the vacant "hole" at the reaction center (P700) is filled with an electron from the soluble copper-containing protein known as plastocyanin.[5]
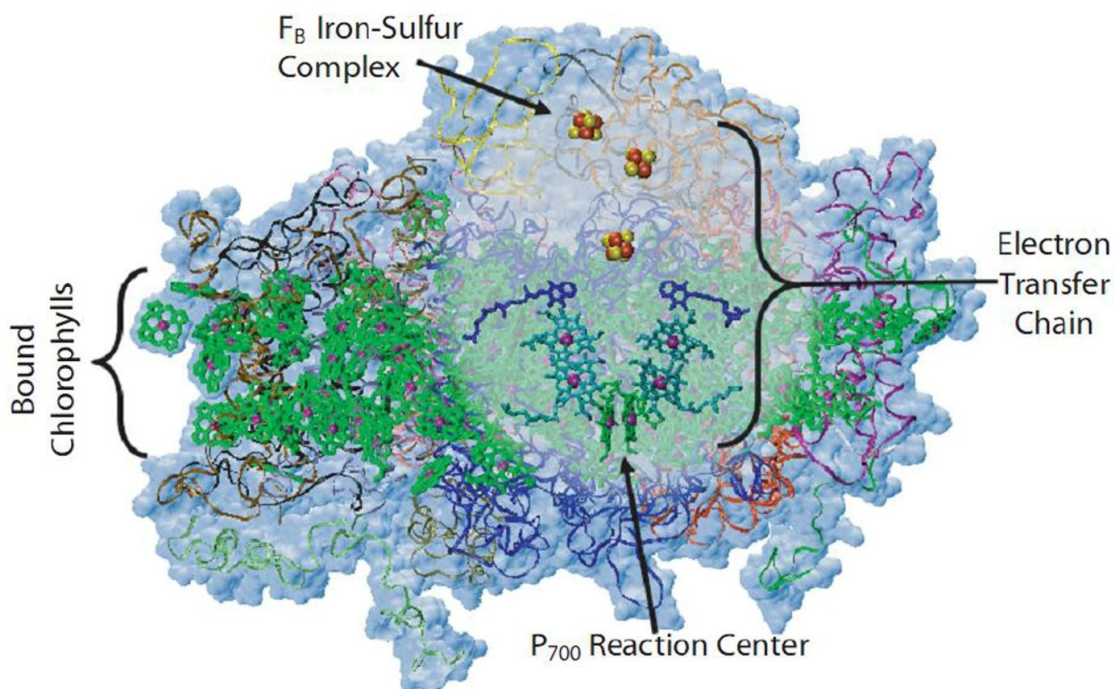
Figure 1.1 The structure of PSI highlighting the bound chlorophylls in the membrane portion of the protein and the electron transport chain. Atomic coordinates used to make this image are from PDB entry 2o01.[7] Image reproduced with permission from Peter N Ciesielski, copyright 2010.[8]

Due to the rapid charge separation and efficiency of PSI, researchers from around the world have investigated the incorporation of this nano-photodiode into functional devices.[9] Research towards this end was first reported by Greenbaum in 1985,[10] in which chloroplasts were modified with platinum for the photo-catalyzed production of hydrogen. Greenbaum took advantage of the reducing power of PSI to photoreduce catalytic platinum on the surface of the chloroplast. Further illumination resulted in the production of hydrogen as the photoexcited electrons were passed directly into the platinum catalyst. Greenbaum then demonstrated how platinum-modified PSI could be immobilized on fiberglass filter paper.[11] In doing so, he was able to make electrical

3

contact with a metal electrode, thus enabling the generation of a sustained current under illumination, and exposing the field to the possibility of using photosynthetic biological materials for the direct conversion of solar energy to either hydrogen or electricity. Since then, several groups have used PSI as a photoactive material for hydrogen production.[12–15] The photoreduction of platinum on PSI has also been used to anchor PSI reaction centers onto metal surfaces[16] and more recently, for the organization of multilayer films of genetically modified PSI.[17] In 1997 Greenbaum and co-workers moved away from PSI-Pt hybrid materials and reported that PSI proteins function as individual photodiodes on an electrode surface[18] by using scanning tunneling spectroscopy to generate current-voltage (I-V) measurements on individual proteins. The orientation of the protein on the electrode surface was correlated with different I-V scan shapes. This study was followed by electrochemical investigations of PSI by other groups,[19,20] and eventually to the incorporation of PSI into a solid-state photovoltaic device in 2004.[21]

Over the past 10 years there have been numerous groups around the world, including our own, that have worked to improve the artificial electron transfer to and from PSI in biohybrid devices. Research at Vanderbilt University alone has demonstrated a photocurrent increase by over five orders of magnitude (**Figure 1.2**). These dramatic increases have resulted from a number of distinct methods for integrating PSI with electrode surfaces. Our first photocurrent measurements were made by simply interfacing a sparse layer of PSI with an electrode via physical adsorption.[22] By creating covalent attachments between PSI and the electrode materials, we found that photocurrent production increased dramatically due to improved electronic interaction and higher coverage of PSI.[23] In order to increase the light absorption of the biohybrid electrode, we

4

increased the surface area of our underlying electrode[24] and utilized thick multilayer films

of PSI.[25,26] Finally, as described in Chapter II, the use of a semiconducting electrode

substrate can be used dramatically improve the photocurrent density.[27] The value for our

highest reported photocurrent density is now approaching values for more traditional

photoelectrochemical cells (5-20 mA/cm^2).[28]
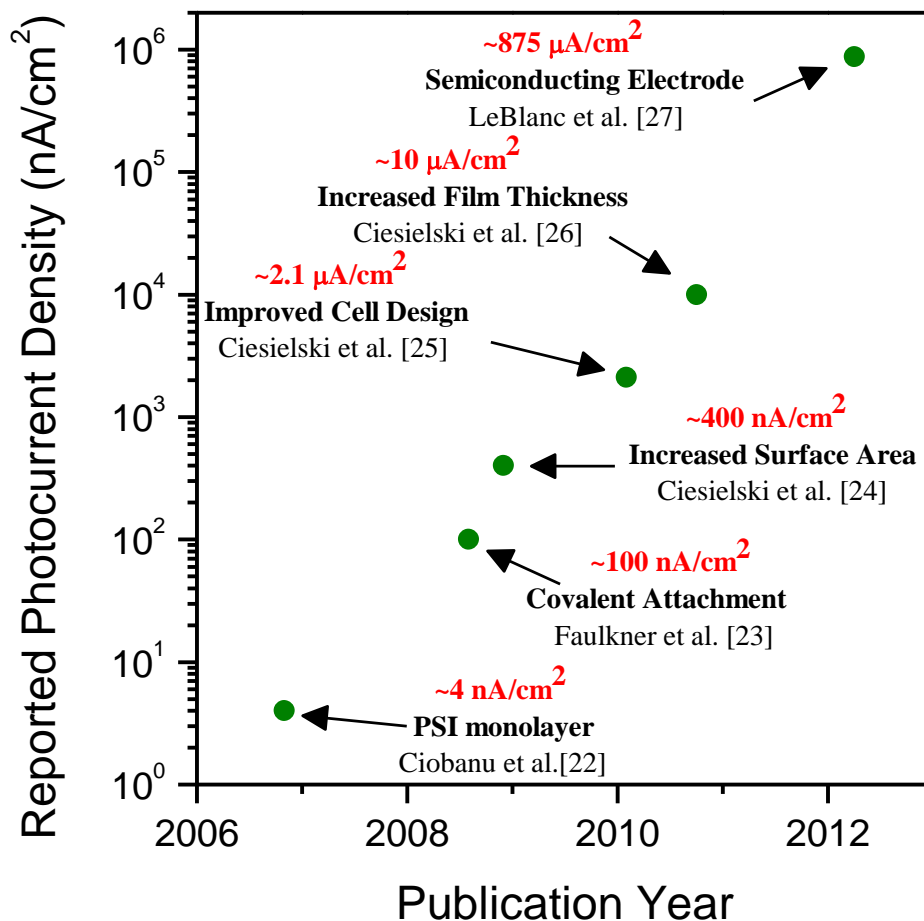
Figure 1.2. Reported photocurrents by the Cliffel/Jennings team at Vanderbilt University over the past seven years. The photocurrent value is listed adjacent to each data point, as is the manuscript from which the data were obtained.

5

Building from these results, the studies presented in this work provide additional insights on strategies to improve the photoactivity of biohybrid electrodes based on PSI. We have demonstrated that the electrochemical mediator and the underlying electrode material can have a significant effect on the electron flow through the PSI-modified electrode (Chapters II, III, and IV).[27,29] Furthermore, we have found carbon-based materials, such as graphene, to be particularly attractive for integration with PSI (Chapter V).[30,31] Chapter VI will discuss the ability for these biohybrid electrodes to generate hydrogen fuel after a platinum catalyst is photoreduced on the surface of the PSI film.[32] Finally, Chapter VII will conclude this dissertation by summarizing these research results and providing a perspective on the future directions that our research team and others may take to help preserve our natural resources by employing the abundant materials that nature has engineered.

GENERAL EXPERIMENTAL AND ANALYTICAL METHODS[*]

Extraction of Photosystem I[33]

PSI used as the integral component in biohybrid electrodes has been extracted from higher green plant leaves as well as cyanobacteria. The most common plant source for PSI in these studies has been spinach, due in part to the widely employed extraction protocols developed by Reeves and Hall.[34] Our adapted version of this protocol is shown in **Figure 2.1**, where PSI is removed from the thylakoid membrane of spinach using Triton-X 100 solubilization followed by filtration and centrifugation steps, as well as dialysis to remove residual salts and surfactant if needed based on the end use.[26] PSI concentrations from this extraction range from of $0.1 - 10$ μM, and the number of externally bound chlorophylls per PSI complex can be varied from 180 down to ~40. Fromme and co-workers[35] developed a notable advance in PSI extraction in 1998 by employing β-dodecylmaltoside as the surfactant in an improved process. Through this method, which is used by many in the biohybrid community, crystal structures of PSI at ultrahigh resolution can be obtained.
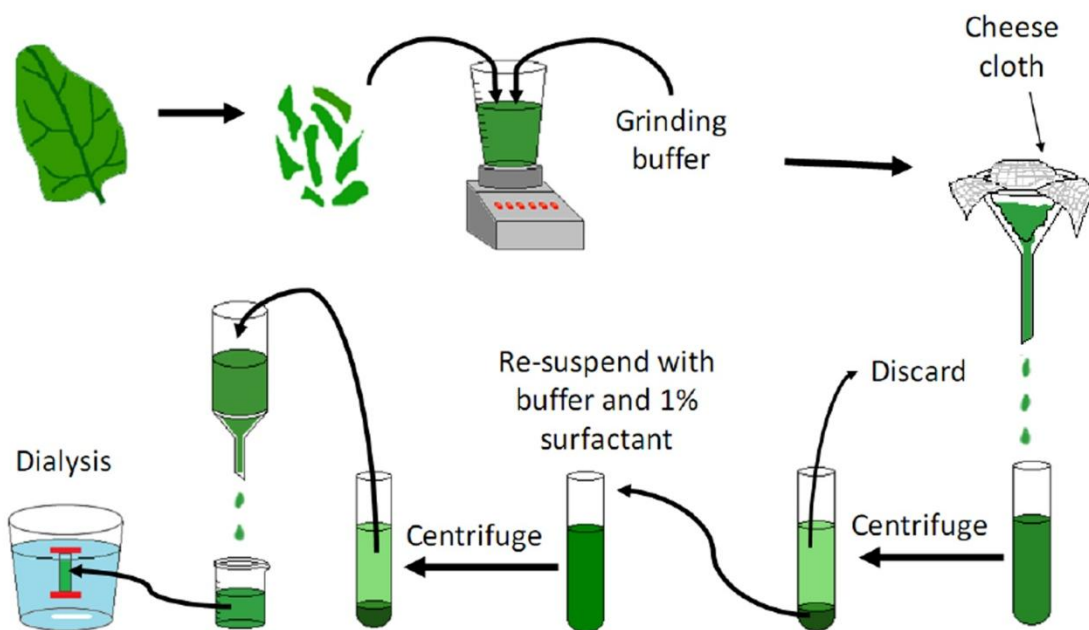
Figure 2.1. General PSI extraction procedure for higher order plants. The procedure follows the general methods described by Baba and co-workers,[36] Shiozawa and co-workers,[37] Reeves and Hall,[34] and Ciesielski and co-workers.[26] Figure reproduced with permission from Peter N. Ciesielski, copyright 2010.[8]

As PSI in higher plants is homologous,[37,38] PSI extracted from different plant sources under similar conditions is expected to exhibit similar performance on an electrode. To demonstrate that PSI can be extracted from non-food plant sources, Gunther and co-workers[39] reported the preparation and performance of PSI films extracted from *Pueraria lobata* (kudzu), a rapidly growing, invasive vine that covers nearly a million hectare of the southern U.S.[40] PSI complexes were extracted from kudzu leaves following the method for PSI extraction from spinach[26] and then deposited onto lightly doped p-Si. While kudzu PSI films on silicon demonstrated significant photocurrent enhancements over uncoated silicon, the yield of kudzu PSI in the extract was 10-fold lower than what is typically achieved with spinach. Thus, additional processing steps were required to

achieve similar film thickness and performance for kudzu PSI as compared to spinach PSI. These results show the critical importance of concentration or yield of active PSI that is extracted, as well as the biomass production of the source, when considering a long-term source of PSI for scale up in potential applications.

Another common source for PSI in biohybrid devices is the thermophilic cyanobacterium, *Thermosynechoccus elongatus*.[12] A key advantage of this source is that PSI exists as a trimer that may be more thermally stable and robust for many solar applications. As an example, Iwuchukwu and co-workers[12] compared hydrogen production from platinized PSI obtained from *T. elongatus* to that from the mesophilic cyanobacterium *Synechocystis* PCC 6803. The thermophilic PSI was better able to maintain its chlorophylls as temperature was increased, and its Pt-catalyzed hydrogen production increased up to 55°C, whereas that for the PCC 6803 continually decreased as the temperature was increased above room temperature. In comparison to platinized monomeric PSI from spinach from earlier studies,[41] the thermophilic PSI achieved plateau hydrogen generation at 4× greater light intensity, perhaps owing to its smaller antenna size.

Preparation of Biohybrid Electrodes[33]

PSI films are commonly deposited as (sub)monolayers for fundamental investigations into adsorption,[42–44] orientation,[18,45,46] or electron transfer.[22] Perhaps the simplest way to form a monolayer of PSI is to allow the protein complex to adsorb onto a surface from aqueous solution, in which the extraction surfactant (e.g. Triton X-100) helps to suspend PSI in solution and inhibit the formation of multilayers on the

surface.[23,42] We showed that the photocurrent for these single-layer PSI films is maximized as their coverage approaches the complete monolayer level and that long (48 h) adsorptions of PSI from solution are required to achieve these sufficiently dense monolayers.[23] To greatly accelerate this process to a fraction of an hour, we introduced an assembly process where the pressure above the aqueous PSI solution is reduced to rapidly evaporate the water and concentrate the PSI into a visibly green film of protein, surfactant, and salt on the surface.[23] Subsequent rinsing removes all but the first layer of bound protein, resulting in dense monolayers that exhibit comparable photocurrents as those where PSI adsorbs from solution over two days.

The substrate in these cases is often a metal or metal oxide that is terminated with an ultrathin self-assembled monolayer (SAM) to facilitate physical, electrostatic, or covalent interactions with the protein[23] without providing an insulating barrier against electron transfer between the substrate and the protein.[22] Gold has commonly been employed as an electrode material for the analysis of PSI films because it is an inert material with a relatively wide potential window for electroanalysis.[16,20,22–24,41,47–49] Many of the SAMs used to interface PSI with the gold electrode can be found in **Table 2.1**. Of these SAMs, n-alkanethiols that expose dense methyl-terminated surfaces generally do not adsorb PSI due to the presence of the extraction surfactant that tends to adsorb to the low energy surfaces in water and present an interface that inhibits protein attachment.[42] Surfaces that provide hydrophilic functional groups,[50] including hydroxyls that interact with PSI via hydrogen bonding and other weak physical interactions, as well as carboxylic acids and amines that interact with PSI via electrostatic interactions, enable greater extents of PSI adsorption. When focusing on a common family of SAMs, the

chain length of the molecular tether plays an important role in both adsorption of PSI and electron transfer between the protein complex and the electrode. In a study of PSI adsorbed onto hydroxyl-terminated SAMs, Ciobanu and co-workers[22] were only able to observe significant photocurrent response with a tether length of 6 or 8 carbons. This ideal chain length was also observed in a separate study by Kondo and co-workers using amine-terminated SAMs.[48] SAMs with shorter tethers are believed to pack poorly and not present a dense 2-D surface for adsorption of the protein, whereas longer tethers provide too great of an electron tunneling barrier that slows electron transfer to the protein.

SAMs that can covalently bind with PSI, such as those exposing terephthaldialdehyde and n-hydroxysuccinimide groups that can bind to lysine residues of PSI, tend to yield high coverage and good photocurrents.[23] However, as lysine residues are abundant on both the luminal and stromal sides of PSI, these covalent approaches are not likely to yield selective orientations. More recently, methods to selectively orient PSI on gold electrodes have been investigated.[23,24,47,49,51] Frolov and co-workers were able to directly attach PSI to a gold electrode by genetically modifying amino acids on the stromal side of PSI to cysteines[51] to directly bind PSI to the gold electrode through a gold-thiolate bond. After demonstrating PSI assembly onto a gold electrode, they demonstrated the photoactivity of the system by measuring the photopotential with KPFM.

Table 2.1. Comparison of various SAMs used to attach PSI to gold electrodes.

SAM on Gold Electrode	Method of Attachment	PSI Adsorption[a]	Electrochemical Signal[a]	Reference
ethanethiol	physical	Low	N/A	50
hexanethiol	physical	None	N/A	22
octanethiol	physical	Low	None	23,48
2-mercapto-1-ethanol	physical	High	Low	22,50
4-mercapto-1-butanol	physical	High	None	22
6-mercapto-1-hexanol	physical	High	Moderate	22
8-mercapto-1-octanol	physical	High	Moderate	22
11-mercapto-1-undecanol	physical	High	None	22
thioacetic acid	physical	Low	N/A	50
mercaptoacetic acid	electrostatic	High	High	20,50
3-mercaptopropionic acid	electrostatic	High	Low	22,23
8-mercaptooctanoic acid	electrostatic	Moderate	High	48
2-amino-1-ethanethiol	electrostatic	Low	Low	20,23,48
6-amino-1-hexanethiol	electrostatic	Moderate	High	48
8-amino-1-octanethiol	electrostatic	High	Low	48
11-amino-1-undecanethiol	electrostatic	High	None	48
2-dimethylaminoethanethiol	electrostatic	Low	N/A	50
4,4'-dithiodipyridine	physical	Low	N/A	20

tiopronin	electrostatic	High	None	22
terephthaldehyde[b]	covalent	High	High	23,24
N-hydroxysuccinimidyl[b]	covalent	High	Moderate	23
Vitamin K wire[b]	reconstitution	Moderate	High	49
Cytochrome-c	molecular relay	High	High	47
Cysteine mutation	covalent	High	N/A	51

[a] Relative levels (high, moderate, or low) are based on comparisons within a given manuscript or between manuscripts using similar methods or SAMs.

[b]The use of these SAMs requires an underlying SAM to bind to the gold surface.

Electrophoretic deposition, in which an aqueous PSI solution is confined between two electrodes bearing an applied potential difference, is an alternative way to deposit PSI onto electrode surfaces.[44,52,53] In these studies, a SAM-coated gold electrode served as the anode where a monolayer of PSI trimers was electrophoretically deposited with a potential difference of -2 V over several minutes. As compared to solution adsorption, the electrophoretic deposition provides enhanced adsorption of PSI[53] and reduces aggregation to yield more uniform PSI monolayers, as evidenced by AFM images.[44]

Another way to deposit PSI monolayers is to exploit the insolubility of PSI in water and thus, its tendency to partition to the air-water interface.[54,55] A film of PSI at this interface can be compressed into a dense monolayer uisng a Langmuir trough and transferred onto a substrate through various approaches. This method offers key advantages, including controllable PSI coverage based on the applied 2-D pressure,[54] a wider selection of substrates, and the capability of forming multilayered structures with a known, precise number of layers. We recently showed that PSI monolayers transferred

from the air-water interface to a hydroxyl-terminated SAM/Au substrate exhibit opposite orientations, depending on whether the transfer is by Langmuir-Blodgett (removing a pre-immersed substrate, oriented perpendicular to the air-water interface, from solution) or Langmuir-Schaefer (pressing a horizontal substrate, face-down, to the air-water interface).[54] Under these conditions, the air-water interface was able to orient 57% of the adsorbed PSI complexes with the electron transfer vector pointed toward the air phase.

While PSI monolayers are highly useful for fundamental studies, the ability to deposit thicker, multilayer films of PSI enable increased absorption of light and vastly improved photoelectrochemical performance.[25–27,32] A key to rapidly obtaining these thicker films is to first dialyze the extracted PSI solution to reduce the concentration of surfactant. Then, we employ the rapid assembly method described above where reduced pressure causes water to evaporate, concentrating the PSI into a dense film (**Figure 2.2**).[26] With little surfactant remaining with the PSI after dialysis, subsequent rinsing of the visibly thick PSI film does not remove it. The PSI film thickness can be enhanced by repeating this process, demonstrating a growth of 390 nm (~40 monolayers of PSI) per deposition based on the concentrations and conditions established in our prior work.[26] Through this approach, we were able to prepare 2.6 μm-thick PSI films that exhibited photocurrents that were 100-times greater than our best PSI monolayers.[26] The dialyzed PSI solution is critical to achieving this multilayer film; an undialyzed PSI solution would contain significant surfactant such that rinsing the deposited film would remove all components except the first, bound layer of PSI.[23] Unless otherwise stated, the deposition of thick multilayer films of PSI is the method that has been used for the studies described in the subsequent chapters of this thesis.
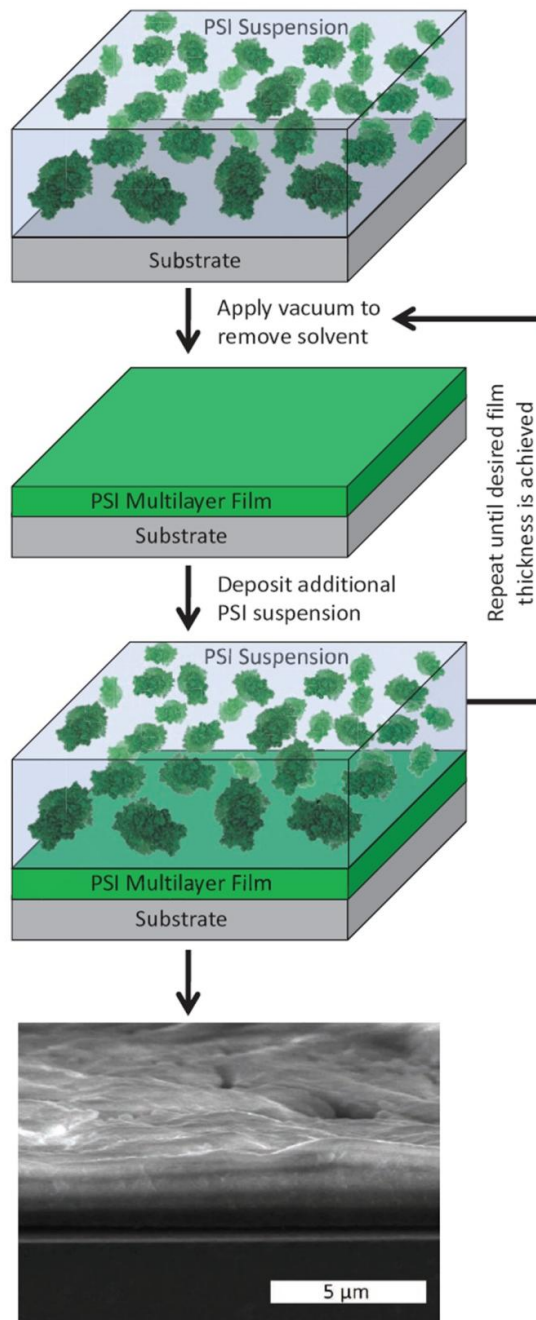
Figure 2.2. General procedure for the deposition of thick "multilayer" films of PSI. As depicted, the thickness of the resulting film can be adjusted by repeating the deposition process or by using different concentrations of PSI in the initial solution. The bottom panel shows an SEM image of the cross-section of the film following seven deposition steps. Image reproduced with permission from John Wiley and Sons, Copyright © 2010 WILEY-VCH Verlag GmbH & Co. KGaA, Weinheim. Image originally published in Ciesielski 2010.[26]

15

Analytical Techniques and Instrumentation

Electrochemistry

Electrochemical analysis is a particularly attractive means for analyzing these biohybrid electrodes. Using a 3-electrode set-up (**Figure 2.3**) allows a direct analysis of the PSI-modified working electrode without large uncompensated resistance causing problems with the measurement.[56] In this arrangement the counter electrode, typically a platinum mesh with a high surface area, is used to monitor the current. The reference electrode, typically Ag/AgCl in aqueous solutions, is used to monitor the voltage. In these experiments the three electrodes are connect via an electrolyte solution commonly containing a salt and a redox mediator.
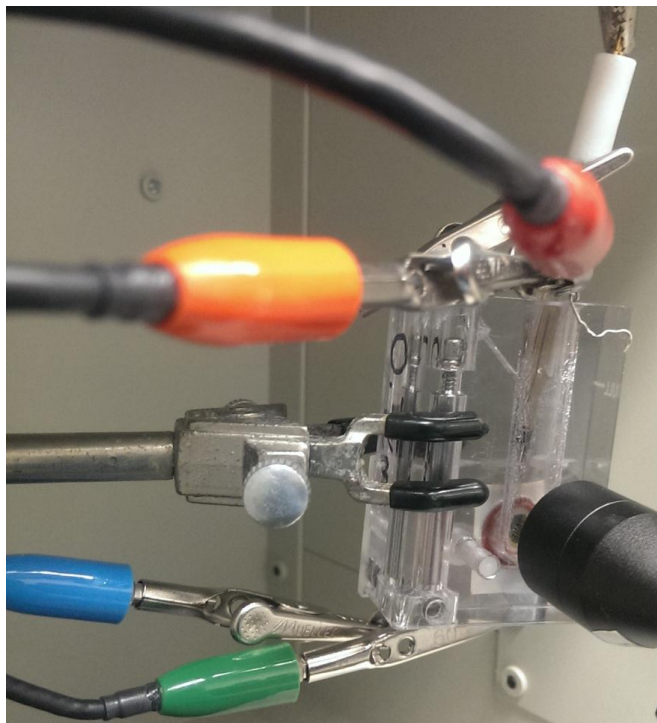
Figure 2.3. Electrochemical cell set-up. Photograph of a 3-electrode cell set up. The working electrode is connected to the green and blue clips. The counter electrode (platinum mesh) is connected to the red and orange clips. The reference electrode (Ag/AgCl) is connected to the white clip. The transparent electrode cell allows a light source to penetrate through to the biohybrid electrode.

In order to determine the photocurrent production of a biohybrid electrode, photochronoamperometry is commonly employed.[22–27,53] In these experiments, the working electrode is held at a constant potential (commonly the open circuit potential under dark conditions) and is eventually illuminated for a short period of time while the current change is measured. As shown in **Figure 2.4**, the current density under illumination decays according to the Cottrell equation,

$$i(t) = \frac{n\text{FAD}^{1/2}\text{C}}{\pi^{1/2}\, t^{1/2}} \tag{1}$$

where i is current density, t is time, n is the number of electrons, F is Faraday's constant, A is the area of the electrode, D is the diffusion coefficient of the mediator, and C is the concentration of the mediator. Thus, according to Equation (1), the current will decay as $t^{-1/2}$. In practice, the values shortly after illumination are unreliable due to non-faradaic contributions to the total current, limitations of the potentiostat, and limitations of the recording device. Additionally, at times longer than 20 s the buildup of density gradients and stray vibrations can cause disruption of the diffusion layer, preventing the assumptions of the Cottrell equation from holding true.[56] Because of these limitations, we often report the photocurrent density after 10 s of illumination, when the values can be compared with higher accuracy (see **Figure 1.2**).
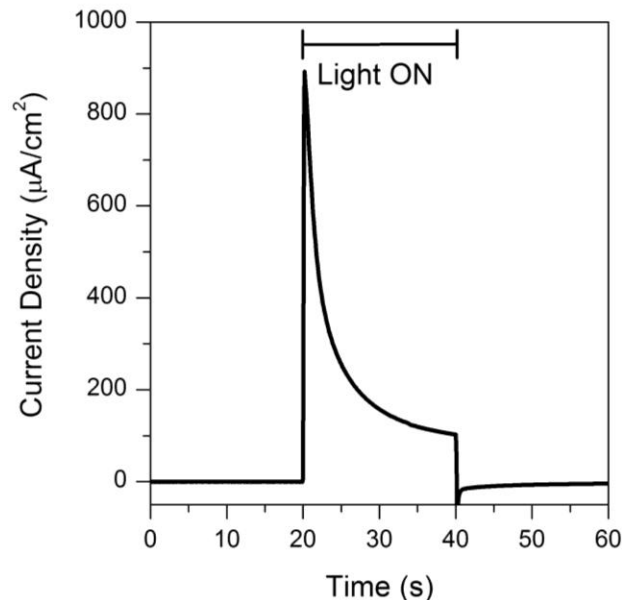
Figure 2.4. Sample photochronoamperometric analysis of a PSI modified electrode. Here, the electrode was held at the experimentally determined open circuit potential under dark conditions and the current was measured as a function of time. The sample was illuminated for 20 s (from 20 s to 40 s).

Because PSI has two redox active sites, P700 and F_B, the protein is capable of either donating or accepting electrons from the underlying electrode. The unique accessibility of these two redox components of PSI has proven to make it quite useful as a biomolecular photodiode for use in biohybrid solar energy conversion. For the successful construction of PSI biohybrid devices, the thermodynamics and kinetics of electron transfer between biological redox centers of PSI and electrode surfaces must be understood. Through the use of electroparamagnetic resonance spectroelectrochemical measurements,[57] the energetics of electron transfer in PSI has been explored. Through the use of electrochemical square wave voltammetry, Ciobanu and co-workers[22] were able to identify the presence of the stromal-side F_A/F_B and the luminal side P700/P700$^+$ redox couples in a single voltammogram for the first time. Hydroxyl-terminated SAMs were

18

used on gold electrodes to adsorb monolayers of the solubilized protein for direct electrochemical measurement. The observation of F_A/F_B and P700/P700$^+$ redox couples present in a single voltammogram indicates the presence of a monolayer of PSI with mixed orientation on the SAM-modified electrode. The experimentally determined redox potentials of -0.36 V (vs. NHE) and +0.51 V (vs. NHE) for F_A/F_B and P700/P700$^+$ respectively, are in good agreement with values from others who observed only the F_A/F_B or P700/P700$^+$ redox couples separately.[19,20]

An important consideration in the design of PSI-derived biohybrid solar energy conversion devices is the selection of redox mediator to facilitate electron transfer from the protein to the counter electrode or *vice versa*. In 2013, Chen and co-workers[29] performed a systematic study of redox mediators in order to maximize photocurrent output of PSI multilayer films on gold. According to the study, two of the most important considerations in mediator performance are the formal potential of the mediator and its optical absorbance properties. Enhanced photocurrent densities were observed in systems that utilized mediators with formal potentials near or more positive than the formal potential of P700, as shown in **Figure 2.5**. A trend of increasing photocurrent is observed as the formal potential of the redox couple becomes more positive; however, a break in the trend occurs with methylene blue (MB) and 2,6-dichlorophenolindophenol (DCPIP) at -0.2 V and 0.09 V (vs. Ag/AgCl), respectively. In order to explore this result, an absorbance study of each mediator was performed. MB and DCPIP both form dark blue solutions in aqueous media and have strong absorbances in the same spectral region as PSI (**Figure 2.7**). Due to the overlap in absorbance between these mediators and PSI, the overall photocurrent output of PSI-modified

electrodes becomes limited. When deposited on gold electrodes, PSI multilayer films must be illuminated through the mediator; thus, for strongly colored mediators that absorb in the same region as PSI's Q_y transition band or Soret band, a diminished photocurrent yield is observed, especially with high mediator concentrations (>20 mM). This study has concluded that for a randomly oriented PSI multilayer on gold electrodes, ferricyanide acts as the most effective electrochemical mediator, producing 900 nA/cm^2 at a concentration of 200 μM. The high performance of this mediator in this study is attributed to its relatively high formal potential, 0.2 V (vs. Ag/AgCl) and minimal spectral overlap with PSI's Q_y transition band. Additionally, metal-based redox mediators generally exhibit faster electron transfer with PSI's cofactors as compared to non-metallic, organic mediators.
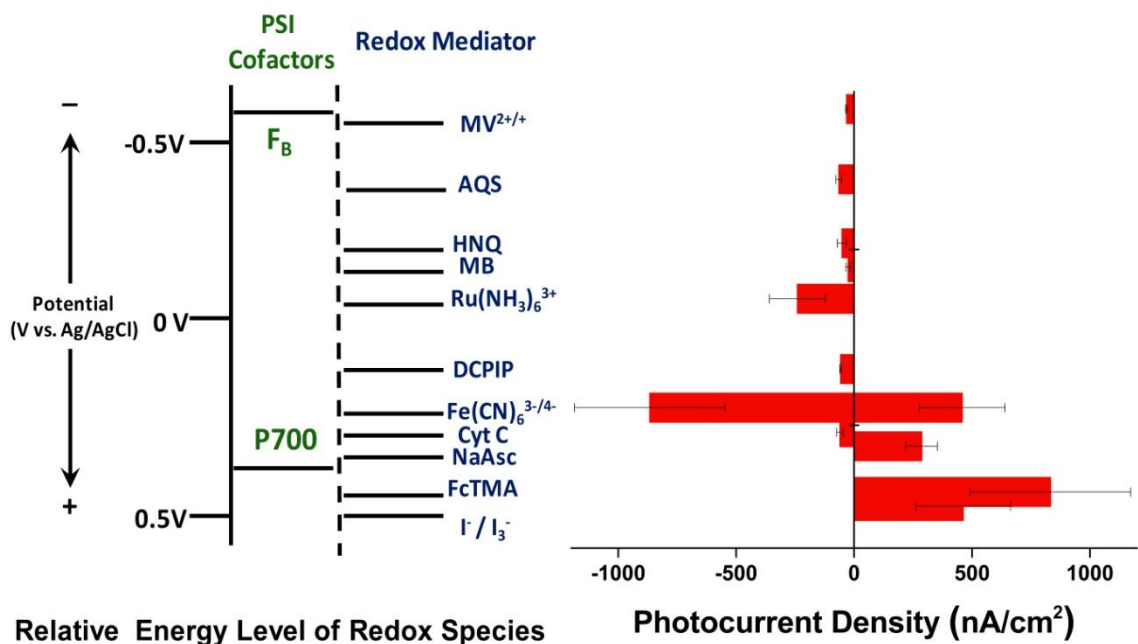
Figure 2.5. Photocurrent as a function of mediator formal potential. Energy diagram relates the formal potential of each studied mediator couple relative to the formal potentials of F_B and P700 of PSI.

20

An interesting question surrounding the use of thick multilayer films of PSI is how electrons are able to transport through the film itself. While the results demonstrate that films of PSI are capable of transporting electrons,[26,32] direct evidence of film conductivity requires more complicated electrochemical techniques. One such method is electrochemical impedance spectroscopy (EIS). In these experiments, the applied voltage is varied in a sinusoidal manner with a peak-to-peak amplitude of approximately 10 mV. During a typical experiment, current is monitored while the frequency of the applied voltage is changed. By analyzing the resulting alternating current and the phase angle of the current with respect to the voltage, the various components of the impedance (resistance and capacitance) can be determined for the electrochemical cell. The data for these experiments is usually displayed in either a Bode or Nyquist plot. In **Figure 2.6** the EIS for a PSI multilayer film on a gold electrode is displayed in a Nyquist plot (Bode plots and their analysis can be found in Chapter V). Under dark conditions, the PSI film has relatively high impedance. However, under illumination the PSI film demonstrates a significant decrease in film resistance and overall impedance. This change becomes even more apparent when a semi-conducting electrode like p-doped silicon is used (Chapters III and V).[27] This indicates that the protein film is capable of improved electron conduction under illumination.
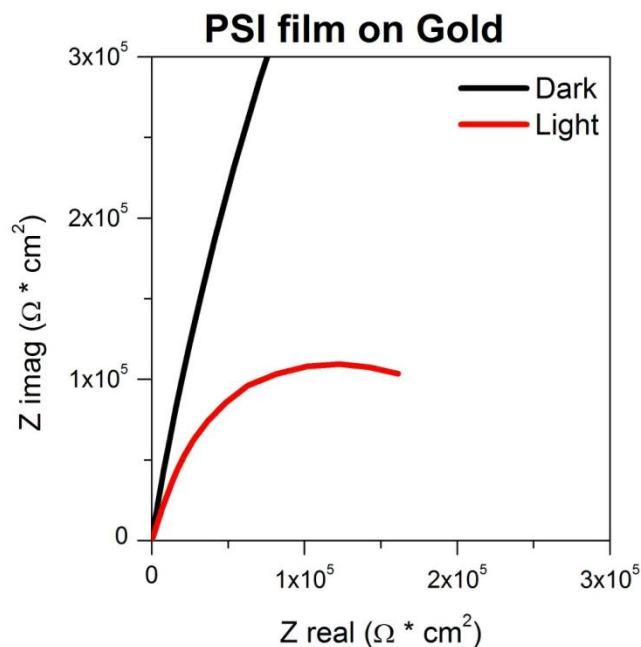
Figure 2.6. Nyquist plots of PSI multilayer film on a gold electrode. EIS of PSI modified gold electrodes under dark (black) or illuminated (red) conditions. The electrochemical cell consisted of a gold working electrode, platinum counter electrode, and a Ag/AgCl reference electrode. The mediator solution consisted of 2 mM methyl viologen and 100 mM KCl.

Another useful electrochemical technique for the analysis of PSI films is scanning electrochemical microscopy (SECM). To perform an SECM experiment, an additional tip electrode is used. This fourth electrode is typically an ultramicroelectrode (UME) with a diameter less than 25 μm. This UME is capable of controlled movement in the x, y, or z direction.[56] In 2013, Chen and co-workers utilized SECM approach curves (movement of the UME in the z direction) under both light and dark conditions to evaluate the feedback loop generated between an UME tip and the PSI-modified substrate.[58] In this study, a negative feedback loop (indicating a drop in current) was observed when PSI films were not illuminated. This observation confirms the hypothesis that PSI acts as an insulating layer on the electrode surface in the dark. Approach curves performed under illumination

conditions resulted in a higher current as compared to the dark case, indicating that the PSI film is regenerating the redox species consumed at the SECM tip. Based on the relatively slow kinetics of the PSI film itself, the tip consumes the redox mediator faster than the PSI film can regenerate it; thus, a true positive feedback loop was not experimentally observed. However, using computational simulations, a rate constant for the PSI film was approximated as 0.0032 cm/s.[58]

Optical Spectroscopy

The ability for PSI to interact with various wavelengths of light is obviously one of the critical reasons that researchers are interested in it for solar energy conversion devices. Here, we will describe the various optical spectroscopies that can be used to analyze PSI both in solution and on the surface of electrodes.

UV-vis spectroscopy is understandably a critical method for the analysis of PSI. As mentioned above, PSI absorbs strongly in the red region (Q_y transition band) and in the blue region (Soret band). The resulting UV-vis spectra (**Figure 2.7**) can be used to determine the concentration of a PSI in solution or to provide evidence for the presence of PSI on a transparent substrate. The absorption coefficient of PSI is so high, that a monolayer film (~10 nm) of PSI can be detected (Chapter V).[30,54] Visible light can also be used to analyze a PSI film on an opaque substrate through the use of reflectance UV-vis[59] or, more commonly, ellipsometry.[23,30]
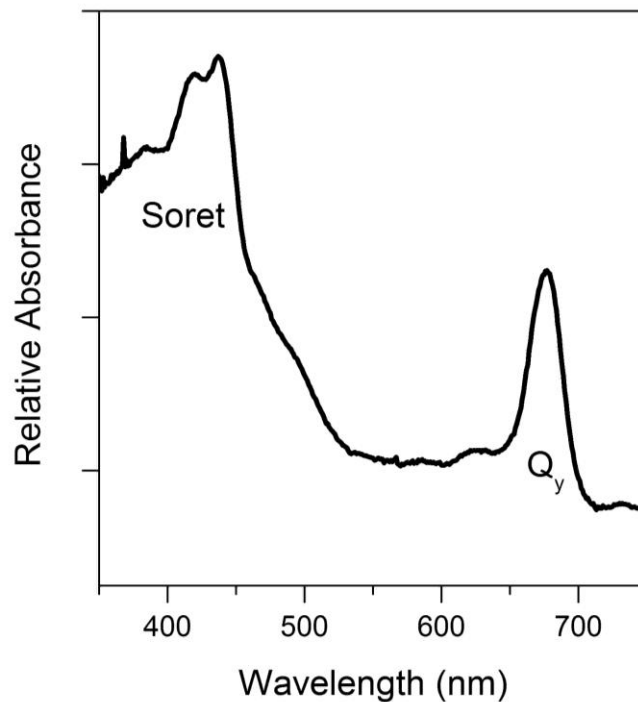
Figure 2.7. UV-vis spectrum of PSI in solution with the Q_y band and Soret band labeled.

Raman and infrared (IR) spectroscopy can also be used to analyze the bonds within PSI (**Figure 2.8**). In Raman spectroscopy, the biohybrid electrode can be illuminated with laser light that interacts with the electron cloud of the bonds in PSI generating inelastic scattering. This inelastic scattering, also known as Raman scattering, can then be analyzed for specific excitations that are characteristic bands for PSI.[60] IR spectroscopy is a more common and complementary method for the analysis of the vibrational modes of molecules. In this case, IR light is absorbed by bond vibrations. In PSI, characteristic amide I and II peaks can be observed near 1667 and 1546 cm^{-1}, respectively.[24] Particularly attractive for analyzing PSI-modified electrodes is reflection absorption infrared spectroscopy (RAIRs). For RAIRs, an IR reflective substrate (*i.e.* gold) allows the IR light to pass through the material of interest, PSI in this case, twice

before being directed to the detector. Both of these methods are typically used for the qualitative analysis of PSI, however additional information such as protein orientation may be possible using careful data collection and analysis.
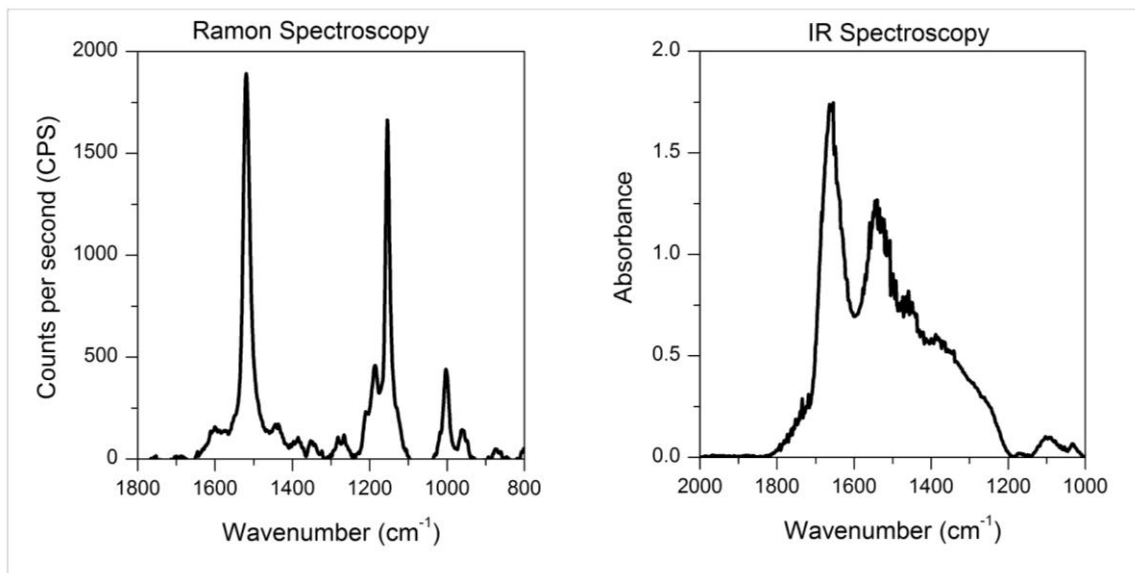
Figure 2.8. Raman and IR spectroscopy of PSI modified electrodes. Raman spectra (left) were performed on a silicon substrate modified with a multilayer film of PSI using 532 nm laser light. RAIRs spectra (right) was performed on using a PSI-modified gold electrode.

Electron and X-ray Spectroscopy

In order to fully characterize the structure and surface of biohybrid electrodes, electron and X-ray spectroscopy can often provide physical and chemical information not possible through other methods of analysis. In scanning electron microscopy (SEM), a beam of electrons is rastered across a specimen under high vacuum. The most common method for analysis utilizes secondary electrons emitted by the sample after bombardment from the primary electron beam. As these secondary electrons are collected by a detector, an image is produced allowing the user to "see" features not possible with

an optical microscope. The increased resolution of SEM is due primarily to the decreased wavelength of electrons compared with visible light. Biological samples are typically coated with a conductive layer prior to imaging to prevent effects cause by surface charging. Interestingly, most of the PSI-modified electrode samples that have been analyzed with SEM as a part of this thesis research did not require metallic coating (Chapter V), possibly due to partial conductivity of PSI films described above.

Products of interacting samples with high energy electrons results not only in secondary electrons, but also in characteristic X-rays. In this form of analysis, known as energy dispersive X-ray spectroscopy (EDX), the characteristic X-rays are used to identify various elements present in the sample. While quantitative analysis is possible with EDX, this technique is primarily used in this thesis work for qualitative purposes (Chapter VI). X-ray photoelectron spectroscopy (XPS) has also been used for more detailed elemental analysis. This technique can be thought in principle as the opposite of EDX; the sample is bombarded with X-rays and electrons with characteristic binding energies are detected. This method of analysis can give additional information such as the oxidation state of metals.

PHOTOCURRENT ENHANCEMENT FROM PHOTOSYSTEM I FILMS ON P-DOPED SILICON[*]

Introduction

As described in the previous chapters, the study of PSI for solar energy conversion has typically been performed with PSI deposited onto a metal electrode.[24,26,46,49] The immobilization of PSI onto an electrode increases the surface concentration of the protein, bringing the photoactive material in close contact with the electrode.[24] While a variety of methods have been developed for immobilizing PSI on metal substrates, reports of immobilizing PSI with a semiconducting electrode have been limited to GaAs, FTO, ZnO, and TiO_2.[61–63] Because the photocurrents resulting from dyes absorbed on metals are typically much smaller than those absorbed on semiconductors,[64] we hypothesize that the same general result would be seen for a photoactive protein. Recent work from Mershin and co-workers has demonstrated how a semi-conducting metal-oxide in conjunction with PSI could be used to generate a biophotovoltaic solar cell.[62] Unlike the dye in a typical dye-sensitized solar cell, however, we are not limited to using a monolayer film because PSI acts as an independent photodiode that can separate charge and perform electron transfer reactions without rapid recombination within the protein complex. Thus we can greatly enhance the observed photochemistry through the

---

[*] Portions of this chapter have previously been published: LeBlanc, G.; Chen, G.; Gizzie, E. A.; Jennings, G. K.; Cliffel, D. E. Enhanced Photocurrents of Photosystem I Films on p-Doped Silicon. *Adv. Mater.* **2012**, *24*, 5959–5962.

use of multilayer films of PSI.[17,26] Recently our group developed a simple and straightforward method for depositing films of PSI onto a wide variety of materials,[26] enabling this systematic study of PSI films on silicon substrates.

Silicon provides an excellent platform for the analysis of photoactive films of PSI for a variety of reasons. The band gap for silicon is approximately 1.1 eV,[65] making it photoactive in the visible region of the electromagnetic spectrum. Additionally, the valence band and conduction band for silicon (0.5 V and -0.6 V vs. NHE respectively) roughly align with the P_{700} and F_B redox centers of PSI (0.43 V and -0.58 V vs. NHE, respectively). Because the Fermi energy of silicon can be easily shifted by introducing impurities, we hypothesized that we could control and enhance the electron flow through the biohybrid system by changing the doping type and doping density. This circumvents the issue of protein orientation that has been found to play an important role in the photocurrent of these systems.[66] The optimized system allows for electrons to flow in a single direction, from the silicon to the protein, and finally to a redox mediator. Here we describe how the doping type and doping concentration in silicon affect the resulting photo-electrochemistry, and how the resulting photocurrent for the system can be optimized.

Results and Discussion

Using heavily p-doped silicon (Hp-Silicon), we found that a significant photocurrent enhancement could be achieved when a film of PSI was deposited on the semiconductor. We attributed this tremendous photocurrent enhancement to the band alignment between the valence band (VB) of the silicon with the P_{700} site of PSI (**Figure**

3.1). Thus, the ideal band alignment for this system, ignoring the effects of band bending, enables electrons to flow from the p-doped silicon to the P_{700} site of PSI. Photons are then used by PSI to excite the electron to the F_B site, where a methyl viologen redox mediator is used to shuttle the excited electrons to the counter electrode.
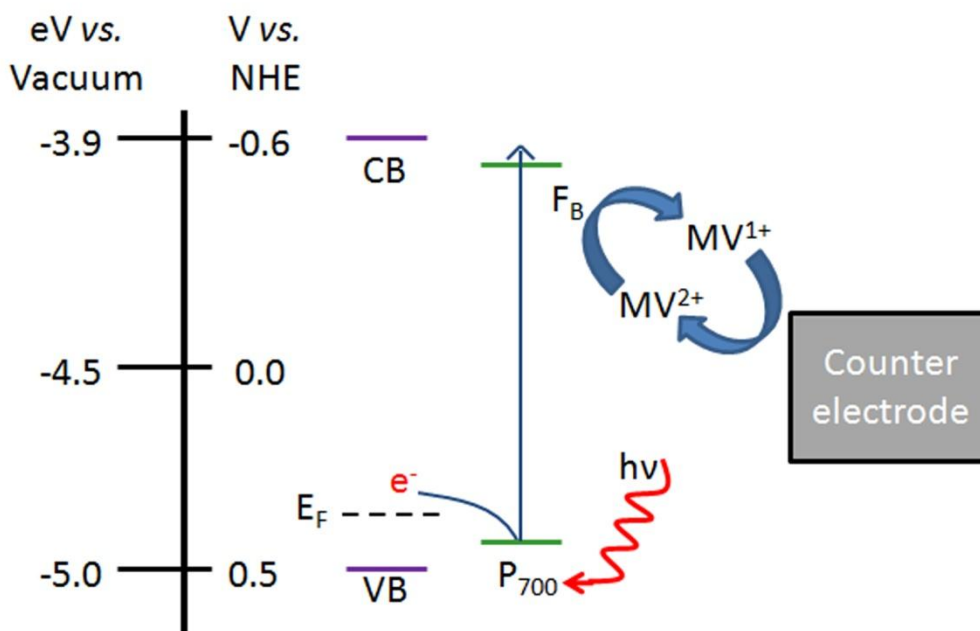
Figure 3.1. Electron flow through the PSI modified p-doped silicon electrode to the platinum counter electrode. Methyl viologen (MV) is used to complete the circuit.

Doping Type and Doping Density

In order to test this hypothesis, a systematic evaluation of the doping type, doping density, and mediator formal potential was performed. As seen in **Figure 3.2**, the direction of electron flow was controlled by the doping type of the system. For n-doped silicon, only photo-oxidations occur at the electrode (negative photocurrent values), while only photo-reductions occur when p-doped silicon is used as the working electrode (positive photocurrent values).[56] Photocurrent enhancement with PSI was only observed,

however, when p-doped silicon was used as the substrate. This provides further evidence for the scheme depicted in **Figure 3.1**, where the electrons can flow "down-hill" from p-doped silicon to the P_{700} site of PSI, but are unable to flow "up-hill" from the F_B site of PSI into n-doped silicon. By changing the doping density of the silicon electrode (from lightly p-doped to heavily p-doped), the band alignment between the P700 reaction center of PSI and the valence band of the silicon is improved. This further facilitates electron flow according to Marcus theory.

Furthermore, the mediator was found to have a profound effect on the resulting photocurrent in the system. The mediators tested included $Fe(CN)_6^{3-/4-}$, RuHex, and MV with redox formal potentials of 0.36, 0.1, and -0.45 vs. NHE respectively. Using p-doped silicon, the greatest photocurrent enhancement was observed when MV was used, where the formal potential of the redox mediator (-0.45 vs. NHE) is the closest to the midpoint potential of the F_B site of PSI, enabling the excited electrons to be quickly removed from the protein film. This confirms the scheme depicted in **Figure 3.1**, as previous experiments on a metal electrode gave relatively low photocurrent values when MV was used (**Figure 2.5**).[29]
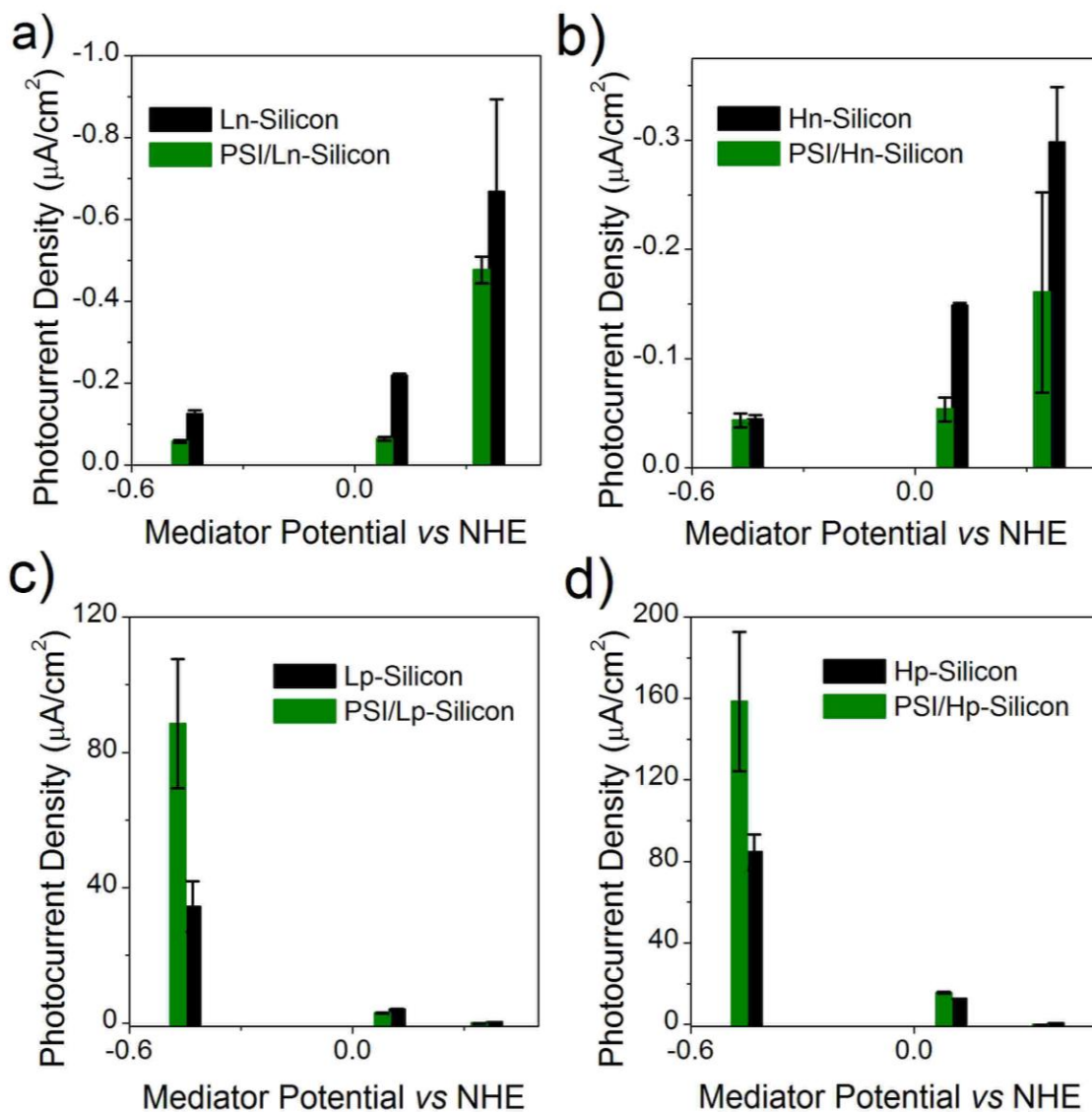
Figure 3.2. Systematic study of doping type and mediator combination. Photocurrent density (n=4) with PSI (green) and without (black) as a function of redox mediator formal potential. Doping type and doping density of the silicon substrate were varied: a) lightly n-doped, b) heavily n-doped, c) lightly p-doped, d) heavily p-doped. Measurements made with or without a PSI film (1.5 ± 0.2 µm) in 0.2 mM redox mediator, 0.1 M KCl, with a Ag/AgCl reference electrode and a platinum mesh counter electrode.

Film Thickness

Once the ideal silicon substrate and redox mediator were determined, the photocurrent from the system was optimized by analyzing both the thickness of the

31

protein film and the concentration of the redox mediator. Previous studies that utilized a gold substrate demonstrated that the photocurrent increased with protein film thickness beyond 2 μm.[26] In our experiments on silicon, however, we found that protein film thicknesses roughly greater than 1 μm did not generate greater photocurrents, and in fact began to decrease the photocurrent density with a film thickness greater than 2 μm (**Figure 3.3**). Fitting the data demonstrates that the photocurrent production follows a parabolic function rather than a linear function. This is likely due to the synergistic effects between the silicon and PSI, which requires a balance between the light absorbed by the protein film and the light reaching the photoactive substrate in order to maximize the photocurrent production.
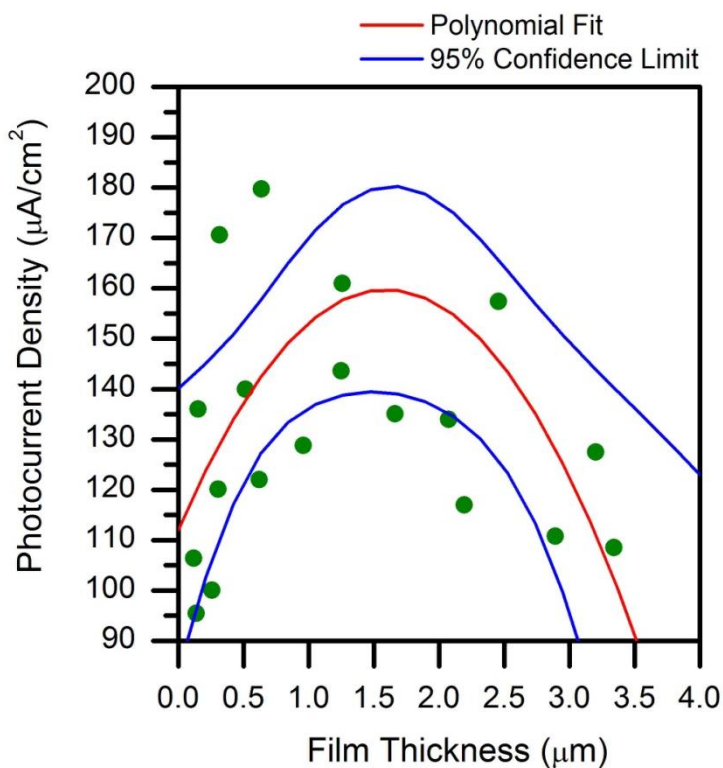
Figure 3.3. Photocurrent density as a function of PSI film thickness. Photocurrent measurements were made using 0.2 mM methyl viologen with 0.1 M KCl as the supporting electrolyte. Film thickness was determined using profilometry.

Mediator Concentration

As seen in **Figure 3.4**, the photocurrent increases with mediator concentration, and the photocurrent enhancement improves dramatically with the concentration of methyl viologen. At the highest concentration tested (0.2 M), an average photocurrent density of 875 μA/cm^2 was observed. This represents a 2500 fold enhancement over a film of PSI deposited on a gold electrode under the same conditions (0.35 μA/cm^2). As a control, the photocurrent for unmodified silicon was measured. The less dramatic increase in photocurrent observed for the unmodified electrode demonstrates how PSI can be used to enhance the photocurrent of p-doped silicon.
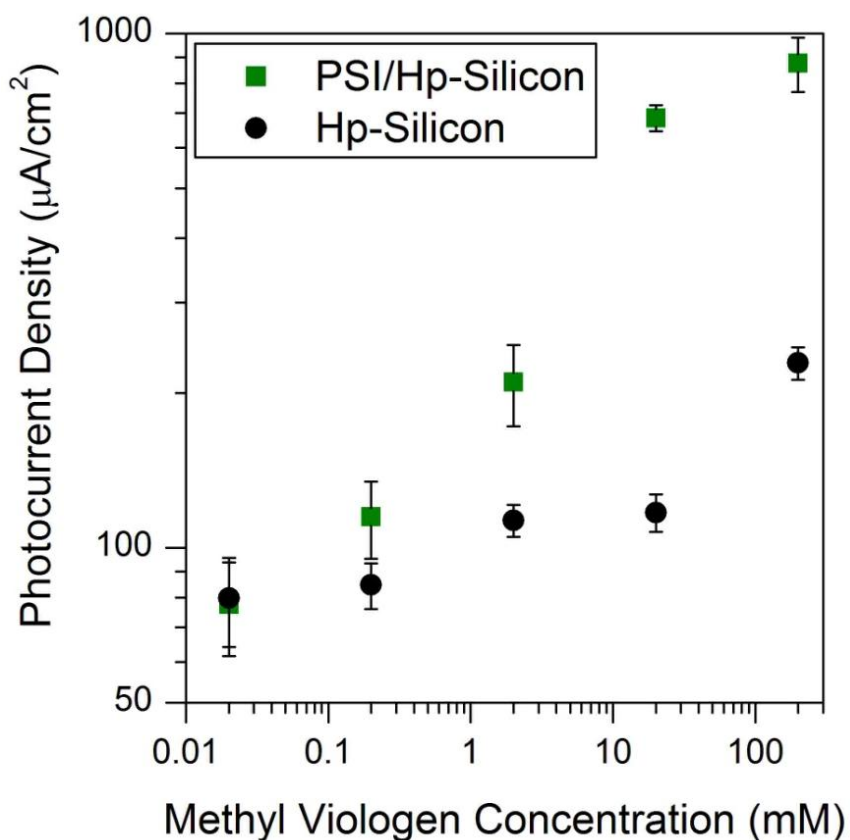
Figure 3.4. Photocurrent density as a function of mediator concentration. Unmodified heavily p-doped silicon (black) or heavily p-doped silicon modified with a 0.9 μm ± 0.1 μm film of PSI (green) was used as the working electrode.

Photovoltage Measurements

Open circuit voltage measurements were performed in order to determine the effect that the protein modification had on the photovoltage of the system (**Figure 3.5**). The PSI modified silicon was found to retain approximately 80% of photovoltage observed for the unmodified p-doped silicon (0.28 V vs. 0.35 V). This small decrease in photovoltage can be attributed to the voltage required to pass electrons through the protein film. The four-fold enhancement in photocurrent, coupled with the minimal reduction in photovoltage makes this system particularly attractive.
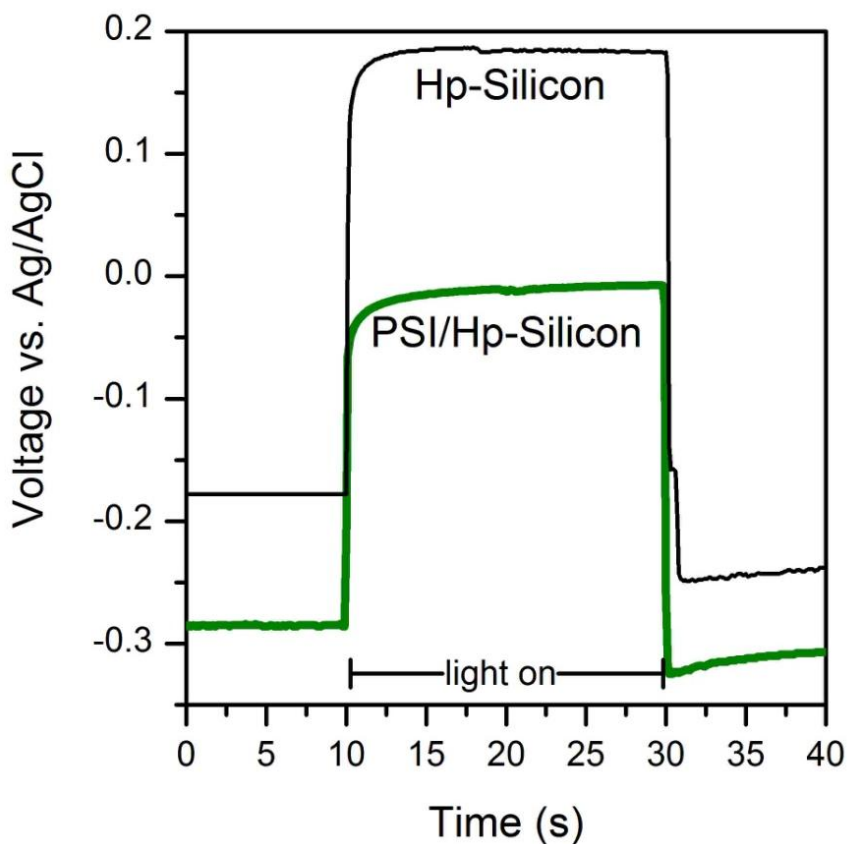
Figure 3.5. Photovoltage analysis of PSI modified (green) and unmodified (black) heavily p-doped silicon. The open circuit potential for modified and unmodified samples was taken in an electrochemical mediator solution consisting of 0.2 M methyl viologen and 0.1 M KCl.

Etched vs. Unetched Substrates

As one may expect, the condition of the underlying electrode can have a substantial impact on the resulting performance of the biohybrid electrode. For the silicon electrodes described thus far, the substrate was first cleaned using a 2% hydrogen fluoride solution. This cleaning step is performed in order to etch the native silicon dioxide layer that results from contact with the oxygen in the atmosphere. Silicon dioxide is an insulating material and therefore impairs electron transfer to the underlying silicon. Performing experiments with unetched silicon resulted in significantly lower photocurrents, as expected. Interestingly, we found that photocurrent *improvement* of the PSI-modified electrodes compared with the unmodified electrodes was much better (**Figure 3.6**). In other words, the background contribution from the silicon was diminished, making more fundamental analysis of the PSI film and electrochemical mediator easier.
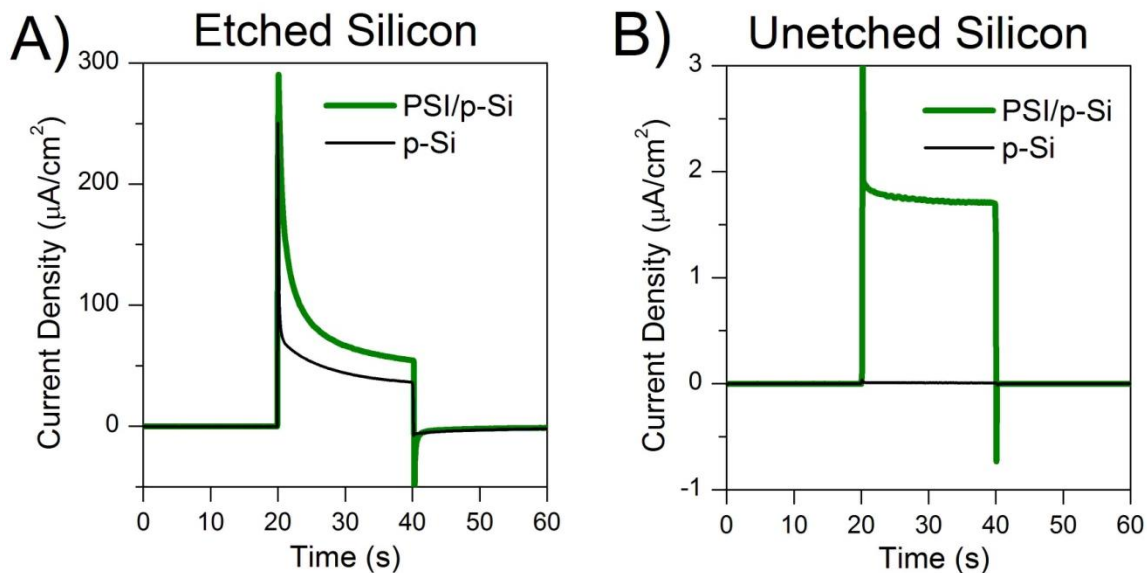
Figure 3.6. Comparison of etched and unetched silicon substrates.
Photochronoamperometric analysis PSI modified (green) and unmodified (black) p-doped silicon working electrodes. A) Silicon electrode was etched using 2% hydrogen fluoride. B) Silicon electrode with the native oxide layer left intact. Measurements made using 2 mM MV mediator, 0.1 M KCl, a Ag/AgCl reference electrode, and a platinum mesh counter electrode.

Inspired by this capability, we decided to analyze a series of viologen-based mediators in order to "fine-tune" the electrochemical parameters of the PSI modified p-doped silicon electrode. A list of the viologen mediators along with their experimentally determined formal potential can be found in **Table 3.1**. While several of these viologens are commercially available (MV and BV), the remaining viologens required synthesis. The synthesis and characterization of these viologens can be found in the experimental section of this chapter.

Table 3.1. Viologen Series with abbreviations and Formal Potentials.

Abbreviation	Common Name	Chemical Name	Formal Potential (E°') V vs. Ag/AgCl*
BV	Benzyl Viologen	1,1'-dibenzyl-4,4'-bipyridinium	-0.53
DQ	Diquat	1,1'-ethylene-2,2'-bipyridinium	-0.57
MV	Methyl Viologen	1,1'-dimethyl-4,4'-bipyridinium	-0.65
TMBP	N/A	1,1'-trimethylene-2,2'-bipyridinium	-0.76
DTMBP	N/A	4,4'-dimethyl-1,1'-trimethylene-2,2'-biyridinium	-0.90

*Formal Potentials were experimentally determined using cyclic voltammetry.

Interestingly, testing this series of viologen mediators with PSI-modified p-doped silicon gave dramatically different results depending on whether the substrate had been etched or left unetched (**Figure 3.7**). For etched silicon, MV, DQ, and TMBP all performed similarly well. DTMBP, however, is unable to efficiently shuttle electrons away from the F_B site of PSI because its formal potential is too negative, -0.9 V vs. Ag/AgCl. Similarly, BV has a formal potential that lies outside the ideal range for interaction with the F_B site, except in this case the formal potential is too positive. Thus, for etched silicon the ideal range for the mediator formal potential is between -0.57 V and -0.76 V vs. Ag/AgCl. Unetched silicon, on the other hand, demonstrates a trend of increasing photocurrent as the formal potential of the mediator becomes more positive. While BV and DQ are not statistically different, it is clear that TMBP underperforms the mediators with a more positive formal potential. This suggests that the addition of the oxide layer on the silicon substrate not only hinders electron transfer, but also shifts the energy alignment of the system. While the effects of band-bending are well studied,[56] the concept of an oxide layer significantly shifting the band-alignment of this system was unexpected.

37
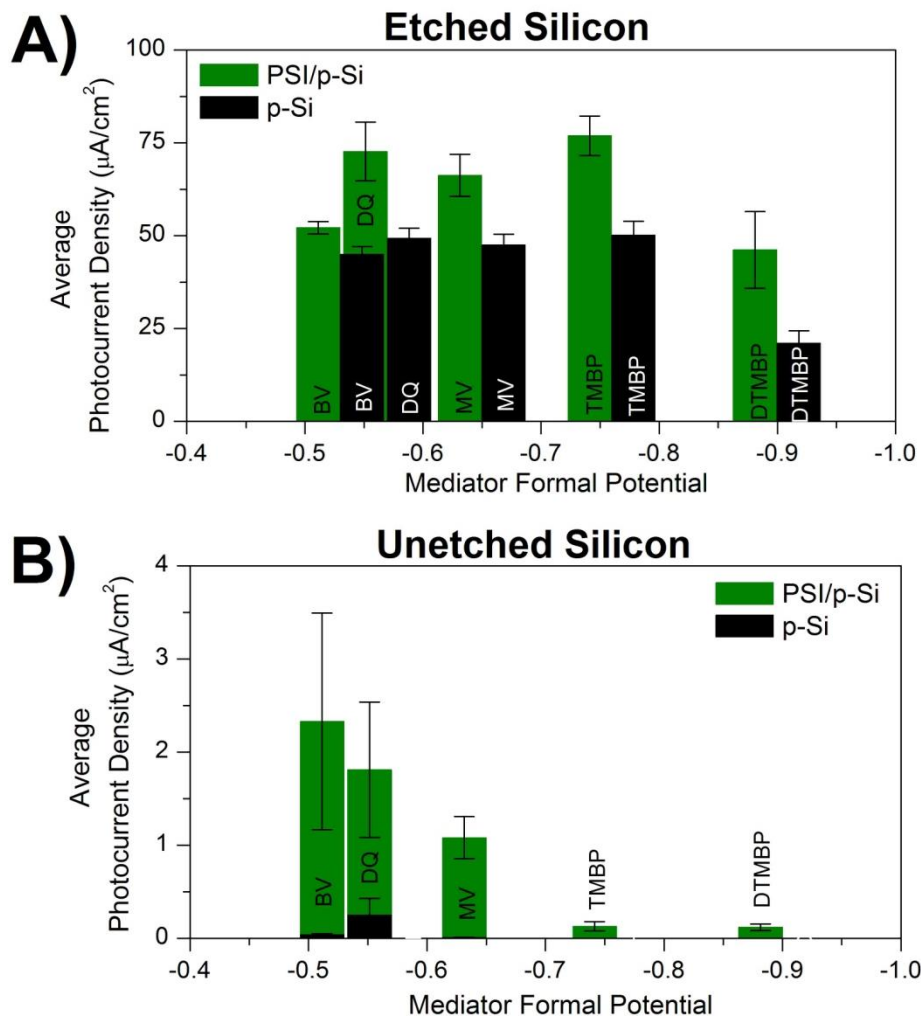
Figure 3.7. Comparison of Viologen Series. The average photocurrent density as a function of the viologen mediator formal potential for PSI modified (green) and unmodified (black) p-doped silicon electrodes that have either been etched (A) or left unetched (B). Measurements made using 2 mM viologen mediator, 0.1 M KCl, a Ag/AgCl reference electrode, and a platinum mesh counter electrode. Abbreviations of the mediator used have been added for clarity.

Unfortunately, it has proved difficult to synthesize additional viologen molecules with more positive formal potentials. Experiments using RuHex, with a formal potential of -0.10 V vs. Ag/AgCl, gave similar photocurrent densities as BV when unetched silicon was used. This may suggest that the ideal mediator formal potential for unetched silicon

substrates lies between that of RuHex and BV. Efforts to synthesize water-soluble mediators in this regime have led us to synthesize polyviologens. The synthesis and characterization of these polymers can be found in the experimental section of this chapter. The analysis of these polymers as electrochemical mediators has not yet been performed.

Conclusions

In conclusion, we have demonstrated how doped silicon can be used to enhance the photocurrent density of PSI films, and conversely how PSI can enhance the photocurrent density of p-doped silicon. After testing different doping types and doping densities, we found that heavily p-doped silicon provided the best substrate for photocurrent enhancement by PSI. Of the mediators tested, high concentrations of methyl viologen were shown to provide the best photocurrent density when etched silicon was used. The extraordinary photocurrent enhancement taken at the open-circuit potential could be generated without protein orientation by directing electron flow via band alignment. Additional photocurrent was also contributed to the system by the photoactive substrate. This method shows promise in next generation biohybrid devices. Interestingly, the photocurrent contribution from the substrate could be reduced by leaving the silicon unetched. While this greatly reduces the overall current density of the system, the use of unetched silicon may provide a useful platform for more fundamental studies with PSI. As both PSI and silicon are widely abundant, the use of these materials in conjunction with one another for photocurrent enhancement provides a promising avenue toward inexpensive solar conversion devices.

Experimental

Extraction and Isolation of Photosystem I.

Photosystem I complexes from commercially available baby spinach were isolated using previously described methods. Briefly, thylakiod membranes were isolated from spinach leaves via maceration and subsequent centrifugation at 4,000 g.[34] The PSI complex was then removed from the thylakiod membrane by adding a high concentration of surfactant and further centrifugation.[67] The protein was then purified using a chilled hydroxylapitite column, and excess surfactants and salts were removed using dialysis.[26] The concentration of the resulting PSI solution consisted of 1.7×10^{-4} M chlorophyll with a chlorophyll a/b ratio of 3.5, and 1.0×10^{-5} M protein complexes as characterized by the methods of Porra[68] and Baba *et al.*[36] respectively.

Preparation of substrates

Silicon substrates were purchased from either University Wafer or WRS materials. Heavily doped silicon had a doping density of 10^{20} cm^{-3}, while lightly doped silicon had a doping density of 10^{16} cm^{-3} (as determined by the resistivity values provided by the supplier). Unless otherwise stated, substrates were cut and rinsed with deionized water prior to etching with a 2% hydrogen fluoride solution to remove the native oxide layer. [CAUTION: *hydrogen fluoride is extremely corrosive and dangerous. Proper protective equipment and procedures should always be used*]. The etched silicon substrates were then rinsed with copious amounts of deionized water before electrochemical analysis or further modification with PSI. Substrates used without etching (unetched silicon) were simply rinsed with water and dried with nitrogen prior to use.

Gold substrates were prepared by thermally evaporating 125 nm of gold onto a silicon wafer with a 10 nm adhesion layer of chromium. Substrates were cut and rinsed with deionized water prior to electrochemical analysis or further modification with PSI.

Modification of substrates with PSI

Films of PSI were deposited onto the silicon substrates following the procedure previously developed by our lab.[26] Briefly, 100 µL of PSI extract solution was pipetted onto the silicon substrate (exposed area of 0.283 cm^2) and a vacuum was applied to remove any solvent. Due to the low surfactant concentration in the protein suspension, the resulting protein film was no longer water soluble and could withstand electrochemical experiments using aqueous mediators. The thickness of the protein film can be easily increased by adding additional deposition steps, or decreased by diluting the concentration of the initial solution. Film thicknesses were determined using a Vecco Dektak 150 stylus profilometer. For these measurements the protein film was scratched to the underlying silicon substrate, and the profilometer tip was run across the scratch. The average thickness of the films used for each experiment was determined from three measurements, and is listed in the figure caption for the various experiments.

Synthesis of viologen mediators

The general synthesis method of the viologen mediators followed the procedures presented by Salmon and Hawkridge.[69] The general synthesis method for the polyviologen mediators followed the procedures presented by Sassoon and co-workers.[70] Note that experiments concerning the use of polyviologen mediators with PSI-modified silicon electrodes is not reported in this chapter.

Synthesis of 1,1'-ethylene-2,2'-bipyridinium

In a 25 mL round-bottom flask, 1.00 g of 2,2'-bipyridinum (6.4 mmol) was mixed with 10.00 mL of 1,2-dibromoethane (115.5 mmol). The mixture was then refluxed for 3 hours at 150°C. The resulting bright yellow precipitate was filtered and dried (0.87 g). The crude product was then purified through recrystallization with isopropyl alcohol to give an off-white product (0.20 g, 9.1% yield). The product was then characterized using NMR (**Figure 3.8**) and cyclic voltammetry (Figure 3.10). ^{1}H NMR (400 MHz, D_2O): δ 5.29 (s), 8.32 (t), 8.85 (t), 8.92 (d), 9.16 (d).

Synthesis of 1,1'-trimethylene-2,2'-bipyridinium

In a 25 mL round-bottom flask, 1.00 g of 2,2'-bipyridinum (6.4 mmol) was mixed with 10.00 mL of 1,3-dibromopropane (98.5 mmol). The mixture was then refluxed for 3 hours at 150°C under a nitrogen atmosphere. The resulting bright yellow precipitate was filtered and dried (2.3481 g). The crude product was then purified through recrystallization with ethanol twice and dried in an oven at 100°C for 1 hour to give a light yellow product (0.75 g, 32.8% yield). The product was then characterized using NMR (**Figure 3.8**) and cyclic voltammetry (**Figure 3.10**). ^{1}H NMR (400 MHz, D_2O): δ 2.91 (m), 8.36 (t), 8.46 (d), 8.86 (t), 9.20 (d).

Synthesis of 4,4'-dimethyl-1,1'-trimethylene-2,2'-bipyridinium

In a 25 mL round-bottom flask, 1.18 g of 4,4'-dimethyl-2,2'-bipyridinum (6.4 mmol) was mixed with 10.00 mL of 1,3-dibromopropane (98.5 mmol). The mixture was then refluxed for 3 hours at 150°C under a nitrogen atmosphere. The resulting pale yellow precipitate was filtered and dried (4.11 g). The crude product was then purified through recrystallization with a mixture of 95% isopropyl alcohol and 5% ethanol twice

and dried under reduced pressure for 1 hour to give a light pink product (1.08 g, 43.7% yield). The product was then characterized using NMR (**Figure 3.8**) and cyclic voltammetry (**Figure 3.10**). ^{1}H NMR (400 MHz, D$_2$O): δ 2.74 (s), 2.84 (m), 8.13 (d), 8.26 (s), 8.95 (d).

Figure 3.8. NMR spectra of synthesized viologen mediators. NMR spectra of DTMBP (top), TMBP (middle), and DQ (bottom) along with their chemical structure and peak assignments.

Synthesis of poly-propyl viologen (PPV)

In a 100 mL round-bottom flask, 1.00 g of 4,4'-bipyridine (6.4 mmol) was dissolved in 50 mL of anhydrous acetonitrile. Using a syringe, 0.65 mL of 1,3-dibromopropane (6.4 mmol) was added to the mixture. The mixture was then allowed to reflux for 24 hours at 85°C under a nitrogen atmosphere. The light yellow precipitate was filtered, washed with anhydrous acetonitrile, and dried under reduced pressure (0.46 g, 35.7% yield). The product was then characterized using NMR (**Figure 3.9**) and cyclic voltammetry (**Figure 3.10**). ^{1}H NMR (400 MHz, D_2O): δ 2.90 (m), 7.83 (d), 8.39 (t), 8.57 (d), 8.69 (d), 9.00 (t), 9.18 (d).

Synthesis of poly-p-xylene viologen (PXV)

In a 100 mL round-bottom flask, 1.00 g of 4,4'-bipyridine (6.4 mmol) and 1.69 g of α,α'-dibromo-p-xylene (6.4 mmol) was dissolved in 50 mL of anhydrous acetonitrile. The mixture was then allowed to stir at room temperature for 24 hours under a nitrogen atmosphere. The dark yellow precipitate was filtered and washed with anhydrous acetonitrile (3.57 g). The crude product was then purified through recrystallization with ethanol and dried under reduced pressure to give a bright yellow product (0.80 g, 29.7% yield). The product was then characterized using NMR (**Figure 3.9**) and cyclic voltammetry (**Figure 3.10**). ^{1}H NMR (400 MHz, D_2O): δ 5.92 (s), 7.56 (s), 8.49 (d), 9.10 (d).

Synthesis of poly-decyl viologen (PDV)

In a 100 mL round-bottom flask, 1.00 g of 4,4'-bipyridine (6.4 mmol) and 1.92 g of 1,10-dibromodecane was dissolved in 50 mL of anhydrous acetonitrile. The mixture was then allowed to reflux for 24 hours at 90°C under a nitrogen atmosphere. The light

yellow precipitate was filtered, washed with anhydrous acetonitrile, and dried under reduced pressure (1.07 g, 36.6% yield). The product was then characterized using NMR (**Figure 3.9**) and cyclic voltammetry (**Figure 3.10**). ^{1}H NMR (400 MHz, D$_2$O): δ 1.26 (s), 2.49 (m), 3.33 (s), 3.51 (t), 4.63 (t), 8.04 (d), 8.64 (d), 8.86 (d), 9.25 (d), 9.44 (m).
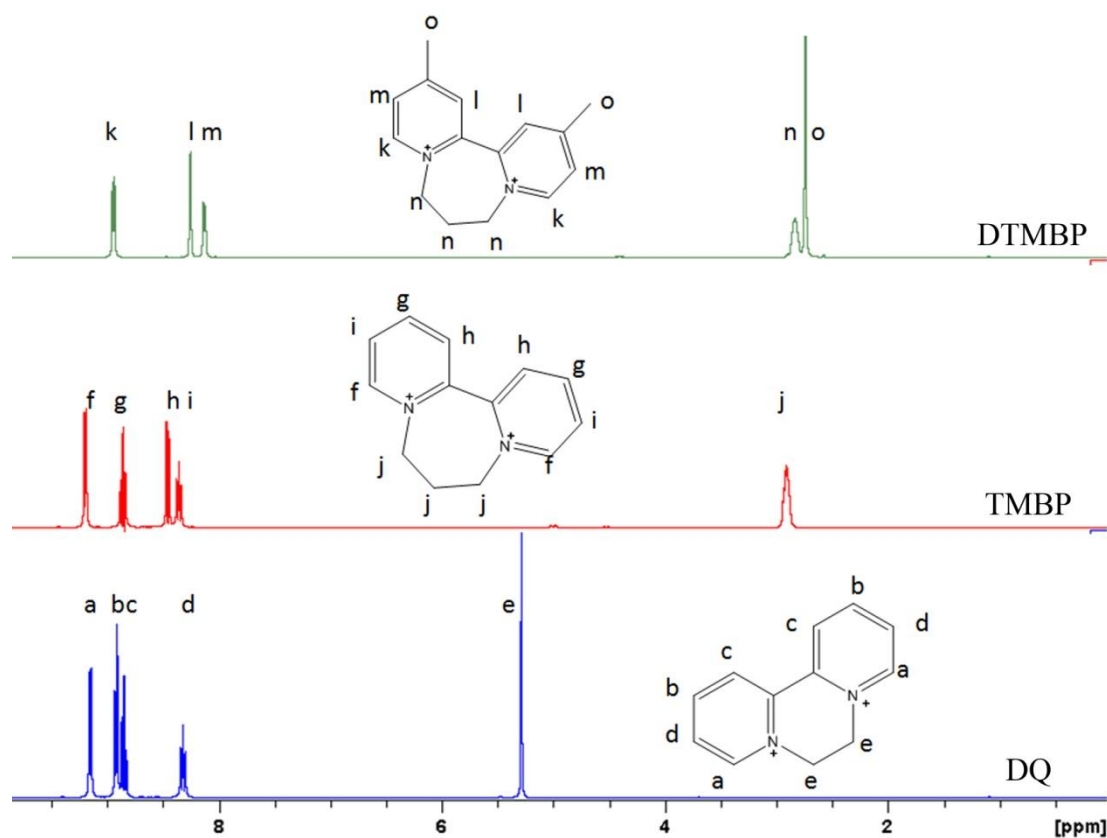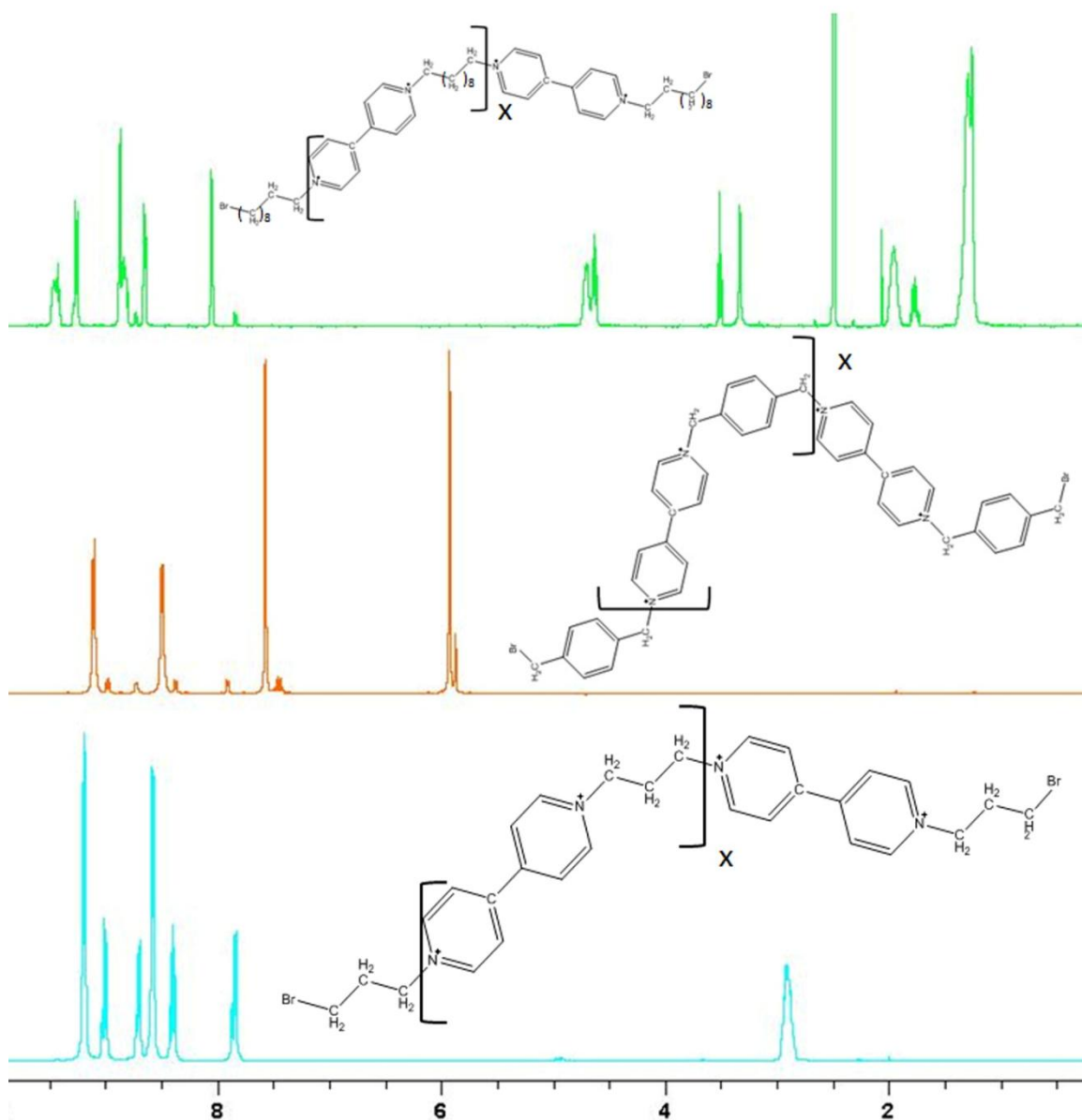

Figure 3.9. NMR spectra of synthesized polyviologen mediators. NMR spectra of PDV (top), PXV (middle), and PPV (bottom) along with their chemical structure. Sections in brackets represent the repeating unit of the polymer. Assignments are not added for clarity.

Electrochemical measurements

Electrochemical measurements were performed using a CH Instruments CHI 660a electrochemical workstation equipped with a Faraday cage as described in Chapter II. The silicon substrate was set as the working electrode, Ag/AgCl used as the reference electrode, and a platinum mesh used as a counter electrode. Electrochemical mediator solutions consisted of 100 mM potassium chloride (Sigma-Aldrich) and 0.2 mM of either ferrocyanide (Sigma-Aldrich), ferricyanide (Fisher), ruthenium III hexammine trichloride (Sigma-Aldrich), or methyl viologen (Sigma-Aldrich). For viologen studies, 2 mM concentrations of the appropriate viologen were utilized. The concentration of methyl viologen was varied for different experiments as described in the main text.

Cyclic voltammetry (CV) was performed on the viologen mediators in order to determine the formal potential (**Figure 3.10**). Mediator solutions were prepared at 2 mM, with 0.1 M KCl added as a supporting electrolyte. The working electrode was a 2 mm diameter gold macro electrode, with a platinum mesh for the counter electrode, and Ag/AgCl used as the reference. The scan rate was set at 0.1 V/s. The sharp peak observed on the return sweep for the polyviologen mediators is caused by a change in the reaction kinetics. These sharp peaks indicate that the mediator is surface bound rather than diffusion limited.
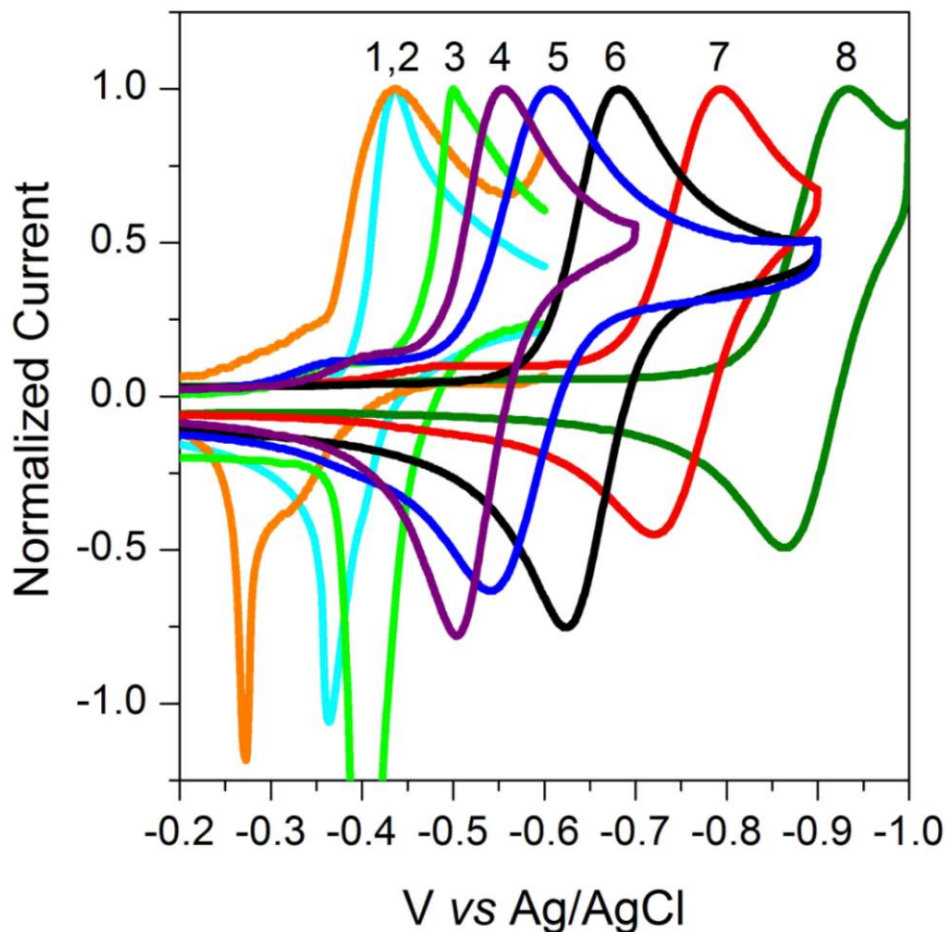
Figure 3.10. Cyclic Voltammetry of Viologen Derivatives. CVs of the various viologens explored in this work. Note that the voltage is referenced against Ag/AgCl and that the cathodic current has been normalized. From left to right, 1) PPV – teal, 2) PXV – orange, 3) PDV – bright green, 4) BV – purple, 5) DQ – blue, 6) MV – black, 7) TMBP – red, 8) DTMBP – green. Measurements made with a scan rate of 0.1 V/s, using 2 mM viologen mediator, 0.1 M KCl, a Ag/AgCl reference electrode, and a platinum mesh counter electrode.

Photochronoamperometric experiments were performed at the open circuit potential of system, which was determined experimentally for each sample. Illumination was provided using a 250 W cold light source (Leica KL 2500 LCD) equipped with a 633 nm high pass filter, generating a light intensity of 0.19 W/cm^2. Illumination with different colors of light demonstrated that the enhancement with PSI was primarily found with red light. The photocurrent values reported were found by taking the difference in the dark

current and the current under illumination after 10 seconds. Values reported represent the average value from four measurements, with error bars representing the standard deviation between those measurements. Photovoltage measurements were performed by measuring the open circuit potential of the system in the dark and under illumination.

CHAPTER IV

ZINC OXIDE AS A TRANSPARENT TOP ELECTRODE FOR BIOHYBRID
ELECTRODES BASED ON PHOTOSYSTEM I

Introduction

As described in the Chapter III, p-doped silicon provides an excellent platform for electron donation to PSI. In other words, p-doped silicon is able to reduce the P700$^+$ center of PSI quickly and efficiently. This occurs for two reasons: one, the p-doped silicon favors reduction events in the electrochemical system; and two, the band alignment of the system allows electrons to flow "down-hill" into the oxidized reaction center of PSI. The next logical step to improve upon this system would be to replace the electrochemical mediator (methyl viologen) with an n-doped semiconductor to conduct electrons away from the F_B site of PSI.

There are a few criteria that can be used to help decide on the appropriate n-doped semiconductor. First, the semiconductor must have a conduction band that is very near, but lower in energy than F_B of PSI. Secondly, if p-doped silicon is used as the electron donating electrode, the n-doped semiconductor should be transparent to visible light that can be absorbed by PSI. This means that the band-gap of this semiconductor should be greater than 3 eV. Finally, the semiconductor would ideally be both easily n-doped and inexpensive to prepare. Following these criterions, TiO_2 and ZnO provide likely candidates.

Coincidently, these are the two semiconductors used in conjunction with PSI recently studied by Mershin and co-workers.[62] According to the authors, these semiconductors were chosen in order to take advantage of their mesoscopic, high-surface area geometry. They were also able to use bioengineered peptides to promote selective adsorption of PSI to the semiconducting electrode. In their studies, however, the semiconducting electrode was only intrinsically n-doped, and thus did not provide an ideal electron accepter by the means described above. Additionally, the dye-sensitized solar cells generated by the authors used a platinum counter electrode, and still relied on an electrochemical mediator to help shuttle the electrons between electrodes. We therefore believe that their system can be improved upon and combined with our p-doped silicon to generate a photovoltaic device capable of extraordinary photocurrents.

Topoglidis and co-workers analyzed the immobilization and bioelectrochemistry of proteins on both TiO_2 and ZnO films.[71] The authors found that ZnO exhibited a higher density of sub-band gap states relative to TiO_2 resulting in significant conductivities at potentials slightly negative of 0 V *vs.* Ag/AgCl. TiO_2, on the other hand, was found to be essentially insulating at applied potentials greater than -0.3 V *vs.* Ag/AgCl. Furthermore, ZnO can be easily doped with ions to greatly enhance its conductivity and decrease its resistance.[72] Thus, the Fermi energy (E_F) of the doped ZnO film can be raised to enhance the acceptance of electrons from F_B and complete the circuit as seen in **Figure 4.1**.
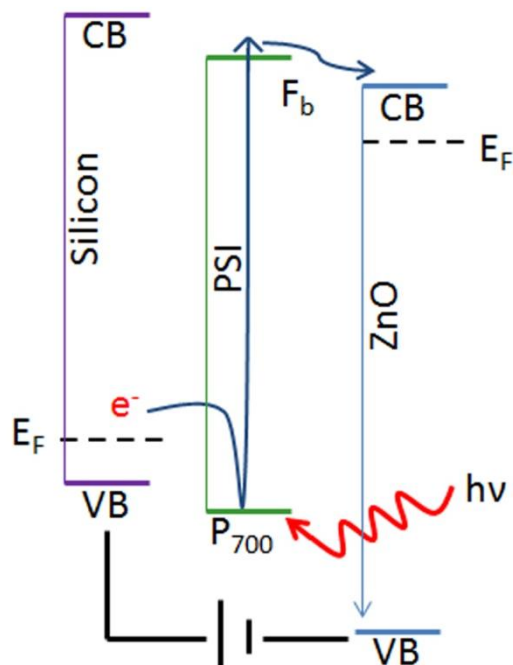
Figure 4.1. Electron flow through the PSI sensitized photovoltaic device. With p-doped silicon, the electrons are able to flow into the P_{700} reaction center, where they are then excited by photons to the F_B site in PSI. The excited electrons are then able to flow from the F_B site of PSI into the n-doped ZnO. Visible light (red line) is able to pass through the doped ZnO electrode due to its large band-gap.

Simultaneously interfacing the PSI film with p-doped silicon and n-doped ZnO provides several challenges. In order to maintain the secondary structure of PSI, any high temperature treatments or harsh chemical treatments must be performed prior to modification with PSI. In other words, the photovoltaic device cannot be annealed to change the crystal structure of the semiconductors. Secondly, the roughness of the protein film makes it difficult to make electrical contact with both the substrate and counter electrodes simultaneously. Therefore one of the semiconductors should be grown on the protein film to ensure maximum contact at the interface.

To meet these challenges, we can look to the vast literature on the synthesis of high quality ZnO films. Several techniques have been employed for the growth of ZnO

films including atomic layer deposition,[73] magnetron sputtering,[74] chemical vapor deposition,[75] pulsed laser deposition,[76] plasma assisted molecular beam epitaxy,[77] sol-gel processes,[72] and electrochemical deposition.[78] Additionally, confined plume chemical deposition (CPCD) has recently been developed for deposition crystalline materials onto organic substrates,[79] making this process an interesting possibility for this application. Of these techniques, electrochemical deposition and CPCD provide the most straight-forward solutions to address both challenges mentioned in the previous paragraph.

Results and Discussion

Electrochemical Deposition

Following the general method described by Goux and co-workers,[80] we have been able to electrochemically deposit films of zinc oxide using zinc chloride and molecular oxygen as precursors. The mechanism for this reaction can be summarized by the following equations:

$$O_2 + 2H_2O + 4e^- \rightarrow 2OH^- \tag{2}$$

$$Zn^{2+} + 2OH^- \rightarrow ZnO + H_2O \tag{3}$$

At temperatures below 34°C, the formation of zinc hydroxide is kinetically favored. Here, the films were grown at 40°C, which has been previously determined to be the lowest temperature at which smooth, dense films can be electrochemically deposited.[80]

Following five hours of electrochemical deposition, a film of ZnO was deposited on top of the PSI film (**Figure 4.2**). The scanning electron microscopy (SEM) image (**Figure 4.2B**) coupled with the EDX spectra (**Figure 4.2C**) demonstrate that the ZnO

film has grown on the contoured surface of the protein film. Furthermore, it appears that the protein film is necessary for significant semiconductor growth, as the same process performed directly on p-doped silicon did not produce a film.
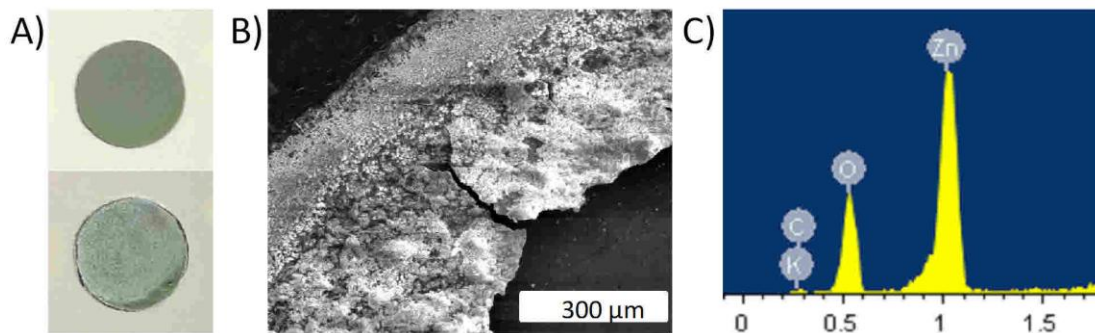
Figure 4.2. ZnO film formation on the surface of a PSI modified electrode. A) Optical image of the PSI modified p-doped silicon sample before (top) and after (bottom) electrochemical deposition of ZnO. B) SEM image of the sample and C) accompanying EDX spectrum.

In order to demonstrate the effect of depositing this second semiconductor on the biohybrid electrode, additional electrochemical experiments were performed. We hypothesized that the addition of a ZnO film on the surface of the PSI would prevent efficient electron flow from the PSI to methyl viologen (MV), however electron flow to ruthenium III hexammine trichloride (RuHex) should be unimpeded or even enhanced due to the new band alignment. This is because the electrons from F_B transfer rapidly to the n-doped ZnO before MV. Subsequently, the electrons transferred to ZnO cannot be used to reduce MV because the formal potential of MV is too high. In other words, the electron cannot flow "uphill" to methyl viologen, but can still flow "downhill" to RuHex, which has a lower formal potential. As seen in **Figure 4.3**, a p-doped silicon substrate modified with PSI demonstrates much higher photocurrents in a mediator solution containing MV compared with a RuHex mediator solution. However, after electrochemical deposition of ZnO the RuHex mediator outperforms MV, as

53

hypothesized. Compared with the PSI film alone, the improved photocurrent production

with RuHex after the addition of ZnO is due to improved kinetics according to Marcus

theory. These results demonstrate that the electrochemically deposited mediator is not

only in close contact with the PSI film, but is capable of efficient electron transfer with

the biohybrid electrode.
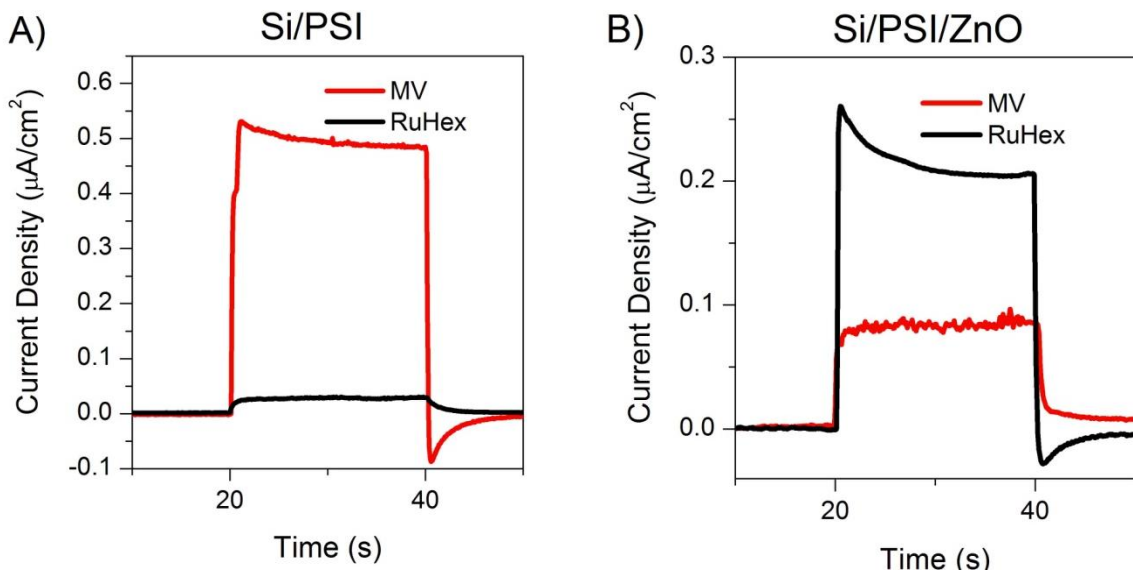
Figure 4.3. Photochronoamperometric analysis of electrochemically deposited ZnO. p-doped silicon modified with a film of PSI (A) and further modified with an electrochemically deposited film of ZnO (B). Samples were tested in mediator solutions consisting of 0.1 M KCl and either 2 mM methyl viologen (red) or 2 mM RuHex (black). The light was turned on and off at 20 s and 40 s, respectively. The working electrode was held at the open circuit potential, and a platinum mesh and Ag/AgCl were used as the counter and reference electrode respectively.

Confined Plume Chemical Deposition

CPCD is a relatively new deposition procedure developed by the Lukehart

research group at Vanderbilt University for depositing crystalline solid material on an

organic or inorganic support material without significant damage to the support

material.[79] The basic principal of this deposition method is to generate a reaction plume

from a chemical precursor that then deposits the desired material onto the surface of the underlying substrate (**Figure 4.4**). This reaction plume is generated through the use of a precursor molecule that can absorb a specific wavelength of light generated by a laser pulse. By confining the reaction plume between a substrate and a transparent barrier, the resulting decomposition product of the precursor is deposited on the nearby substrate. In order to coat the entire surface of the substrate, the laser beam is rastered across the surface of the sample. Damage to the substrate is avoided through two advantages that laser illumination provides. First, laser light is composed of a single wavelength of light. Therefore using a wavelength of light that the sample does not absorb well prevents this form of radiation from damaging the substrate directly. Second, the collateral thermal damage that could be generated by the reaction plume can be avoided by using short pulses of laser irradiation. This allows the generated heat from the reaction to be dissipated prior to thermal degradation of the substrate.
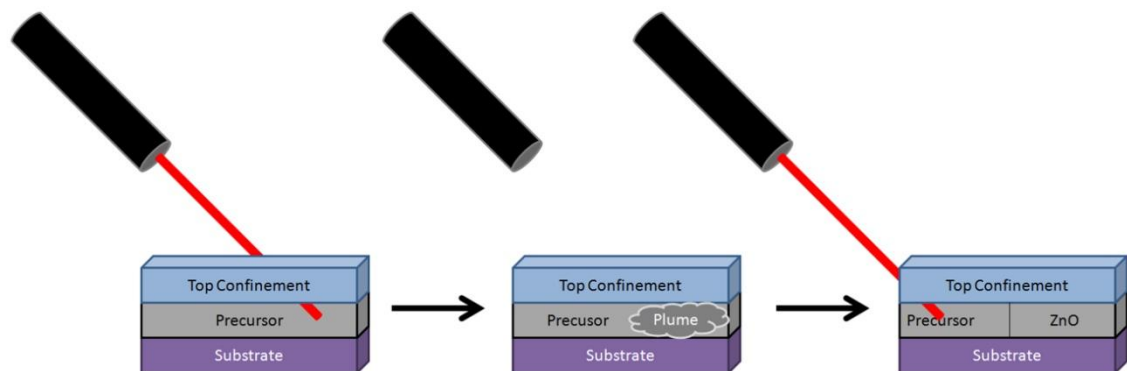
Figure 4.4. Experimental schematic for CPCD. The general method for CPCD is comprised of illuminating a precursor material with a pulsed laser light in a confined area. This illumination generates a chemical plume resulting in crystalline ZnO to deposit on the substrate surface. The laser is then moved and the process continues until the desired area is covered.

For the deposition of ZnO, the zinc precursor bis (n-propylcarbamate) zinc

(**Figure 4.5**) was synthesized by Jeremiah Beam. The amide structures are capable of

absorbing laser light, in this case 2.94 μm illumination from an Erbium YAG laser. This

precursor, which is soluble in dimethyl sulfoxide (DMSO), was then deposited onto the

substrate through simple drop-casting.
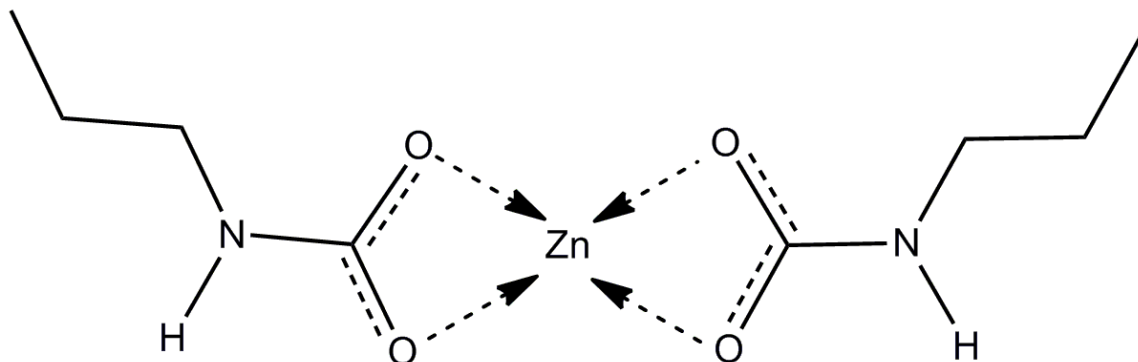
Figure 4.5. Chemical structure of ZnO precursor. Bis (n-propylcarbamate) zinc
provided by Jeremiah Beam.

The precursor was confined using a glass slide and illumination from the laser

resulted in a chemical plume. Removing the sample from the stage resulted in a dense

ZnO film on the surface of the PSI modified silicon electrode. The presence of crystalline

ZnO was confirmed through the use of X-ray diffraction (XRD) and Raman spectroscopy

(**Figure 4.6**). The XRD demonstrates a very sharp diffraction peaks, demonstrating a

highly crystalline material with hexagonal wurtzite structure. Typically, achieving ZnO

films with sharp diffraction peaks requires annealing at 300°C or higher.[81] The Raman

spectrum serves as further evidence of the wurzite structure of the ZnO that was

deposited on the surface of the PSI film. The C_{6v} symmetry of ZnO generates optical

phonon modes classified as $A_1+E_1+2E_2+2B_1$. According to selection rules, only E_2 and

A_1 modes are expected to be observed. As seen in **Figure 4.5B**, sharp peaks are present at approximately 98, 440, and 520 cm^{-1}, which is in good agreement with the E_2 and A_1 modes reported previously in the literature.[82]
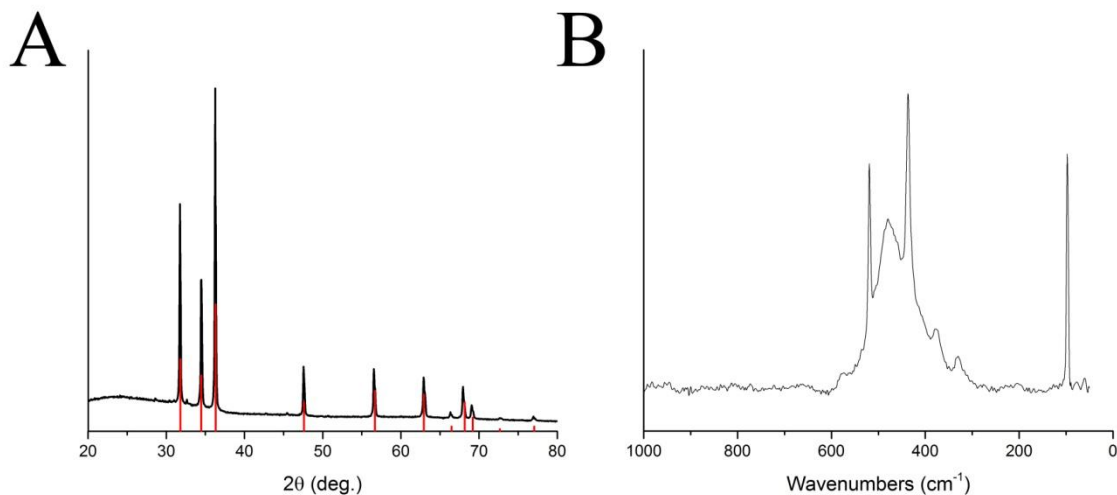
Figure 4.6. XRD and Raman of CPCD ZnO. A) XRD of ZnO film deposited on top of a PSI-modified silicon electrode. Red lines correspond to the JCPDS card number 36-1451. B) Raman spectrum of ZnO film deposited on top of a PSI-modified silicon electrode.

Similar to previous experiments using electrochemically deposited ZnO, we analyzed the complex interface generated by CPCD ZnO on a PSI-modified silicon electrode with electrochemistry (**Figure 4.7**). From the photochronoamperometric analysis with MV, there are a number of interesting observations that can be made. First, the irradiation of a PSI film with the pulsed laser used in CPCD does not directly hinder the photoactivity of PSI. Second, the addition of either the precursor or the CPCD ZnO directly to the silicon substrate does not sufficiently block electron transfer to MV. The addition of CPCD ZnO to the PSI-modified silicon electrode, however, does demonstrate a significant blocking effect. This suggests that ZnO is able to act as an effective electron sink for the photoexcited electrons generated by the PSI film. Interestingly, experiments

with RuHex did not demonstrate enhanced photocurrent generation with CPCD ZnO on PSI-modified silicon. This may be due to increased n-doping in the ZnO film as compared with the electrochemical deposition of ZnO. Increasing the n-doping would make the reduction of RuHex less favored, as n-doped semiconductors favor oxidation reactions.[56]
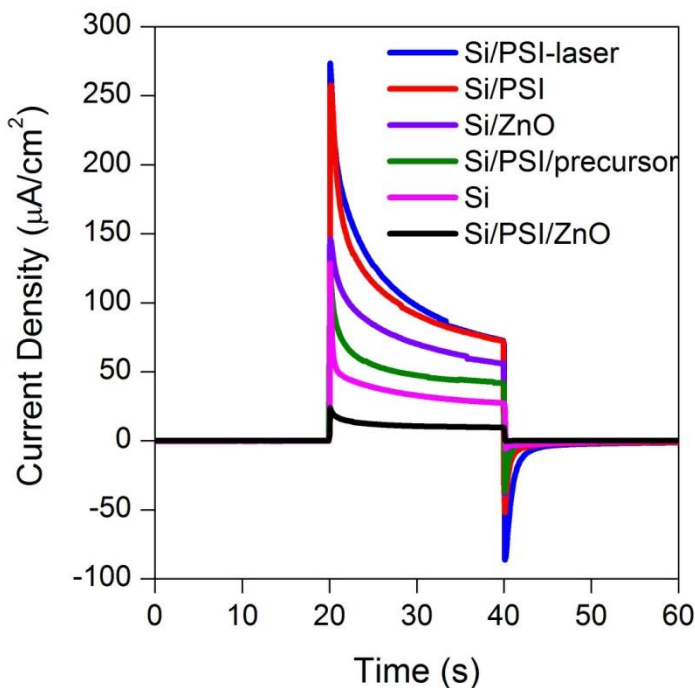
Figure 4.7. Photochronoamperometric analysis of CPCD ZnO films. Samples are listed in the legend in order of decreasing photocurrent density. Samples with ZnO and the PSI-laser sample were exposed to laser irradiation prior to the electrochemical experiments. The remaining samples were not exposed to laser irradiation. Samples were tested in mediator solutions consisting of 0.1 M KCl and 2 mM methyl viologen. The light was turned on and off at 20 s and 40 s, respectively. The working electrode was held at the open circuit potential, and a platinum mesh and Ag/AgCl were used as the counter and reference electrode, respectively.

Knowing that electrons were effectively being collected from the PSI film by ZnO, more direct experiments were performed to analyze the solid-state solar cell device. For this experiment, electrical connectivity to the ZnO was generated by physical

connection to conductive glass, FTO. Thus the complete cell was composed of p-doped Si/PSI/ZnO/FTO. The cell was then analyzed using a two probe measurement in the dark and under 1 sun illumination. The I-V curve presented in **Figure 4.8** demonstrates that the cell is in fact electrically connected and photoactive. The cell gave a short-circuit current (J_{sc}) of 7.34 μA/cm^2 and the open-circuit voltage (V_{oc}) of 114 mV. The fill-factor (ff) was 0.275, and the cell demonstrated an external efficiency (η) of 2.4x10^{-4} %. While these values are relatively low, this data represents an important proof-of-concept. We anticipate dramatic improvements for these values as the CPCD process for ZnO on PSI is optimized. Additional areas for improvement include smoother PSI film formation and improved contact methods for connectivity to the ZnO film.
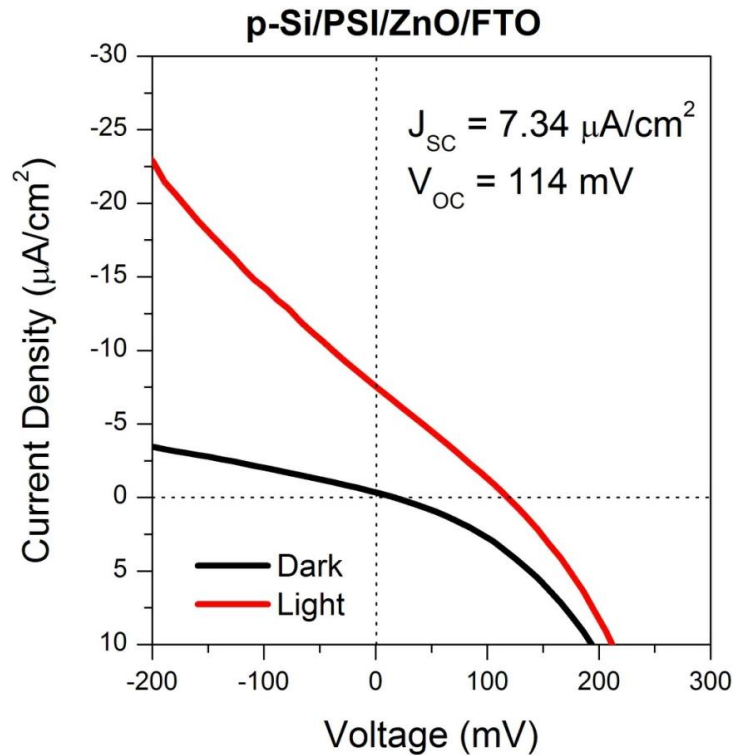
Figure 4.8. I-V analysis of a PSI-based solid-state solar cell. The cell, comprised of p-Si/PSI/ZnO/FTO, was analyzed under dark (black) and 1 sun illumination (red). The voltage was swept from -250 to 500 mV.

Conclusions

In conclusion, we have demonstrated how ZnO can be directly deposited onto the surface of a biohybrid electrode at conditions that do not jeopardize the functionality of the biological material. Specifically, we described the electrochemical deposition and CPCD of ZnO on a film of PSI. Both systems demonstrated photoactivity when tested with electrochemical methods, demonstrating the power of these types of studies for the analysis of a complex interface. Electrochemical deposition allowed the system to remain in an aqueous environment, while the use of CPCD required the PSI film to be exposed to DMSO, although efforts to develop a water soluble ZnO precursor are underway. CPCD also provided a much faster deposition process that was completed in minutes rather than hours, as is required for the electrochemical deposition process. Ultimately, we found CPCD to be the more promising method for ZnO deposition, and used this method to form a prototype solid-state solar cell device composed of p-Si/PSI/ZnO/FTO. Efforts to improve upon the performance attributes of this solid-state device will enable the use of these inexpensive and abundant materials to have an impact on the current energy crisis.

Experimental

Preparation of substrates

Lightly p-doped (10^{16} cm^{-3}) silicon substrates were purchased from University Wafer. Substrates were cut and rinsed with deionized water prior to etching with a 2% hydrogen fluoride solution to remove the native oxide layer. [CAUTION: *hydrogen fluoride is extremely corrosive and dangerous. Proper protective equipment and procedures should always be used*]. The etched silicon substrates were then rinsed with

copious amounts of deionized water before electrochemical analysis or further modification with PSI and/or ZnO.

For the development of a solid-state device, a resist layer was patterned onto a silicon substrate using photolithography. Briefly, a Shirley 1830 photoresist solution was coated onto the surface of a 7.62 cm diameter etched silicon wafer. The resist was added using a spin coating method at 5000 rpm for 60 s using a Brewer Science Cee 200CB. The wafer was then "soft-baked" at 115°C for 60 s before a patterned mask was used to illuminate the regions of interest with UV light for 8.2 s using a Karl Suss MA6 optical mask aligner. The wafer was then rinsed in a base solution for 60 s, rinsed with water for 60 s, and then "hard-baked" for 120 s at 115°C. This enabled rectangular wells (4 mm x 2 mm) with a depth of 1.2 μm to be modified with PSI and eventually CPCD ZnO.

Modification of substrates with PSI

PSI was extracted from baby spinach leave as described in Chapter II. Films of PSI were deposited onto the silicon substrates following the procedure previously developed by our lab.[26] Briefly, 100 μL of PSI extract solution (10^{-6} M) was pipetted onto the silicon substrate (0.283 cm^2 exposed area) and a vacuum was applied to remove any solvent. This process was repeated a second time in order to completely cover the silicon substrate.

Electrochemical deposition of ZnO

Electrochemical deposition of ZnO on the surface of the PSI-modified silicon substrate followed the general procedure described by Goux and co-workers.[80] Here, we prepared a 5 mM zinc chloride solution with 100 mM KCl added as a supporting electrolyte. This solution was then bubbled with oxygen for 30 minutes prior to the

experiment and then continuously through the deposition process. The solution was heated to a temperature of 40°C. The biohybrid electrode was then held at a potential of -1.1 V vs. Ag/AgCl for 5 hours. Following electrochemical deposition, the sample was gently rinsed with water and allowed to air dry prior to further analysis.

CPCD of ZnO

CPCD was performed following the same concept described by Ivanov and co-workers.[79] Here, the ZnO precursor, bis (n-propylcarbamate) zinc, was suspended in DMSO and deposited via dropcasting onto the PSI-modified silicon electrode. After drying in air, the sample was confined using a glass slide and a custom made aluminum frame. The sample was then irradiated using a 2.94 μm erbium YAG laser. The laser, with a power output of 100 mJ, was pulsed at 20 Hz. The laser was rastered over the surface of the sample 5 times, generating a noticeable plume during each scan. The sample was then removed from confinement and excess ZnO and carbon material was removed using compressed air. In the case of the solid-state solar cell device, an FTO coated glass slide was placed on top of the ZnO modified electrode and held in place using binder clips.

ZnO characterization

After modification with ZnO, the samples were characterized using a number of analytical techniques. SEM and EDX were performed using a Hitachi S4200 with an accelerating voltage of 20 keV. Raman analysis was performed using a Thermo Scientific DXR Raman microscope. XRD was performed using Scintag X-1 Powder XRD. Samples were run at 45 kv, 40 mA using Cu k-alpha radiation (1.54 Å).

Electrochemical measurements

Electrochemical measurements were performed using a CH Instruments CHI 660a electrochemical workstation equipped with a Faraday cage as described in Chapter II. The silicon substrate was set as the working electrode, Ag/AgCl used as the reference electrode, and a platinum mesh used as a counter electrode. Electrochemical mediator solutions consisted of 100 mM potassium chloride and 2 mM of either RuHex or MV.

Photochronoamperometric experiments were performed at the open circuit potential of system, which was determined experimentally for each sample. Illumination was provided using a 250 W cold light source (Leica KL 2500 LCD) equipped with a 633 nm high pass filter, generating a light intensity of 0.19 W/cm^2.

I-V measurements

Evaluation of the solid-state solar cell device described in the main text was obtained immediately after device assembly by way of a Sciencetech SF150B solar simulator with AM1.5G filter (class A spectral match, class B non-uniformity) connected to a Keithley 2400 sourcemeter controlled by Labview software. The lamp was calibrated to 1.00 full sun with an NREL certified silicon reference diode.

CHAPTER V

INTEGRATION OF PHOTOSYSTEM I WITH GRAPHENE, REDUCED GRAPHENE
OXIDE, AND GRAPHENE OXIDE[*]

Introduction

As described in the previous chapters, PSI can be immobilized on a wide variety

of electrodes resulting in enhanced properties such as photocurrent[27,62] and

photovoltage.[61] Recently there has been tremendous enthusiasm concerning the

integration of biomaterials with carbon-based materials.[83] In 2007 Carmeli and co-

workers described the integration of PSI with carbon nanotubes,[84] however little has been

done since then to analyze the interaction of PSI with other carbon-based materials. Much

of the recent excitement surrounding carbon-based electrodes was sparked by the

discovery of graphene.[85] Improvements in synthesis and characterization methods have

provided the opportunity to exploit this novel material as a transparent, highly conductive

electrode. Graphene sheets are one-atom-thick, consisting of sp^2 carbon, possessing

unique properties such as a tunable bandgap,[86] high carrier mobility

($200\ 000\ cm^2V^{-1}s^{-1}$),[87] the quantum Hall effect at room temperature,[88] high elasticity

(breaking strength of 43 N m^{-1}),[89] high thermal conductivity (~3000 W/m-K in plane)[90] and high transparency over the visible spectrum (97.7%).[91] These extraordinary electronic, mechanical, and optical properties of graphene are inviting for applications from solar cells to transistors.[92]

There are several methods for generating graphene and graphene-like materials. The first method, described by Novoselov and co-workers, is the mechanical exfoliation method, more commonly known as the "scotch-tape method".[85] In this method, small areas of pristine graphene are produced by placing graphite onto a piece of tape and repeatedly sticking and pulling-apart the tape until a monolayer of carbon atoms is present. This is possible due to the strong forces holding the carbon atoms together in the lateral direction and the weak forces holding the layers of carbon together in the vertical direction. Unfortunately this inexpensive method is both time-consuming and incapable of producing large areas of graphene. This led to the wide spread use of chemical vapor deposition (CVD) to grow single to few layers of carbon on various substrates.[93,94] In this process, a mixture of gases, usually hydrogen and methane, are passed over a metal substrate, typically nickel[93] or copper,[94] at high temperatures. The carbon deposited on the metal can then be transferred to another substrate by etching the metal substrate away. Using this CVD method, large areas of graphene can be produced, with the size limited only by the tube furnace diameter used during the deposition process. The disadvantages of the CVD method include the production of defect sites, the complex nature of the process, and the expensive equipment required. This has led to a renewed interest in two additional carbon-based materials: graphene oxide (GO) and reduced graphene oxide (RGO).[95] GO is essentially a graphene sheet with additional oxygen functional groups

throughout the structure. GO can be produced through the chemical exfoliation of graphite, making its production both facile and scalable.[96] The oxygen functional groups act to prevent the GO sheets from stacking together, however they also disrupt the conjugation of the carbon lattice. In order to regain this conjugation, and thus improve the conductivity of the material, GO can be reduced through a number of methods to generate RGO.[97] While not as transparent or conductive as pristine graphene or even CVD graphene, RGO provides a simple method for generating large areas of semi-transparent, organic, and conductive films for a wide variety of applications.

In this chapter we will describe how each of these carbon-based materials can be interfaced with PSI for improved cell characteristics. We will begin with a discussion of integrating PSI with pristine, mechanically exfoliated graphene to generate a photoactive field-effect transistor (FET). We will then describe how CVD graphene and RGO can be used to provide a transparent electrode for studies with PSI. Finally, we will discuss the effects of integrating GO and RGO into the PSI film deposited onto a semi-conducting substrate. The results of these studies demonstrate the potential for developing carbon-based, photoactive electrodes that are inexpensive and environmentally friendly.

Results and Discussion

Graphene[30]

The most direct method for interfacing PSI with graphene is to simply immerse a sample of pristine graphene, produced through mechanical exfoliation, in a solution of PSI. This method generates a disperse, sub-monolayer, film of PSI on the surface of the graphene substrate due to physical adsorption. Using a graphene sheet that has been

prepared with gold contacts and deposited onto 300 nm of SiO_2 with an underling n-doped silicon substrate, the biohybrid system becomes a simple FET.

The resulting system, as well as a control FET without PSI, was tested using 4-probe impedance measurements. In this type of measurement, also known as Kelvin sensing, two of the gold contacts are used as voltage leads while the other two are used as current leads. By using four contacts the impedance contribution of the wiring and contacts resistance can be eliminated, which has been shown to be important in graphene-based FET.[98] The gate electrode, n-doped silicon, is located below the insulating SiO_2 in order to alter the channel resistance. In our experiments we found that exposure to PSI solution provided a 5-fold enhancement on the photoresponse of the FET (**Figure 5.1**). Furthermore, we observed that the photoresponse could be reversed by simply changing the gate voltage of the underlying silicon. Interestingly, if the gate voltage was held at more positive potentials (*i.e.* +10 V), the system would irreversibly respond to illumination (data not shown). These results demonstrate the ability for PSI to interact electronically with a graphene electrode and provide a simple method for generating an improved, graphene-based, FET device.
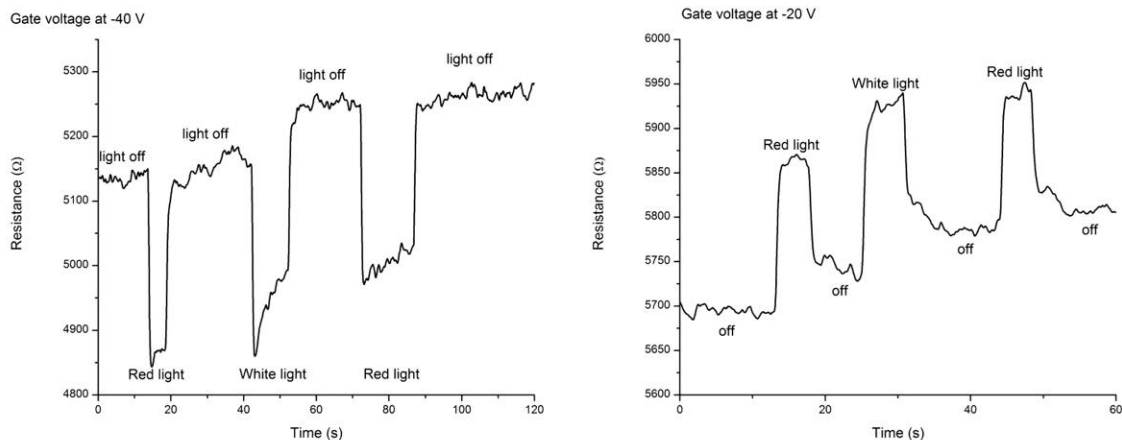
Figure 5.1. Analysis of PSI-graphene FET. 4-probe impedance measurement of a PSI-modified graphene FET as a function of time. The device was tested under vacuum (10^{-5} Torr) with a gate voltage of either -40 V (left) or -20 V (right). The device was illuminated with either red filtered or unfiltered (white) light as indicated in the graphs.

In order to further elucidate the advantages of this nanoscale, photoactive biohybrid electrode, we performed additional analytical tests. In order to perform these experiments, however, we required larger areas of graphene and therefore utilized CVD graphene. To ensure that PSI was, in fact, deposited onto the graphene electrode, we performed RAIRs and UV-Vis on the biohybrid electrode (**Figure 5.2**). The RAIRs data revealed Amide I and Amide II peaks at ~1662 cm^{-1} and ~1540 cm^{-1}, respectively, indicative of the protein complex.[42] Additionally, UV-vis spectra revealed two distinct peaks at ~680 nm and ~440 nm, consistent with the chlorophylls of PSI present on the surface of the graphene electrode. Together, the RAIRs and the UV-vis spectra indicate that PSI is adsorbed onto the graphene surface.
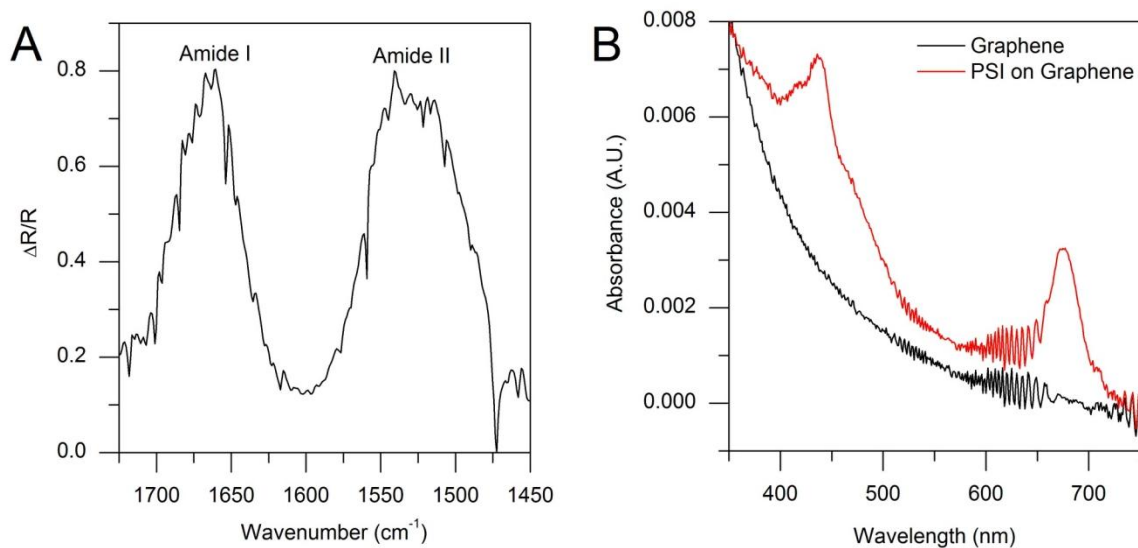
Figure 5.2. RAIRs and UV-vis analysis of PSI on graphene. A) RAIR spectrum of a PSI modified graphene electrode. The CVD graphene was transferred to a gold electrode in order to perform the reflection analysis. B) UV-vis spectrum of a graphene (black) and a PSI-modified graphene (red) electrode. The CVD graphene was transferred to a glass slide to perform the absorbance measurement.

Ellipsometric thicknesses were measured on the PSI films to assess the coverage of protein deposited on the graphene substrate. The average thickness measurement for PSI films was 58 Å with a standard deviation of ± 15 Å, using a Cauchy model. Based on the reported size of PSI[7] and the considerable free volume contained in a complete monolayer of PSI in which the proteins are oriented with their electron transfer vectors normal to the substrate, it is estimated that a complete monolayer would yield an ellipsometric thickness of ~80 Å, which agrees well with the greatest thicknesses reported for PSI monolayers.[23] Therefore, a measurement of 58 Å represents approximately 70% surface coverage of PSI on the graphene surface.

To further investigate the effective coverage of PSI on the electrode, electrochemical experiments were performed in the dark to assess the ability of the PSI film to block the access of redox-active species to the underlying graphene. **Figure 5.3**

shows cyclic voltammograms (CV) recorded in the absence of light. The underlying

substrate (SiO$_2$) acts as an insulator, and no current is observed at any potential. The

unmodified graphene substrate reveals an increasing current as the voltage sweep

becomes more negative, which is attributed to reduction of the oxidized RuHex species,

demonstrating that the graphene film is conductive and an appropriate electrode for this

process. Previous experiments have demonstrated that PSI functions as an insulating

material under dark conditions.[58] Thus, after deposition of a PSI monolayer, the observed

reductive and oxidative current decreases, as PSI blocks mediator access to a majority of

the electrode surface. A PSI surface coverage of ~70% was estimated from the decrease

in integrated charge for the reduction peak after adsorption of PSI, consistent with that

gleaned from ellipsometric measurements.
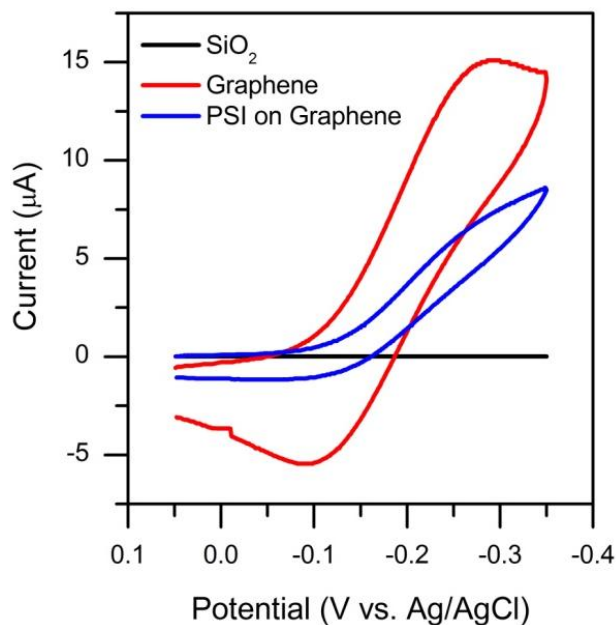
Figure 5.3. CV analysis of PSI-modified graphene electrodes. CV of the SiO$_2$ substrate (blue), unmodified graphene electrode (black), and PSI-modified graphene electrode (red), taken in the dark, using 2 mM RuHex in 5 mM phosphate buffer solution with 0.1 M KCl. The potential of the working electrode was scanned from -0.35 to 0.05 V vs. Ag/AgCl at a rate of 0.1 V/s.

70

One benefit of using graphene as a transparent, conducting electrode is the flexibility it allows with mediator choice and concentration. A previous study by our research group demonstrated that mediators that absorb red light, such as DCPIP or MB, limit the photocurrent because the light is unable to be absorbed by the PSI film.[29] By mounting graphene on glass, we can irradiate the cell through the transparent electrode rather than through the solution, enabling the use of opaque mediators. This also allows us to utilize high concentrations of the mediator, which has been shown to significantly improve photocurrent production of PSI-based photoelectrochemical cells.[27] **Figure 5.4** shows the results of the photochronoamperometric experiments where we have used MB as an opaque, redox-active mediator. Illumination through the MB mediator demonstrated no measureable photocurrent production, as expected. Illumination through the graphene electrode, however, produced a significant photocurrent. At a mediator concentration of 20 mM, the PSI-modified electrode exhibited a 10-fold enhancement over the unmodified graphene electrode. As seen in **Figure 5.4**, the current density for these PSI-modified graphene electrodes increases by a factor of ~20 as the MB mediator concentration increases from 0.2 to 20 mM. The increase in photocurrent production does not increase linearly as well would expect. This may be due to some photoactivity of MB itself. This would then alter the photocurrent production of the system as the concentration at the electrode interface could differ significantly from the bulk solution. Here, the integration of PSI monolayer films with graphene as an atomically thin, transparent electrode enables the achievement of these high photocurrents, while traditional opaque electrodes would not allow testing under these conditions.
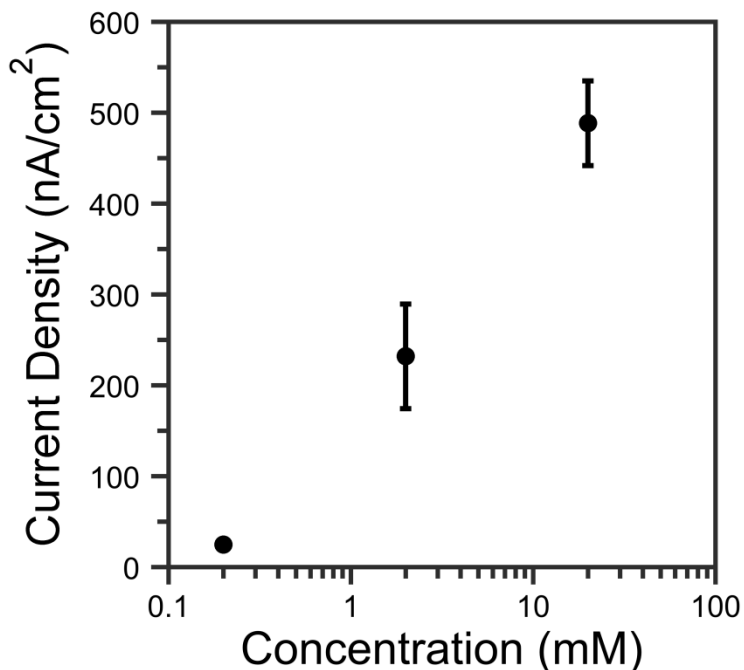
Figure 5.4. Photocurrent of PSI-modified graphene as a function of mediator concentration. Photocurrent measurements made using various concentrations of MB, with 5 mM phosphate buffer and 0.1 M KCl added as supporting electrolytes. Experiments performed at the experimentally determined dark OCP. Photocurrent values taken after 10 s of illumination.

Reduced Graphene Oxide

As mentioned in the introduction, CVD graphene can be time-consuming and expensive to produce, leading to renewed interest in the use of RGO. RGO has similar properties to graphene but generally has imperfections because of unreduced oxygen functional groups. This leads researchers to commonly employ few-layer RGO so that conductivity across the entire film is continuous. We hypothesized that RGO would demonstrate even greater photocurrent improvement than we observed in the CVD graphene case because of the ability to use thicker multilayer films of PSI. We were unable to consistently deposit multilayer films on CVD graphene as the process for this

multilayer film formation often damaged the graphene substrate and prevented electrical contact from being made. We prepared the RGO electrode by spin coating GO onto functionalized glass and then reducing the GO with hydrazine vapor. The resulting RGO film was characterized by its thickness, resistance, absorbance, Raman peak shift, and CV peak splitting (discussed further in the experimental section of this chapter). We subsequently deposited thick, multi-layer films of PSI on the RGO electrode using methods previously developed in our lab.[26]

To measure the photo-electrochemical performance of the PSI-RGO and RGO electrodes we preformed photochronoamperometric measurements (**Figure 5.5**). We determined the current density in seven different mediator solutions with varying formal potentials. The mediators tested were MV, MB, RuHex, DCPIP, ferri/ferro cyanide, and sodium ascorbate. For all the tested mediators, the system generated negative photocurrents, indicating oxidation reactions. In RuHex, DCPIP, and sodium ascorbate mediator solutions, the PSI-modified RGO electrode outperformed the unmodified RGO electrode.
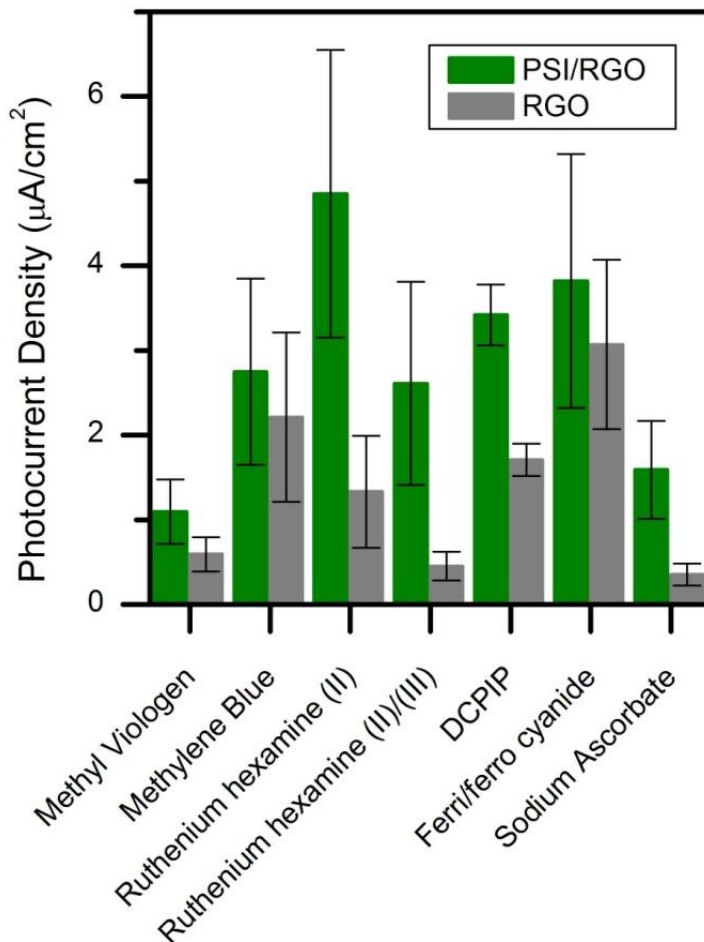
Figure 5.5. Mediator evaluation for PSI-modified RGO electrodes. The average photocurrent (n=4) of PSI-modified RGO compared to unmodified RGO electrodes in various mediator solutions at mediator concentrations of 2 mM.

From these experiments, DCPIP was found to be the most attractive mediator because it is organic, inexpensive, and non-toxic. While previous studies using gold electrodes found DCPIP to be an inferior mediator due to its absorbance in the red region of the spectrum,[29] the transparency of the RGO electrodes provides the opportunity to use this opaque mediator as it is no longer necessary to illuminate the electrode through the mediator (**Figure 5.6**). DCPIP absorbs light in the same 600-700 nm region as PSI preventing the PSI-modified electrode from absorbing the light necessary for

74

photoactivity. Therefore, the transparency of the RGO electrode is necessary for the use of DCPIP as a mediator solution. The PSI-modified RGO electrode demonstrates photocurrents comparable to a PSI-modified gold electrode (1.2 to 7.9 $\mu A/cm^2$)[26] and significantly higher than a PSI-modified graphene electrode (0.5 $\mu A/cm^2$).[30] Furthermore, RGO is a more attractive electrode material because it is significantly less expensive than gold and more processable than graphene.
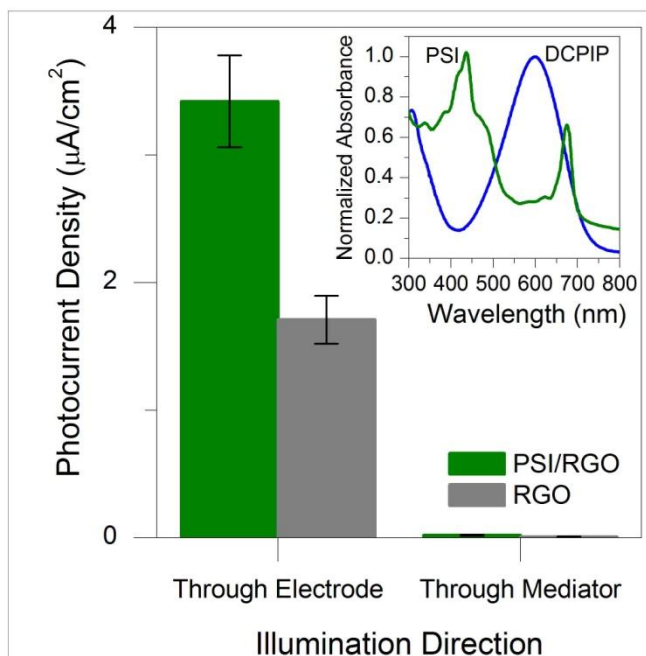
Figure 5.6. Effect of illumination direction for PSI-RGO electrodes.
Photochronoamperometric analysis of PSI-RGO (green) and RGO (grey) in DCPIP when the direction of the light is varied. The mediator solution was 2 mM DCPIP with 100 mM KCl. The inset shows the UV-Vis spectra of DCPIP (blue) and PSI (green).

As demonstrated previously with CVD graphene,[30] increasing the concentration of the mediator solution can further improve the photocurrent density (**Figure 5.7**). Higher mediator concentrations increase photocurrent density by minimizing diffusional limitations of reduced mediator to the PSI film; thus, the mediator is able to donate

electrons to the PSI-RGO more rapidly. A significant increase in photocurrent was observed from 0.2 to 2 mM. Further increasing the concentration showed a marginal improvement in the photocurrent, indicating that the concentration of the mediator solution is not a significant limiting factor in photoactivity beyond concentrations of 2 mM. Additionally, concentrations higher than 20 mM we began to exceed the solubility limit of DCPIP. Thus, the optimal current density is achieved with a mediator concentration of 20 mM.
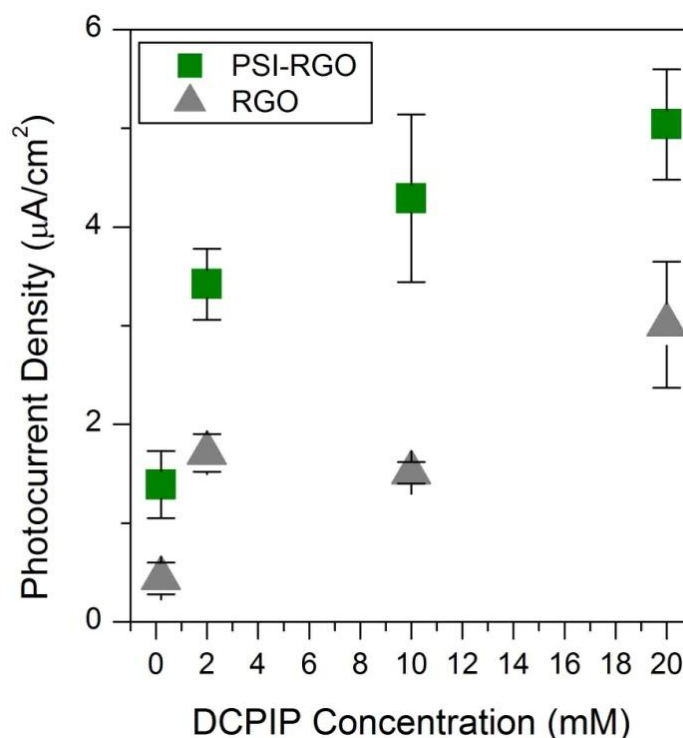
Figure 5.7. Photocurrent of PSI-RGO electrodes as a function of mediator concentration. Photocurrent measurements made using various concentrations of DCPIP, with 0.1 M KCl added as a supporting electrolyte. Experiments performed at the experimentally determined dark OCP. Photocurrent values taken after 10 s of illumination.

Graphene Oxide[31]

In addition to using RGO as a conductive transparent electrode, the use of RGO and even GO as a supporting matrix material is of considerable interest.[99,100] The addition of GO and RGO is particularly attractive for PSI-based devises for a number of reasons. GO and RGO are both water-soluble, making the integration of these materials with PSI straightforward. Furthermore, the low cost and facile synthesis of GO and RGO make these materials ideal candidates for making inexpensive composite materials. The functional groups present on GO make possible the interaction with both the polar groups of PSI as well as the electrochemical mediator (**Figure 5.8**). On the other hand, the improved conductivity of RGO can facilitate electron transfer between the PSI complexes and the underlying electrode.
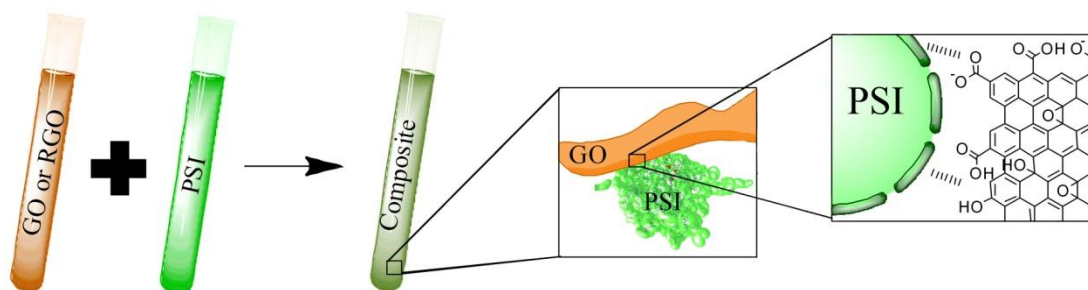
Figure 5.8. Schematic of PSI composite formation. GO, RGO, and PSI are all soluble in water. Therefore these materials can simply mixed in solution prior to film formation to generate a composite solution that results in a composite film after deposition onto a substrate. The materials interact due to the interactions between the oxygen functional groups present on GO or RGO and the hydrophilic regions of PSI as indicated by the insets.

In chapter III we described dramatic improvements in the measured photocurrent of PSI based systems by using a p-doped silicon substrate in conjunction with a methyl viologen mediator.[27] Here we hypothesized that interfacing the PSI film with a water-soluble, carbon-based material would improve the organization of the film and improve

its conductivity. We began by preparing aqueous solutions of the various materials and depositing them on silicon substrates. A scanning electron micrograph of the PSI-GO composite cross-section demonstrates relatively ordered layering (**Figure 5.9**). This ordering has previously been observed with amyloid-GO composites and was attributed to the hydrophilic interactions between the protein and GO.[101] The luminal and stromal ends of the PSI protein, which contain large amounts of hydrophilic lysine residues,[7] generate a strong interaction with the oxygen functionalities present in GO and RGO.
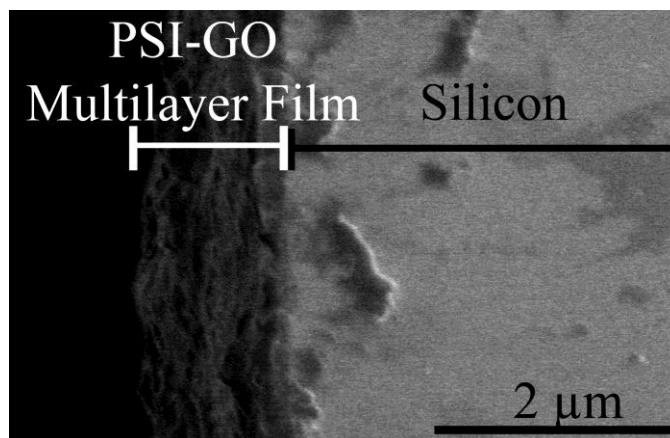
Figure 5.9. SEM of PSI-GO composite. SEM image of an angled cross-section of a PSI-GO composite film on a silicon substrate. Image taken at 1 keV.

In order to determine the effect of the GO and RGO on the impedance of the PSI film, we performed electrochemical impedance spectroscopy (EIS) in the presence of methyl viologen, an electrochemical mediator (**Figure 5.10**). In the dark (**Figure 5.10A**), PSI behaves as an insulating film and provides resistance against the transport of aqueous mediator to the silicon surface. The resulting impedance spectrum contains two time constants: one for the PSI film and one for the silicon interface (space-charge layer, oxide, *etc.*). In the light (**Figure 5.10B**), the PSI/p-Si electrode behaves as a single

interface where electrons can be exchanged with the mediator either at the silicon surface or at the active sites of the PSI complexes within the film. Thus, the time constant exhibited by PSI in the dark disappears from the spectrum, revealing a single time constant. Because there are more sites for electron exchange with the mediator in the PSI system, the impedance at low frequencies in the light is reduced below that of the uncoated p-Si electrode, which is consistent with higher photocurrents observed for PSI modified electrodes versus p-Si controls.[27] The addition of conductive elements (RGO) or charged structuring elements (GO) does not significantly affect the impedance response of the PSI film in the dark, suggesting that these components do not hamper the mediator transfer into the film. However, in the light, two interesting effects are observed. First, the GO-PSI and RGO-PSI films exhibit only a single time constant, suggesting that the entire composite acts as a single interface as observed for the PSI film alone. Second, we observe a significant decrease in resistance with the addition of GO or RGO. At high frequencies the resistance decreases as PSI>GO-PSI>RGO-PSI, which is consistent with the expected conductivities of these films. This resistance is the uncompensated resistance, which is a function of both the solution conductivity and the electrode conductivity. The impedance at low frequencies decreases as PSI>PSI-GO≈PSI-RGO. This impedance element reflects the actual electron exchange with the mediator, showing that the addition of *either* GO or RGO improves the interfacial electron transfer between the biohybrid electrode and the MV electrochemical mediator.
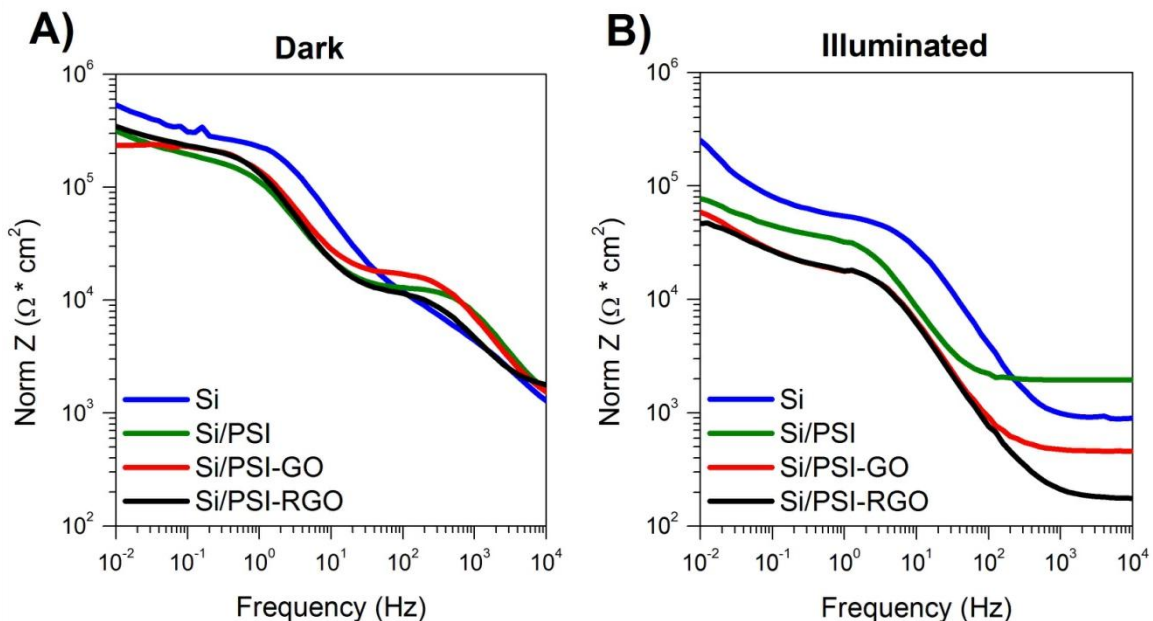
Figure 5.10. EIS of PSI-GO and PSI-RGO composites. Bode plots of samples under dark (A) and illuminated (B) conditions. EIS was performed using a 10 mV AC voltage over a frequency range of 10^5 to 10^{-2} Hz.

To test the photocurrent production of these composite electrodes, we performed photochronoamperometric and linear sweep voltammetry measurements on films of PSI, PSI-GO, and PSI-RGO containing the same quantity of PSI. As expected from the impedance measurements, the addition of either GO or RGO to the PSI results in a significant photocurrent improvement at the open circuit potential due to the improved interfacial electron transfer with the MV mediator (**Figure 5.11A**). Interestingly, the PSI-GO composite has a significantly higher photocurrent density than the PSI-RGO composite. To understand this unexpected result, we performed linear sweep voltammetry (**Figure 5.11B**). Two interesting observations can be made from this data. First, the PSI-GO composite shifts the photoreduction potential of the mediator system more positive. Thus, more current is expected at the dark open circuit potential (-347 ± 7 mV vs. Ag/AgCl). The PSI-GO composite film and the PSI-RGO composite film

demonstrated a positive 75 mV and a 45 mV shift, respectively, in peak current compared

with the PSI film alone. Second, the increased peak current density observed for the PSI-

GO composite suggests that the film is able to increase the local concentration of the

electrochemical mediator. We attribute this effect to the charged nature of the GO when

compared to RGO. This observation correlates well with our impedance measurements

for this film.
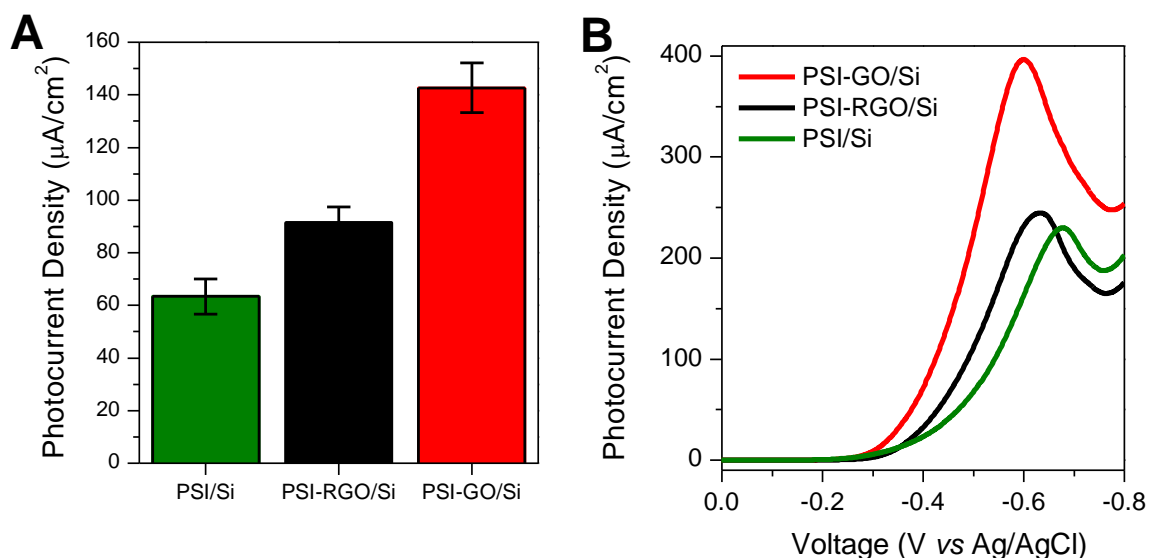
Figure 5.11. Electrochemical analysis of PSI-GO and PSI-RGO composites. A)Bar
graph with the average photocurrent density (n=4) for each sample after 10 s of
illumination with red filtered light (633 nm high pass filter). Photochronoamperometric
analysis of PSI and PSI-composites was performed on p-doped silicon substrates in 2
mM methyl viologen mediator solution. B) Linear voltammetry of PSI and PSI-
composites on p-doped silicon substrates under illumination and in 2 mM methyl
viologen mediator solution. The potential was varied at a rate of 0.01 V/s. The
concentration (mg/mL) ratio of chlorophyll to RGO or GO was 3 for both A and B.

In order to determine the ideal mixture of PSI with GO or RGO, we varied the

ratio of chlorophyll to GO or RGO and measured the resulting photocurrent (**Figure

5.12**). As expected, the PSI-GO composites outperformed the PSI-RGO composites at all

ratios. This provides further evidence towards the hydrophilic interactions between PSI

and the oxygen functional groups present in GO. Additionally, relatively little PSI is required to generate significant improvements to the photocurrent. The highest performing ratio, 1.5 mg chlorophyll to 1.0 mg GO, roughly corresponds to 1 PSI protein complex per 76 nm^2 of GO. Since a single PSI protein complex has an area footprint of roughly 80 nm^2,[54] this result suggests that each PSI complex interacts with the graphene oxide surface in a homogeneous film.
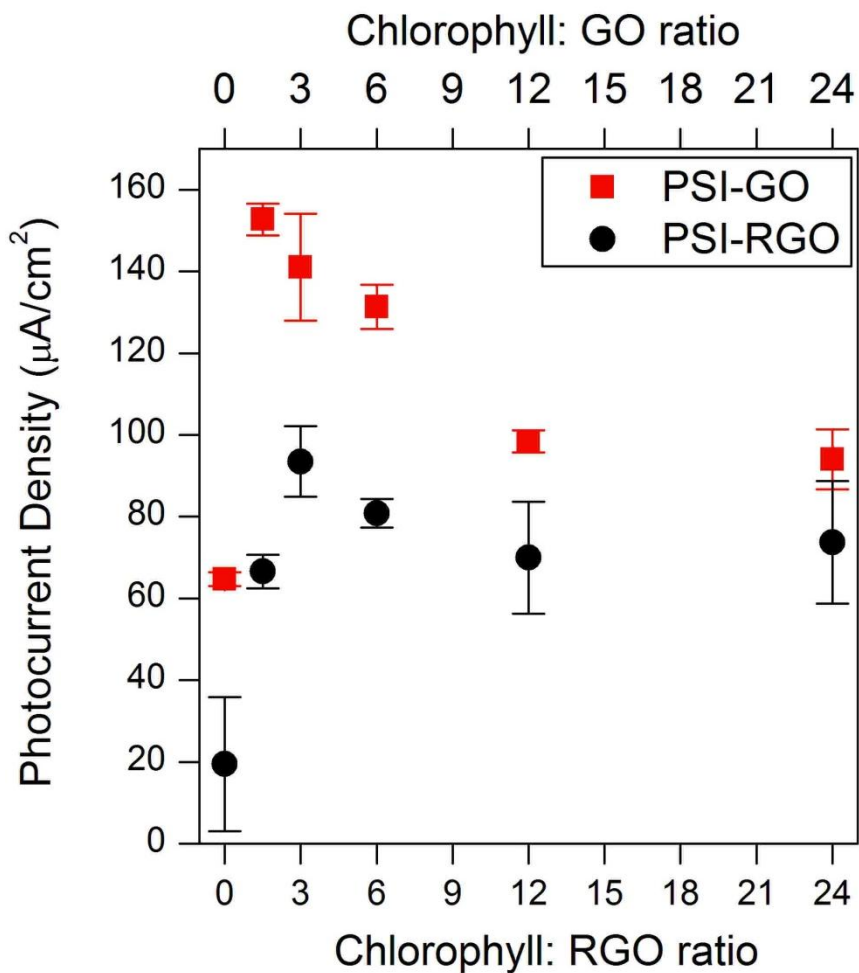
Figure 5.12. Effect of chlorophyll to GO or RGO ratio on photocurrent production.
The average photocurrent (n=3) observed for films of PSI-GO or PSI-RGO on a p-doped silicon substrate are plotted against the ratio of chlorophyll vs. GO or RGO in mg/mL.

Finally, the photovoltage of the system was analyzed by monitoring the change in the open circuit potential from dark to light measurements. This information can be easily obtained from a log plot of the current as a function of voltage (**Figure 5.13**). The open circuit potential is indicated by a sharp decrease in the current value. Thus, the photovoltage can be found by measuring the voltage difference between these values under dark and illuminated conditions. For the PSI-GO composite film, the photovoltage measured was 400 mV, an improvement of 30 mV over the PSI film alone. Curiously, the PSI-RGO composite demonstrated a photovoltage of only 330 mV.
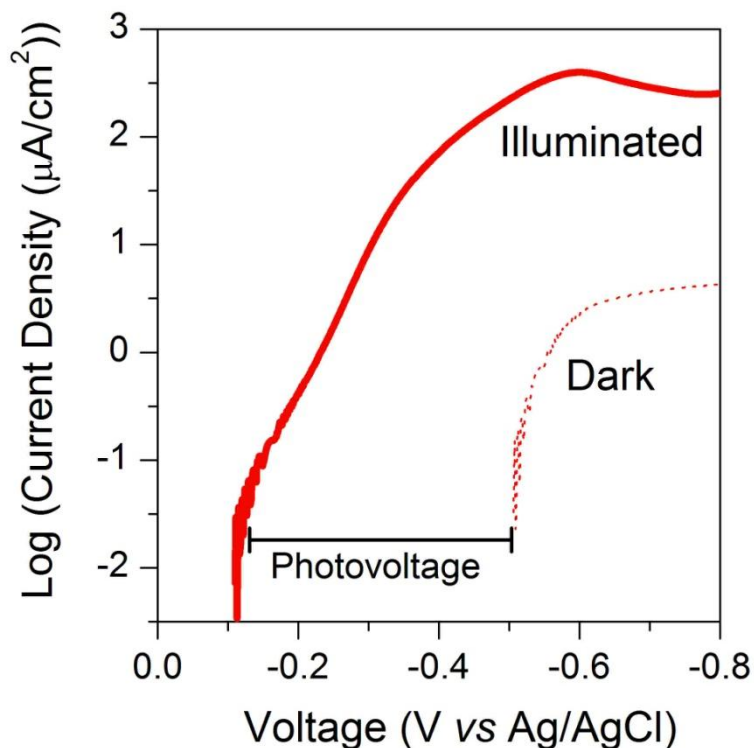
Figure 5.13. Photovoltage of PSI-GO composite. Comparison of the log current density for the PSI-GO film under illuminated (bold) and dark (dashed) conditions. Experiments were performed using a PSI-GO composite with a chlorophyll to GO ratio of 3. The composite was deposited on a p-doped silicon substrate. The potential was varied at a rate of 0.01 V/s. A 2 mM methyl viologen mediator was used with a Ag/AgCl reference electrode and a platinum mesh counter electrode.

Conclusions

We have successfully integrated PSI with a variety of graphene and graphene-like materials. Using pristine graphene we were able to generate a novel FET device with enhanced photoactivity generated by PSI. We then utilized CVD graphene to generate a photoactive biohybrid electrode that was thinner than 10 nm. The use of this graphene electrode enables us to illuminate the PSI film through the electrode rather than the mediator. This provides researchers the opportunity to use opaque mediators such as MB or DCPIP. This was further demonstrated through the use of RGO, which is more processable than CVD graphene. Finally, we demonstrated how GO and RGO could be integrated with a film of PSI to improve the photocurrent generation of PSI-modified p-doped silicon. These results demonstrate the advantages of integrating inexpensive carbon-based materials with PSI. Further studies will aim to improve upon the electrical interaction of PSI with these graphene materials, as well as the development of a photovoltaic device that is completely metal free with the exception of metals naturally present in the protein complex.

Experimental

Fabrication of PSI-graphene FET

The graphene devices investigated here were prepared by AKM Newaz. Briefly, micromechanical exfoliation was performed from Kish graphite crystals onto a 300nm of SiO$_2$ on n-doped-Si substrate. The monolayer graphene flakes were identified by their optical contrast and confirmed by Raman spectroscopy (**Figure 5.14**). Typical size of these flakes was 2-4 μm wide and 8-10 μm long. Standard electron beam lithography

followed by thermal evaporation of Cr (2nm)/Au (100nm) was employed to deposit

electrical contacts to the graphene sheet. Samples were then immersed in a PSI solution

(isolation and characterization of PSI described in previous chapters), for 48 hrs. The

modified electrodes were then rinsed with water and dried with N_2 gas before resistance

analysis using a 4-point-probe method at 10^{-5} Torr.
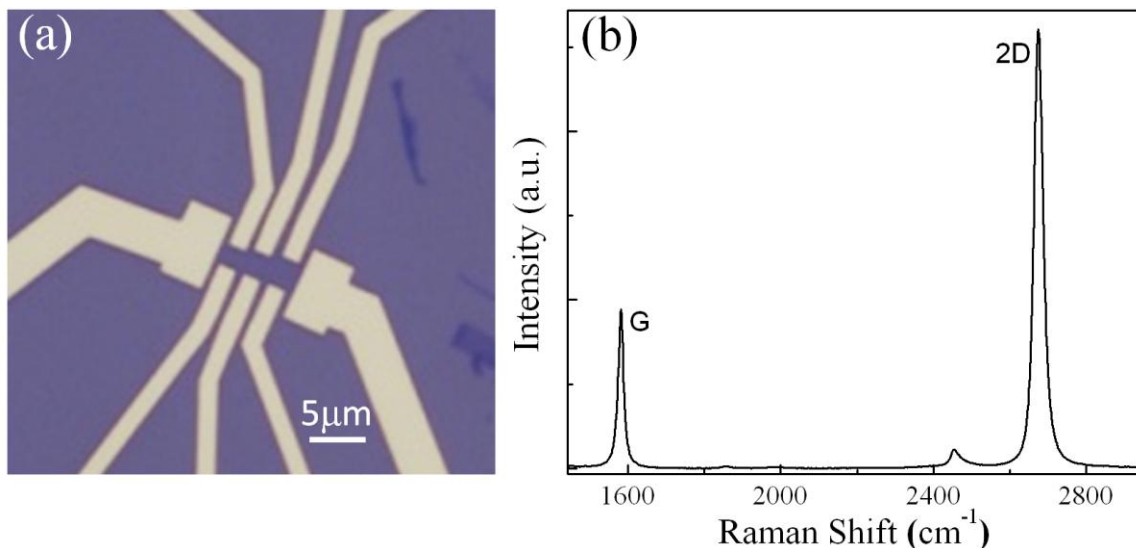
 Figure 5.14. FET device structure and Raman spectrum of pristine graphene. A) An optical image of a representative graphene-based FET device prior to exposure to PSI. B) Raman spectroscopy confirming the graphene flake is single layer and pristine. The 2D and G peaks are labeled for clarity.

CVD of graphene and transfer methods

CVD graphene was prepared and transferred to various substrates following

previously published methods.[102] Briefly, following CVD deposition onto 25-μm

thick Cu foils (Alfa Aesar), poly(methyl methacrylate) (PMMA) was spun onto the

graphene surface, and the copper was etched away using copper etchant type CE 100

(Transene Company). The PMMA-graphene substrate was then floated on deionized

water to remove copper etchant before transfer onto the substrate of interest. CVD

graphene was also analyzed using Raman spectroscopy (**Figure 5.15**). Samples could

then be modified with PSI by immersion in a suspension of PSI for 24-48 hr.
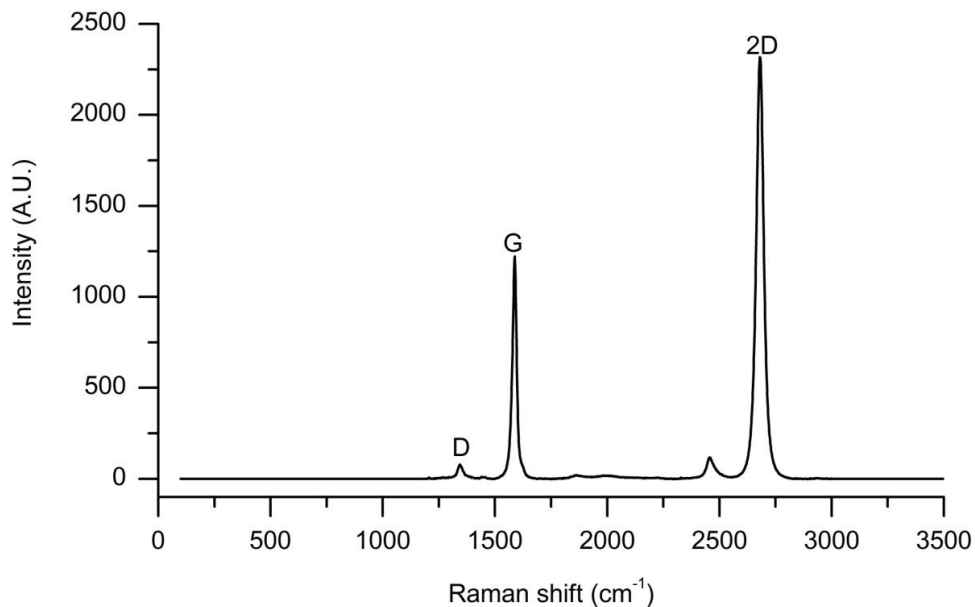
Figure 5.15. Raman spectrum of CVD graphene.

Preparation of RGO electrodes

The preparation method for the RGO electrodes used here is depicted in **Figure**

5.16. To prepare the reduced graphene oxide (RGO) electrode, a glass slide was first

functionalized by soaking the glass in 1% aminopropyl triethoxysilane (APTES) in

ethanol for 1 hour. The slide was then rinsed with ethanol and allowed to dry on the

bench-top. Originally, the slide was rinsed with water but this caused the slide to become

opaque. Additionally, slides were originally cleaned with piranha solution prior to

APTES functionalization, but eliminating this step did not appear to change the results

and made the process much faster, safer, and easier. [CAUTION: *Piranha solution can*

react violently with organic materials. Proper procedures and personal protective

equipment should always be used. Piranha solution should not be stored in tightly sealed

containers].

The functionalized glass slides were then spin-coated with 5mg/mL GO (graphene-supermarket.com) with an average flake size of 0.6-5 µm. 500 µL of 5 mg/mL GO in ethanol was added to the functionalized glass slide and spun at 800 rpm for 4 min. Attempts to spin-coat the samples with GO dissolved in water resulted in uneven film formation. The graphene oxide film was then reduced using a hydrazine vapor reduction method.[97] The GO coated slides were placed in a small petri dish that was subsequently placed in a larger petri dish that contained 1 mL of hydrazine. The larger petri dish was covered and sealed before heating to 30°C for 3 hrs. The GO film slowly changed from a light brown to a grey color during the reduction process.
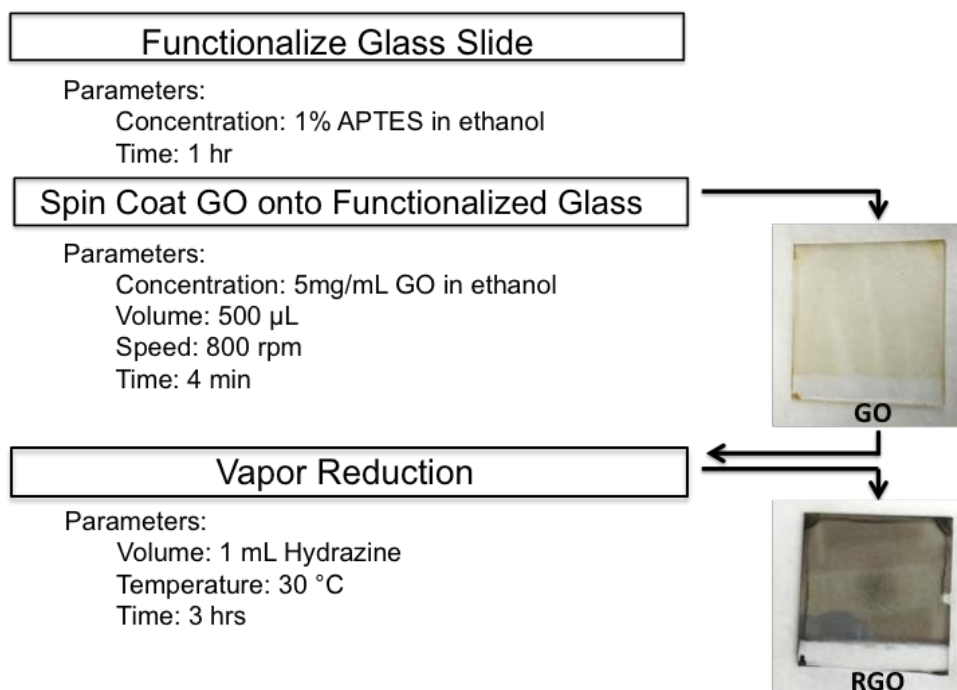
Figure 5.16. Schematic of RGO electrode preparation.

Characterization of RGO substrate electrode

The resulting RGO film was characterized for thickness, resistance, Raman spectroscopy, and UV-vis absorbance. Profilometry (Veeco Dektak 150) was used to determine the film thickness. Although the films had a significant amount of roughness associated with them, the average RGO thickness was determined to be 50 nm.

The resistance of the RGO film was determined using a four point probe resistivity measurement. The average resistance from three measurements was 4.8 ± 1.7 kΩ. The resistance of the GO before reduction was too high to measure. These results support our previous reasoning that graphite loses conductivity when it is oxidized to GO but can regain this conductivity when it is reduced.

Raman spectra of GO and RGO are presented in **Figure 5.17**. It is clearly evident that the RGO generated in this process is significantly different than the graphene generated through the scotch-tape method or from CVD. The distinct peaks observed here are the D and G peaks, at ~1340 cm^{-1} and 1600 cm^{-1}, respectively. A measure of the disorder in the system can be found using a ratio of the D and G peak intensities that correlates with the sp^3 and sp^2 carbons in the system.[103] In these experiments, the D/G peak intensity increases from 1.08 for GO to 1.61 for RGO. The increase of the D/G ratio indicates the reduction of the GO film as order is returned to the carbon lattice.
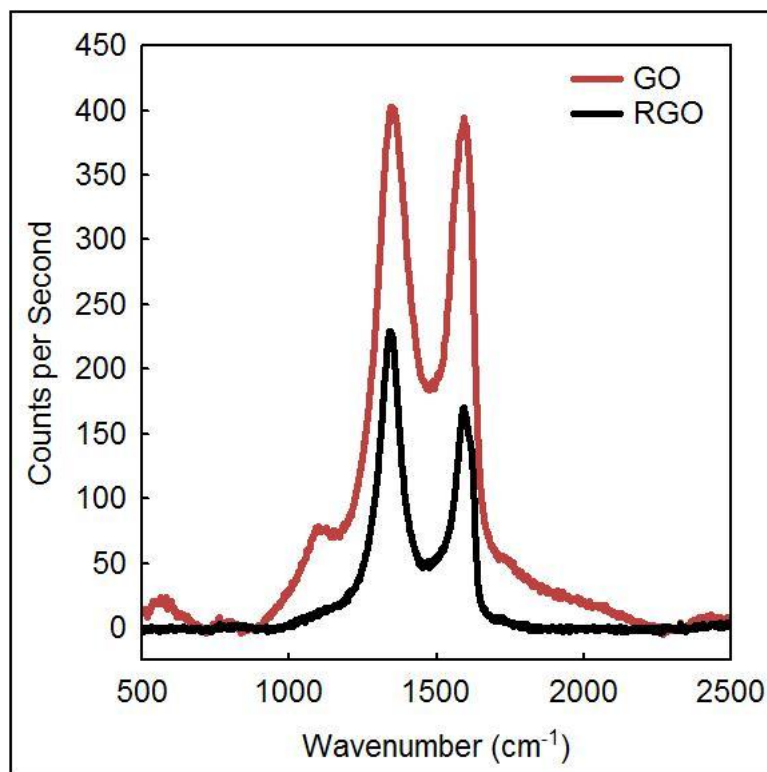
Figure 5.17. Raman spectra of GO and RGO. The D peak occurs at approximately 1350 cm^{-1} and the G peak occurs at approximately 1600 cm^{-1}.

UV-vis spectroscopy was used to measure the absorbance of the RGO film and as another method to verify the reduction process from GO to RGO has reached completion (**Figure 5.18**). In GO, an absorbance maximum is observed at ~230 nm, corresponding to a π→π* transition from aromatic C-C bonds. Additionally, a shoulder is observed at ~300 nm due to the n→π* from the C=O bonds.[104] After reduction, the absorption maximum shifts to 260 nm, indicating increased conjugation in the C-C bonds.[105] Furthermore, while the shoulder at 300 nm is no longer apparent, the absorbance of RGO is significantly higher across the UV-vis spectrum.
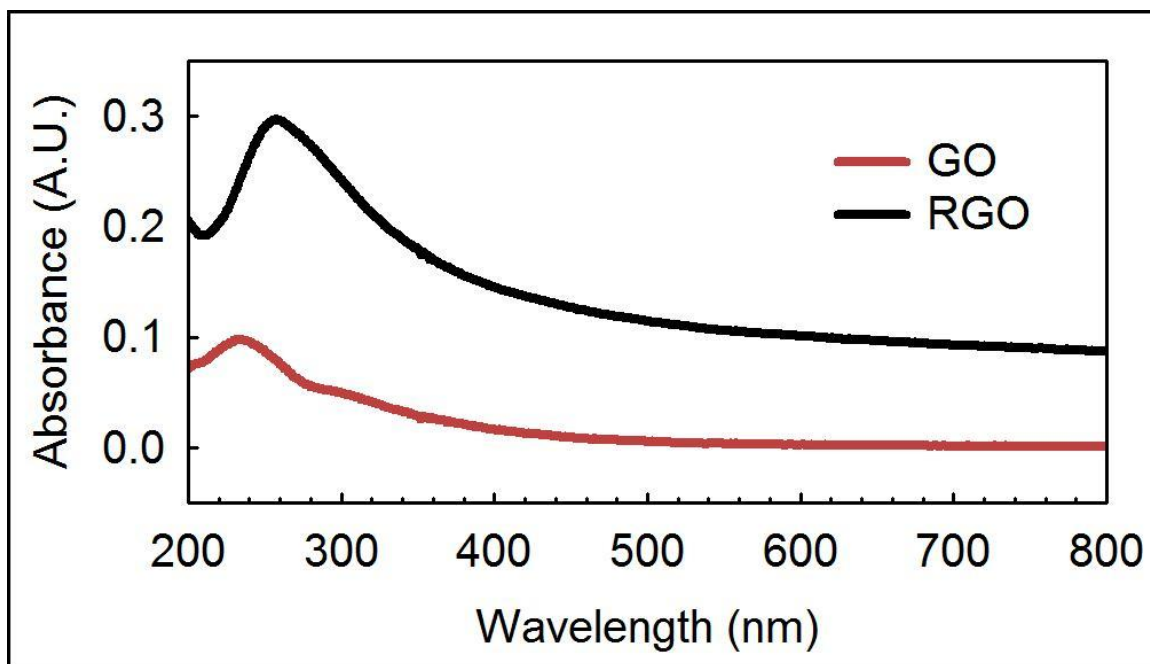
Figure 5.18. UV-vis spectrum of GO and RGO. Measurements were made using aqueous dispersions at concentrations of 0.002 mg/mL.

Deposition of PSI multilayer films on RGO or p-Si electrodes

PSI multilayer films were deposited onto electrodes using previously published methods.[26] Briefly, 50 μL of PSI solution (10^{-6} M) was placed on the surface of the electrode (0.283 cm^{-2} exposed area). In experiments using p-Si, the substrates were etched with 2% HF solution prior to deposition, as described in Chapter III. [CAUTION: *hydrogen fluoride is extremely corrosive and dangerous. Proper protective equipment and procedures should always be used*]. The system was then placed under vacuum until the film was dried. Experiments involving GO or RGO composites with PSI, aqueous solutions of PSI were mixed with various ratios of GO or RGO as indicated in the figure captions. RGO used in composite studies was generated using sodium ascorbate as described by Zhang and co-workers.[106] Briefly, highly concentrated graphene oxide

(graphene-supermarket.com) with an average flake size of 0.6-5 μm was diluted to a concentration of 0.1 mg/mL. The GO was then reduced using 5 mM ascorbic acid at 95°C for 30 minutes.

Electrochemical measurements

A CH Instruments CHI 660A electrochemical workstation equipped with a Faraday cage was used to perform photochronoamperometric and linear voltammetry measurements. EIS was performed using a Gamry Instruments CMS300 Impedance system. A custom built, three electrode cell was used to analyze the biohybrid electrodes. The biohybrid electrode was used as the working electrode, Ag/AgCl used as the reference electrode, and a platinum mesh used as the counter electrode.

EIS was performed using a 10 mV AC voltage over a frequency range of 10^{-2} to 10^5 Hz, with 10 points per decade recorded. Photochronoamperometric experiments were performed at the experimentally determined dark open circuit potential for each system. Linear voltammetry in **Figure 5.11** was performed from 1 V to -1 V vs. Ag/AgCl with a scan rate of 0.01 V/s.

Illumination for all electrochemical experiments was generated using a 250 W cold light source (Leica KL 2500 LCD) equipped with a 633 nm high pass filter, generating a light intensity of 0.19 W/cm^2. Comparison of this illumination with 1 sun illumination was performed using a Sciencetech SF150B solar simulator with AM1.5G filter (class A spectral match, class B non-uniformity). The lamp was calibrated to 1.00 full sun with an NREL certified silicon reference diode. Results using 1 sun demonstrated roughly a 15% decrease in photocurrent density when compared to the illumination generated by the 250 W cold light source.

CHAPTER VI

PHOTOREDUCTION OF CATALYTIC PLATINUM PARTICLES USING
IMMOBILIZED MULTILAYER FILMS OF PHOTOSYSTEM I[*]

Introduction

As described in Chapter I, one of the earliest applications of PSI in a non-biological role was to precipitate platinum to the stromal side of the protein via a previously reported mechanism.[107] Previous accounts have suggested that the source of the electrons for this reaction can be molecular hydrogen[16] or the irradiated PSI reaction center itself.[10] The extended lifetime of the excited electron at the F_B site of PSI[108] makes this location ideal for platinum photoreduction. Blankship and co-workers[109] have outlined an ideal semi-artificial device for H_2 bioproduction utilizing the photoreducing power of PSI. Recent publications have demonstrated the utility of platinum-PSI particles for hydrogen production,[12–14,110] enhanced photoactivity,[17] protein orientation,[107] and ordered multilayering capabilities.[111] However, in all of these methods the photoreduction of platinum occurs prior to or without immobilization of PSI. Our group[22–25] and others[46,49,112] have demonstrated that PSI can be immobilized on a substrate in a variety of ways while maintaining its functionality. In this chapter, we report the photoreduction of platinum onto a previously immobilized multilayer assembly of unmodified PSI from

---

spinach. Additionally, in order to demonstrate the catalytic ability[113,114] of these photoreduced platinum particles, the surface generation of H_2 was imaged using scanning electrochemical microscopy (SECM).

Results and Discussion

Platinum Reduction with a Sacrificial Electron Donor

Our group has previously demonstrated that thick multilayer films of PSI are capable of producing large photocurrents.[26] Here we demonstrate that these immobilized multilayer films of PSI can be used to photoreduce platinum salt to catalytic particles. Upon illumination, electrons are excited from the P700 reaction centers present in these films. Our results show that these electrons then reduce platinum from its original oxidation state (II or IV) to 0, producing a catalytic particle. It is important to note that the photoreduction of platinum was performed in an isolated chamber, while subsequent proton reduction to hydrogen gas was evaluated in an electrochemical cell after rinsing off any residual platinum salts. During the process of platinum photoreduction, electrons are reintroduced to the P700 reaction center by a sacrificial electron donor (sodium ascorbate). Interestingly, multilayers of PSI are capable of photoreducing platinum (IV) to platinum (0) without a sacrificial electron donor (see next section of this chapter). Though less platinum (0) is produced due to the limited number of electrons present in the film, these data suggest that electrons from proteins within the thick PSI film can be transferred to surrounding PSI molecules until they reach the surface of the film, at which point the electrons are used in the reduction of platinum. This provides further information for understanding why higher photocurrents are observed with increasing

93

thickness of PSI films,[26] as the electrons could be passed from the F_B^- site of one protein to the P700$^+$ site of another protein. In order to enhance and optimize the ability to produce photogenerated platinum particles that have catalytic characteristics, all the experiments described in this section used the sacrificial electron donor sodium ascorbate during the photoreduction of platinum salts on protein films.

In order to optimize the amount of time light was exposed to the protein film in the presence of the platinum salt solution, photochronoamperometric measurements in acidic buffer were utilized to analyze the photoreduction of protons at the biohybrid electrode. Photoreduction of platinum salt for 2 hrs was determined to provide the highest amount of hydrogen production as seen by the resulting reductive photocurrent (**Figure 6.1A**). Photoreduction of the platinum salt beyond this time frame resulted in a decrease in the measured photocurrent; however XPS analysis demonstrated that platinum salt continued to be photoreduced beyond 2 hrs of illumination (**Figure 6.1B**). The 4f doublet observed at 71.5 eV and 74.5 eV in the XPS spectrum corresponds to photoreduced platinum.[115] The binding energies are shifted from those expected for either Pt^{II} or Pt^{IV}, as evidenced by experiments performed without a sacrificial electron donor in the next section. The small peaks present for the sample exposed to 0 min of illumination is likely due to residual platinum salt that was reduced by the ambient light in the lab, and thus provides a good baseline measurement to evaluate the other samples. Because multilayers films of PSI have been shown to remain active for at least 280 days,[25] we attribute the decrease in proton reduction for illumination times greater than 2 hrs to a shadowing effect. As the platinum photoreduces on the surface of the protein, it begins to shadow the protein, limiting the amount of light that can be absorbed by the protein film.
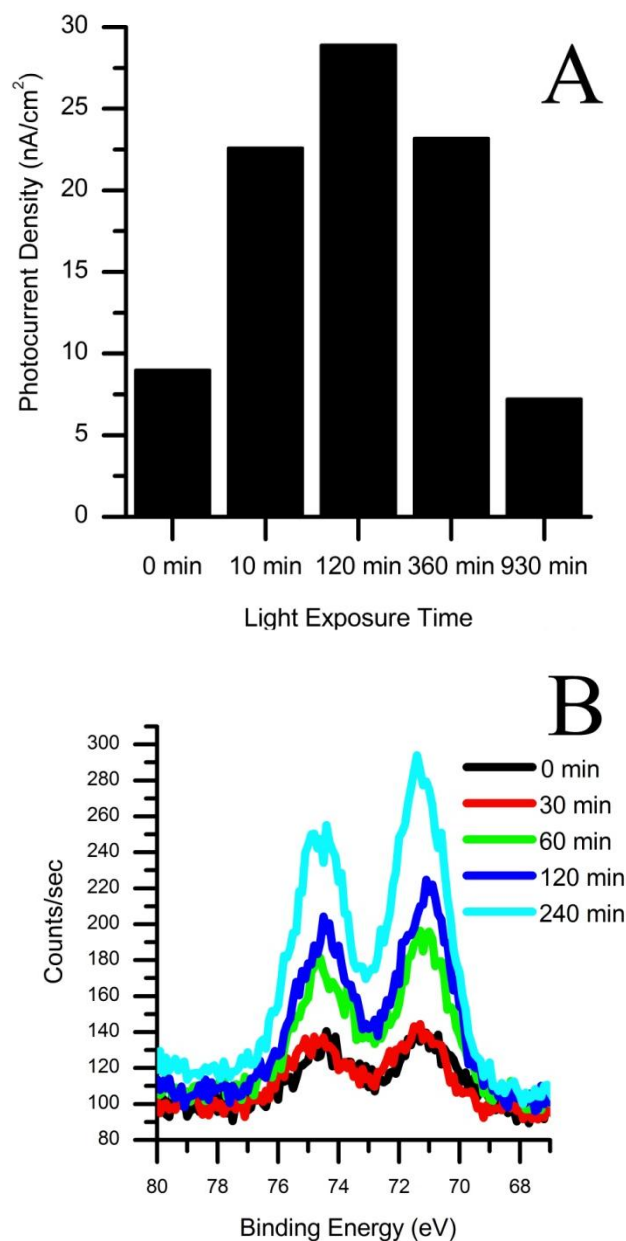
Figure 6.1. Optimization of the photoreduction of platinum onto PSI films (3 deposition steps with a film thickness of approximately 700 nm). A) Photochronoamperometric substrate reduction of protons measured for samples that underwent platinum photoreduction for various lengths of time. Values indicate the change in current following illumination from red light in a pH 4 buffered solution. The working electrode (sample) was set at the open circuit potential (~0.2 V vs. Ag/AgCl) for these measurements. B) XPS analysis of platinum that has been photoreduced on multilayer films of PSI for various lengths of time. Notice that the distinctive platinum 4f doublet increases in intensity with increasing light exposure time.

In order to gain a greater understanding of the size of the platinum particles present on the surface, SEM and EDX analyses were performed (**Figure 6.2**). As seen in the images, platinum particles are scattered over the surface of the sample (**Figure 6.2A**). Performing EDX directly on one of these particles revealed a strong platinum signal (**Figure 6.2C**). The presence of various sized platinum regions would indicate that the photoreduction begins with a small nucleation event, presumably at the F_B^- site, which then allows for larger platinum regions to form as electrons are continually fed to the platinum particles by the protein complexes. This method of particle growth is supported by the fact that smaller platinum particles are observed when photoreduction occurs in solution.[12] Furthermore, the darker regions of the SEM image produce a platinum signal under EDX analysis, however the signal is greatly reduced in comparison to the bright areas in the image suggesting the presence of smaller platinum particles. The ability for particle growth to larger sizes appears specific to this immobilized PSI photoreduction technique.
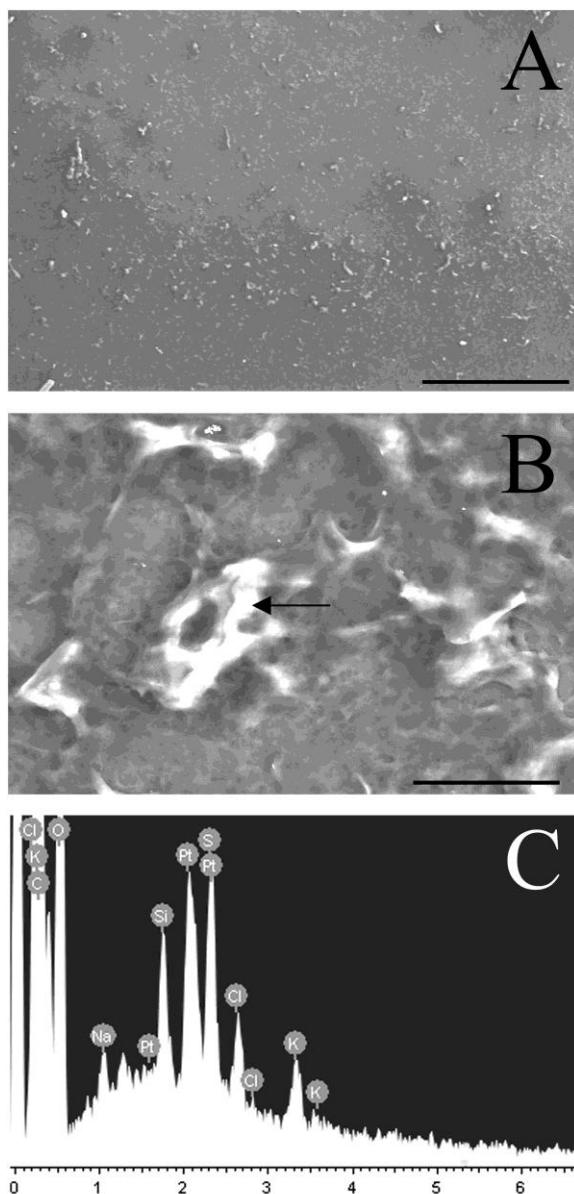
Figure 6.2. SEM and EDX analysis of an optimized sample. Images were collected with an accelerating voltage of 20 kV A) SEM image demonstrating both the abundance and various sizes of platinum particles that have been photoreduced for 2 hrs onto the surface of PSI multilayer films that were previously immobilized on a silicon substrate (scale bar 750 µm). B) SEM image depicting the geometry and size of platinum particles (scale bar 49.5 µm). C) EDX performed at the point indicated by the arrow in Figure 2B with an accelerating voltage of 20 kV and an emission current of 20 µA.

SECM experiments were then performed to demonstrate the catalytic ability of the photoreduced platinum present on the biohybrid electrode. A SECM image was

collected using an ultramicroelectrode (UME) close to the substrate surface in order to electrochemically image individual platinum particles (**Figure 6.3**). To generate the image, the UME was rastered above the biohybrid working electrode in an acidic buffer. When the tip comes in close proximity to an area producing hydrogen, a feedback loop is produced between the tip and substrate electrode, resulting in "hot-spots" of catalytic activity that can be observed as increases of current. From the image seen in **Figure 6.3** it is obvious that there are large areas of increased current present on the surface of the protein film that correspond well with the size of platinum particles observed in the SEM images. "Tails" can be observed following each of these platinum particles due to scan direction of the tip.[116] These "tails" are caused by the diffusion of electrochemical products away from the catalytic particles, enabling the feedback loop to continue beyond the physical dimensions of the particles themselves.
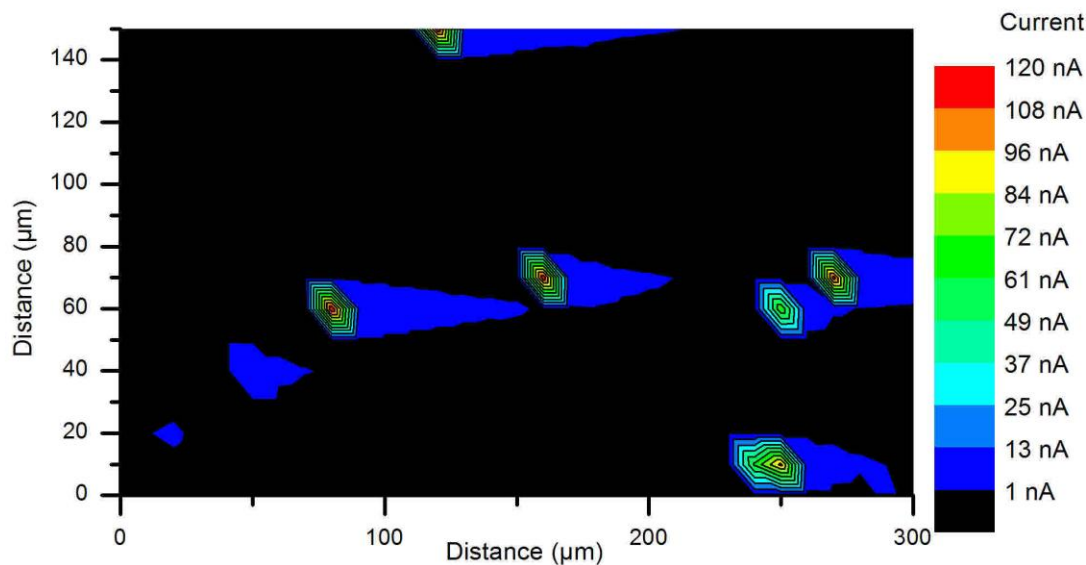
Figure 6.3. SECM analysis of catalytic platinum particles on a PSI film. Tip image produced using a 25 µm platinum UME as the tip electrode, a gold electrode modified with three multilayer films of PSI and photoreduced platinum particles (platinum salt photoreduced for 2 hrs) as the substrate electrode, and a pH 4 mediator solution containing 100 mM KCl as a supporting electrolyte. Green to red areas indicate "hot spots" generated by the electrochemical feedback loop between the tip electrode and the catalytic platinum particles present on the surface of the protein film. The blue "tails" are caused by the diffusion of electrochemical products away from the catalytic particles and follow the scan direction of the tip electrode.

Platinum Reduction without a Sacrificial Electron Donor

In this section we photoreduced platinum onto an immobilized multilayer film of PSI without the use of a sacrificial electron donor. In order to confirm the addition of each component of the system, profilometry and XPS analyses were performed at each stage of the process (**Figure 6.4**). A non-statistically significant increase in the root mean squared (RMS) roughness of the sample was observed upon the SAM modification of the gold substrate which is to be expected given the sensitivity of the profilometer. Following three vacuum deposition steps of PSI, the RMS roughness of the sample increased to ~30 nm. Following the photoreduction of platinum, the RMS roughness increased to ~85 nm.

This dramatic increase in roughness suggests that the platinum particles are both large and rest on the surface of the PSI film rather than being confined within the pocket of the individual protein complexes. XPS was then performed to both confirm the presence of unique bonds and elements as well as determine the ratio of carbon or platinum to gold. Upon addition of PSI layers, the carbon to gold ratio increased in accordance with the number of layers added to the substrate in a linear fashion. The addition of PSI also brought about a shoulder on the carbon peak and the appearance of a nitrogen peak (**Figure 6.5A**). Both of these can be attributed to the large concentration of both nitrogen and various carbon bonds present in the amino acids that make up the protein complex. After the photoreduction of platinum, a distinctive shift in the platinum doublet (4f) was observed (**Figure 6.5B**). This indicates that the platinum has undergone a photoreduction process. Fitting the platinum doublet using XPS software enabled the observation that the photoreduced platinum is present in both the II and 0 oxidation states. The presence of Pt (II) suggests that some of the Pt (IV) was only partially reduced during the photoreduction process. We attribute this observation to the lack of sacrificial electron donor. Thus, once all the electrons present in the multilayer film have been used, the platinum salt can no longer be photoreduced. While minimal platinum signaling was observed in the control samples, software analysis of the peaks indicates that no Pt (0) was present. Additionally, the platinum to gold ratio increased according to the number of PSI layers present, with a significantly larger increase once 3 deposition steps were used (**Figure 6.4**).
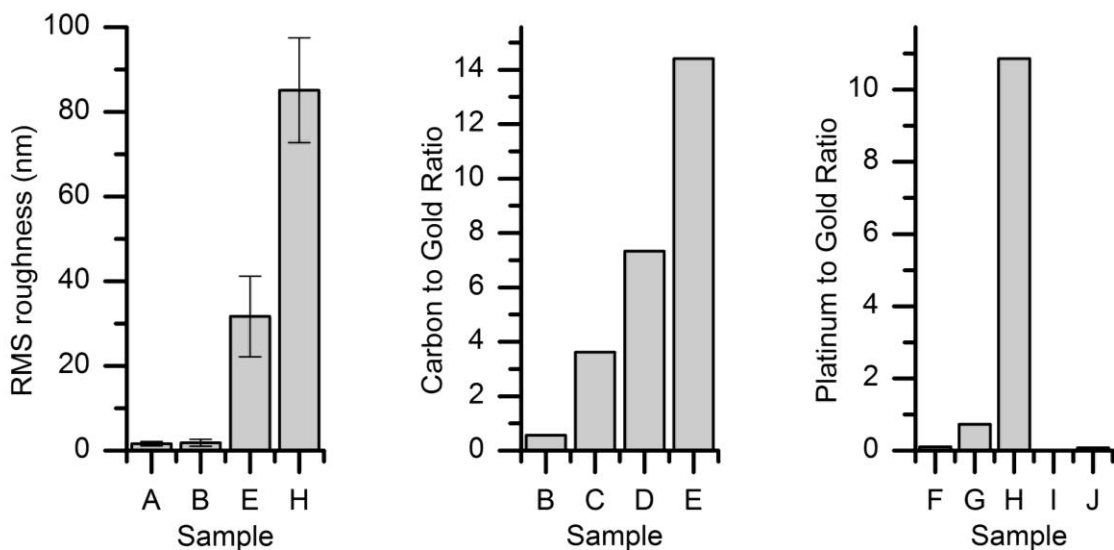
Figure 6.4. Profilometry and XPS of samples prepared without a sacrificial electron donor. Profilometry (left) and XPS (middle and right) of samples A-J. A: Bare Au substrate, B: SAM-modified Au substrate, C: 1-step multilayer film of PSI, D: 2-step multilayer film of PSI, E: 3-step multilayer film of PSI, F: Photoreduced Pt onto 1-step multilayer film of PSI, G: Photoreduced Pt onto 2-step multilayer film of PSI, H: Photoreduced Pt onto 3-step multilayer film of PSI, I: 3-step multilayer film exposed to Pt solution but not light, J: Photoreduced Pt on SAM modified Au substrate.
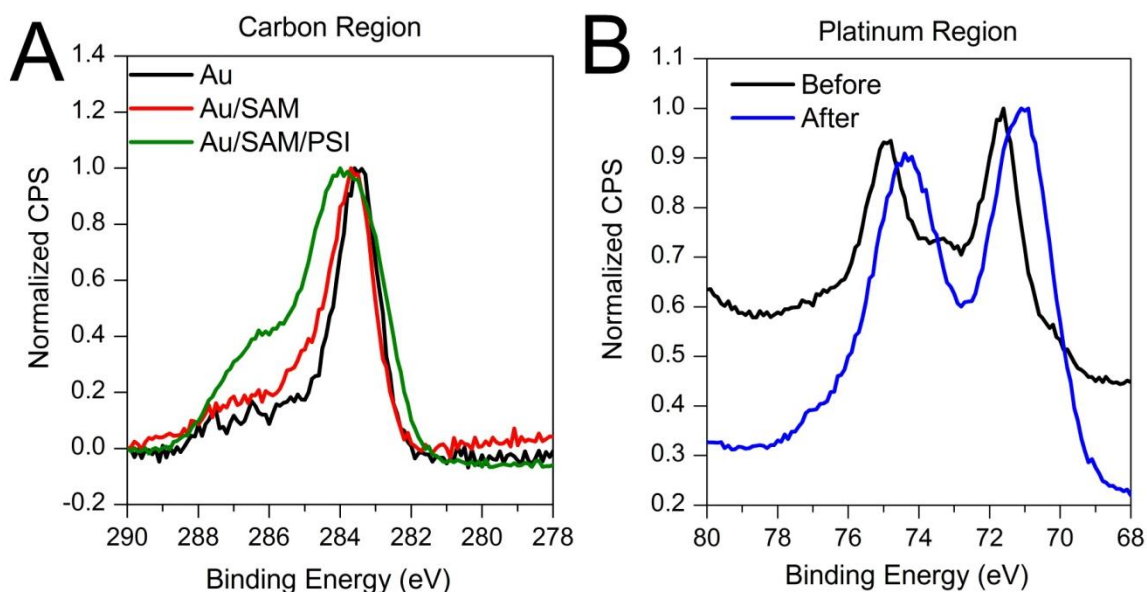
Figure 6.5. XPS of carbon and platinum regions. A) Normalized XPS spectra of the carbon region. B) Normalized XPS spectra of the platinum region before (black) and after (blue) photoreduction with PSI film.

In order to gain a greater understanding of the size of the platinum particles present on the surface, SEM and EDX analyses were performed (**Figure 6.6**). The SEM images show the platinum particles scattered over the surface of the substrate (**Figure 6.6A**). Performing EDX directly on one of these particles revealed a platinum peak (**Figure 6.6C**), while the same analysis performed just beside the particle did not contain any platinum (**Figure 6.6D**). This analysis allowed the characterization of particles in the size range of 1-5 µm. The large size of these particles is in good agreement with the profilometry measurements. Smaller bright spots were also present in the SEM images; however EDX analysis could not confirm the presence of platinum on these smaller spots due to the large background signal generated by the gold substrate. Additionally, the particles produced with a sacrificial electron donor were significantly larger (>20 µm) than those observed by this method.
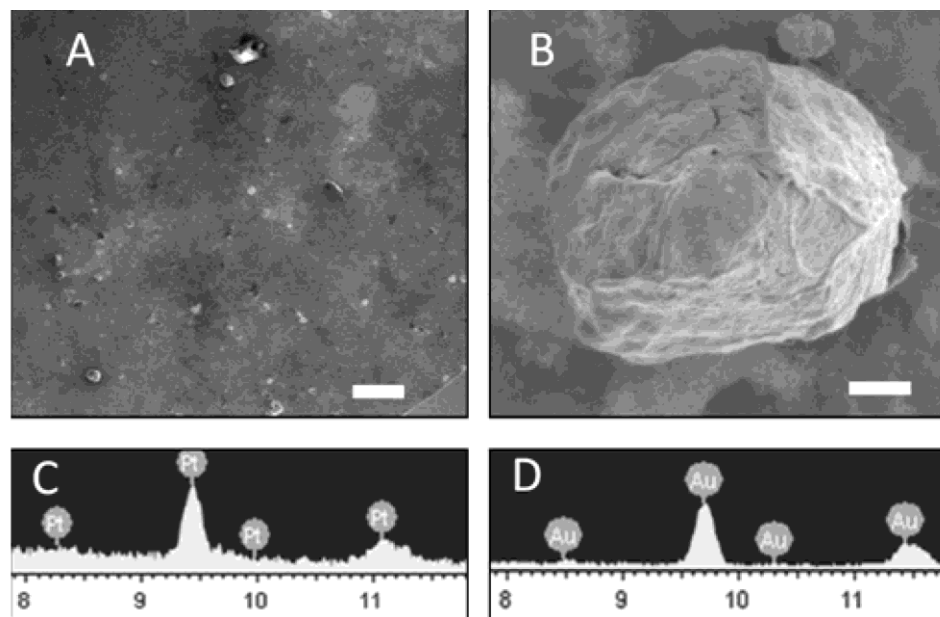
Figure 6.6. SEM and EDX of samples prepared without sacrificial electron donor. A SAM-modified gold substrate that was further modified by a 3-step multilayer film of PSI that was used to photoreduce platinum without the use of a sacrificial electron donor. **A.** SEM image demonstrates large number of platinum particles present on the PSI surface (scale bar: 50 μm). **B.** Magnified SEM picture of a single platinum particle (scale bar: 1 μm). **C.** EDX analysis performed directly on the platinum particle. **D.** EDX analysis performed adjacent to the same particle. The EDX used an accelerating voltage of 20 kV and emission current of 20 μA.

SECM experiments were then performed to electrochemically image the photoreduced platinum particles present on the biohybrid electrode. The red to green "hot spots" seen in **Figure 6.7**, demonstrate the location of the platinum particles and the ability for these particles to act as catalytic sites. The image is in good agreement with the SEM experiments that suggest the particles are present and distributed in various sizes and clusters. The particles are much smaller and less active than those produced in the presence of a sacrificial electron donor (**Figure 6.3**). It should be noted that no electrochemical "tails" were observed, most likely caused by the reduced step size and smaller tip electrode size used to generate this image.

103
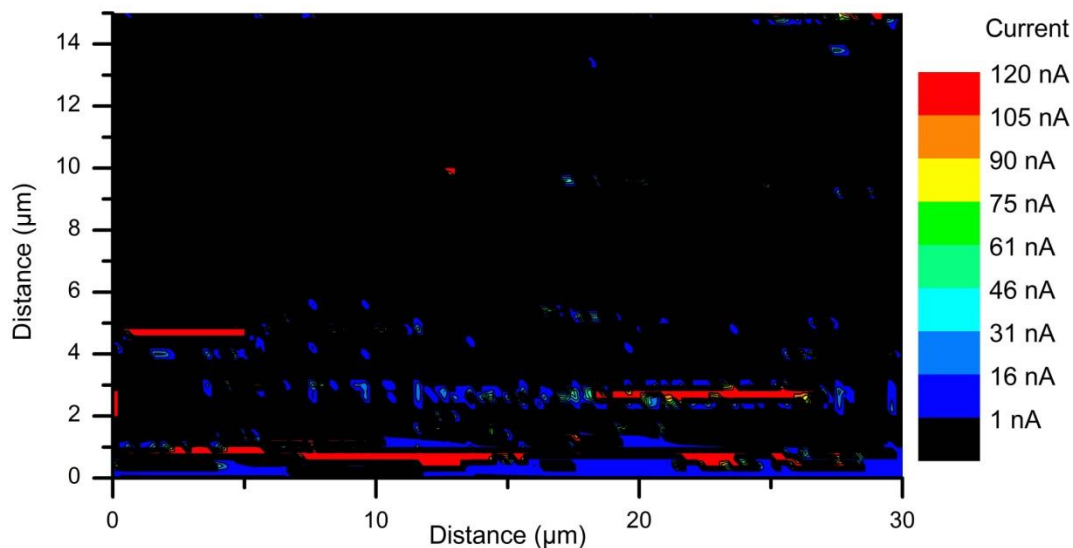
Figure 6.7. SECM image of a sample prepared without sacrificial electron donor.
The SECM image of the catalytic behavior of the platinum particles to produce H_2 gas
from protons present in the solution. Areas in green to red indicate "hot spots" where
there is an increase in catalytic activity. A 2 μm platinum microelectrode was used as the
tip electrode and the platinized PSI-gold sample as the substrate electrode. The image
was taken in a 100 mM KCl solution adjusted to a pH of 1.5 using HCl. The tip and
substrate potentials were set to 0.2 V and -0.8 V, respectively (all potentials vs.
Ag/AgCl). A step size of 0.2 μm was used while the tip was held close to the average
substrate surface.

Conclusion

Platinum particles have successfully been photoreduced onto the surface of PSI

that had been pre-immobilized onto either a gold or silicon substrate. There was found to

be a balance between the amount of photoreduced platinum and the amount of hydrogen

production possible. To the best of our knowledge, this is the first report of imaging the

catalytic activity of photoreduced platinum particles on the surface of a photoactive

protein film using SECM. The size of these catalytic particles is much larger than

previously reported particles photoreduced in PSI solution.[10,12,16] Our results provide an

increased understanding of these biohybrid catalysts that may be later employed for

enhanced utility of these systems in current and future applications. Because the

multilayer protein film can be immobilized on any substrate of choice, this method can be easily modified for incorporation into functional devices. Additional advances in the production of hydrogen using this process may be met by employing the concepts developed in previous chapters with the photoreduced platinum particles demonstrated in this chapter.

Experimental

Materials

Substrates for electrochemical measurements were prepared by thermally depositing ~125 nm of gold onto a silicon support (Montico Silicon, <100> orientation). Unmodified silicon supports were used for some of the non-electrochemical measurements. 50 mM buffered solutions of either potassium biphthalate (pH 4) or potassium phosphate monobasic-sodium hydroxide (pH 7) were purchased from Fisher Scientific. 2-Aminoethanethiol was purchased from Sigma as were sodium hexachloroplatinate (IV) hexahydrate and potassium tetrachloroplatinate (II). Triton X-100 and L-ascorbic acid sodium salt were purchased from Acros. Dialysis was performed using 10 000 MWCO dialysis tubing (Spectrapore).

Photosystem I extraction

Photosystem I complexes were extracted from commercially available baby spinach as previously described.[25] Briefly, thylakoid membranes were separated from the spinach leaves via maceration and subsequent centrifugation following the method of Reeves and co-workers[34] with adaptations.[67] The PSI complex was then removed *via* additional centrifugation and purified using a chilled hydroxylapatite column.[36] The

concentration of surfactant and salt in the resulting effluent was then reduced using dialysis.[26] The concentration of the resulting PSI solution used consisted of 3.7×10^{-5} M chlorophyll, with a chlorophyll a/b ratio of 3.0, and 9.4×10^{-7} M P700 as characterized by the methods of Porra[68] and Baba and co-workers[36] respectively.

Multilayer formation and platinum photoreduction

PSI multilayer films were prepared on either an unmodified silicon substrate or a gold substrate that was modified via immersion in a solution of 2-aminoethanethiol (2 mM) to increase the hydrophilicity of the gold. The extracted PSI solution was placed on the substrate and vacuumed to dryness. This vacuum deposition process was repeated 3 times in order to generate thick multilayer films of PSI with thickness of approximately 1 μm.[26] To photoreduce platinum onto the protein, the dried substrate was immersed in a solution of either 2 mM sodium hexachloroplatinate (IV) hexahydrate or 2 mM potassium tetrachloroplatinate (II), and 50 mM phosphate buffer at a pH of 7. For experiments using a sacrificial electron donor, 8 mM sodium ascorbate was added. The substrates in solution were illuminated for 2 hrs unless otherwise indicated using a Fiber-Lite Fiber Optic Illuminator (Model 190, Dolan-Jenner Industries). The resulting assemblies were rinsed with DI water and dried with N_2 gas before further analysis.

Instruments and Equipment

Electrochemical measurements were performed using a CH Instruments CHI 660a electrochemical workstation equipped with a Faraday cage. A custom built, three electrode cell was used where the modified gold sample was set as the working electrode, platinum mesh as the counter electrode, and Ag/AgCl as the reference electrode. An aqueous solution of potassium biphthalate buffer (50 mM) at a pH of 4 was used as the

mediator. Illumination for photochronoamperometric measurements was provided by a 250 W cold light source (Leica KL 2500 LCD).

X-ray Photoelectron Spectroscopy (XPS) was performed on a Physical Electronics PHI 5000 VersaProbe spectrometer equipped with a monochromatized Al Kα X-ray source (1486.6 eV). Samples were analyzed with an incident angle of 45°. All peaks were referenced to the Au $4f_{7/2}$ peak at 84.0 eV. XPS data analyses were performed using CasaXPS software with Gaussian-Lorentzian profiles using a Shirley background.

Scanning Electron Microscopy (SEM) and Energy Dispersive X-ray spectroscopy (EDX) analyses were performed on a Hitachi S-4200 instrument. SEM images were collected with an accelerating voltage of 20 kV. EDX analyses were performed using an accelerating voltage of 20 kV and an emission current of 20 μA.

Scanning Electrochemical Microscopy (SECM) experiments were performed on a CH Instruments CHI 900 electrochemical workstation. For the image presented in **Figure 6.3**, a 25 μm platinum microelectrode was used as the tip electrode and a platinized PSI-gold sample (2 hrs photoreduction time with sacrificial electron donor) as the substrate electrode. A 100 mM KCl solution adjusted to a pH of 4 using HCl was used as the mediator solution. The tip and substrate potential were set at their respective open circuit potential values. A step size of 10 μm was used with the tip brought near the substrate electrode using a feedback approach curve technique. For the image presented in **Figure 6.6**, a 2 μm platinum microelectrode was used as the tip electrode and the platinized PSI-gold sample described previously as the substrate electrode. The image was taken in a 100 mM KCl solution adjusted to a pH of 1.5 using HCl. The tip and substrate potentials

were set to 0.2 V and -0.8 V, respectively (all potentials vs. Ag/AgCl). A step size of 0.2

μm was used while the tip was held close to the average substrate surface.

CHAPTER VII

CONCLUSIONS AND FUTURE SUGGESTIONS[*]

Summary

In this thesis we have demonstrated the effect of integrating PSI with various electrochemical materials. In Chapters I and II, we introduced the history of PSI biohybrid electrodes and the methods by which we can examine these materials experimentally. Importantly, we found that the electrochemical mediator used in these photoelectrochemical cells can have a significant impact on both the photocurrent density and the direction of electron flow.[29]

In Chapter III we described the impact of using a semiconducting substrate.[27] Using doped silicon, we could control the direction of the electron flow through the system. Because of the unique band alignment between silicon and the active sites of PSI, p-doped silicon could efficiently pass electrons onto the $P700^+$ site in PSI. The band gap of the silicon, which is larger than the charge separation value of PSI, prevented photoexcited electrons from flowing back to the silicon. This meant the random organization of the PSI film has less of an impact than it does on metal electrodes that can both donate and accept electrons from PSI.[66] The result of this study culminated in

---

[*] Portions of this chapter have previously been prepared: LeBlanc, G.; Gizzie, E. A.; Yang, S.; Cliffel, D. E.; Jennings, G. K. Photosystem I Protein Films at Electrode Surfaces for Solar Energy Conversion. *Langmuir* **2014** submitted.

the highest reported photocurrent density for a biohybrid electrode based on PSI (**Figure 1.2**).

Chapter IV built off our findings with silicon and describes our efforts towards a solid-state solar cell using ZnO as the counter electrode. The band alignment of ZnO is ideal for accepting electrons from the F_B site of PSI. Unfortunately, there are a number of challenges associated with depositing a crystalline ZnO film on the surface of a biological material. We address these issues through the use of electrochemical deposition[80] and a novel deposition method known as CPCD.[79] While both of these methods were capable of generating ZnO films on the surface of PSI, we determined CPCD to be the better process. In a proof-of-concept experiment, we demonstrated how CPCD could be used to generate a functioning solid-state solar cell based on PSI.

In Chapter V we discussed our results of integrating PSI with graphene,[30] reduced graphene oxide (RGO), and graphene oxide (GO).[31] These relatively new 2-D materials provide an exciting platform for next-generation solar conversion devices. Studies with pristine, mechanically exfoliated graphene provided a 5-fold enhancement when PSI was added to the FET device. Using CVD graphene, we generated a photoactive electrode with a thickness of 10 nm and produced photocurrents with values up to 0.5 $\mu A/cm^2$. With RGO, we could use multilayer films of PSI to dramatically increase the photocurrent density to 5 $\mu A/cm^2$. The transparent nature of both CVD graphene and RGO enabled the use of opaque redox mediator, as illumination could be performed through the biohybrid electrode. Finally, we discussed how GO and RGO could be added

to the PSI film to improve the photocurrent production of PSI-modified p-doped silicon up to 150 μA/cm^2.

In Chapter VI we described the ability for PSI films to photoreduce catalytic platinum particles.[32] Using multilayer films of PSI to perform the photoreduction process enabled the production of much larger platinum particles than previously reported in solution.[12] After optimization, we were able to generate the first electrochemical images of the photocatalytic hydrogen production from a biohybrid electrode based on PSI. Furthermore, the ability to perform the photoreduction of platinum without the use of a sacrificial electron donor provided new insights on the electron transfer process within the thick, multilayer PSI film.

Perspectives and Future Suggestions

While the photocurrent density for systems based on PSI continues to increase (**Figure 1.2**), the ability to generate photocurrents on the same scale of current photovoltaic materials is still necessary. This will require the generation of ~10mA/cm^2 or more using standard 1 sun illumination (a 10-fold improvement over our best performing systems). Furthermore, the ability to generate greater photovoltages will be necessary to improve the overall power generation of biohybrid electrodes based on PSI. Recent advances by both our research group at Vanderbilt and elsewhere provide exciting opportunities and ideas to achieve these goals in the near future.

Looking at methods that have previously increased photocurrent production in PSI, increasing the surface area of the electrode material is a simple yet effective

technique.[24] By changing from a planar gold electrode to a highly porous gold electrode, photocurrent densities improved by 3-4 times. Applying this concept to the semiconducting electrodes described in Chapters III and IV could provide similar improvements. Because the generation of porous silicon is well understood,[117] the methods for producing various pore sizes and configurations will be straightforward, enabling a systematic study. Interestingly, by making silicon highly porous, the band structure of the electrode changes and makes the electrode more transparent to visible light.[118] This means that the electrochemical system may need to be altered in order to retain the electron transfer potential between the silicon electrode and the PSI film. The alterations could come in the form of silicon doping types or densities, or by using different electrochemical mediators to force the semiconductor's electron bands to bend appropriately.[56]

Using a complete photoelectrochemical cell, Ciesielski and co-workers found that the diffusion of the electrochemical mediator to and from the biohybrid electrode has a significant impact on the photocurrent production of the system.[25] This effect was further demonstrated by our more recent studies focused on the effect of mediator concentration.[27,29,30] While increasing the concentration of the redox mediator in solution will provide enhancement to a certain extent, this approach will always be limited by the solubility of the mediator. A different approach would be to make a solid-state system like the one we described in Chapter IV. Problems with our system, however, were primarily caused by the rough PSI film that is produced during multilayer film formation. Smoother films of PSI that still retain significant light absorption properties can be achieved through the use of electrochemical polymerization techniques. In a proof-of-

concept study by Gizzie and co-workers, PSI was embedded into a poly-aniline matrix using an electrochemical deposition procedure.[59] This process quickly generated a smooth film that could be controlled by deposition time, PSI concentration, and aniline concentration. Other methods may include the use of polymer redox molecules, such as the polyviologens described in Chapter III, which can efficiently shuttle electrons to and from the PSI film. These polymers could either be deposited on-top of the PSI film or embedded within the PSI film.

Finally, while the use of semiconducting electrodes has eliminated the back-flow of electrons that reduce the photocurrent production in our unorganized PSI films, the ability to orient the PSI molecules with respect to the electrode and to other PSI complexes should further improve the photocurrent and photovoltage.[66] Of particular interest is a recent study by Toporik and co-workers.[119] By crystallizing PSI complexes, the researchers presumably forced the proteins to self-align. Using Kelvin probe force microscopy (KPFM) on individual crystals, the researchers were able to generate photovoltages up to 45 V at 1 W/cm^2 and internal electric fields as large as 100 kV/cm^{-1}. These values exceed any reported inorganic material system and provide insight into the power of orienting PSI complexes with respect to one another. By developing methods to orient PSI across an entire electrode, rather than single crystals, could lead to major advances in the performance of biohybrid electrodes.

Conclusions

PSI, a naturally abundant and highly efficient photoactive protein complex, is testament to the type of optimization that nature is capable over through the process of

113

evolution. Nature, however, optimized the PSI to be integrated within the process of photosynthesis, with the ultimate goal of generating carbohydrate molecules. Thus, while the individual components of the photosynthesis process are incredibly efficient, the number of steps involved causes the system to be relatively inefficient (1-5% overall efficiency). This is the fundamental problem with the concept of biofuels. By using the most efficient material that plants produce (PSI) in a setting that reuses its photoactive charge separation power, we hope to improve the energy conversion efficiencies that are possible.

In this thesis we have described the recent advances in the field of biohybrid electrodes based on PSI. By simply changing the electrode and electrochemical system that PSI interacts with, we can provide more ideal systems for the electron flow through this system. Looking to the future, we anticipate that the development of these biohybrid technologies will focus on optimally designed materials to interface with PSI to produce robust systems with synergistic properties, as well as the facile assembly of PSI to achieve highly oriented and organized thin films. The selection of electrodes, mediators, and composite matrices with optimal properties (Fermi levels, formal potentials, selective conductivities, etc.) for the seamless integration with PSI are required to continue the trend of exponential performance improvements over the next few years. Special attention should be focused on the development of both solid-state and wet-based biohybrid composite materials with good long-term stabilities, expanding well beyond the > 280 day activity that we have demonstrated for PSI films in a cell.[25] Further efforts to capitalize on the dramatic improvements observed when PSI can be organized are currently underway in a number of research groups around the world. Building on the

past 30 years of interfacing PSI with electrode surfaces, our research team and others seek to preserve our natural resources by employing the abundant materials that nature has engineered.

REFERENCES

1. Hall, D.; Rao, K. *Photosynthesis*; 6th ed.; Cambridge University Press: Cambridge, 1999.

2. Lovins, A. *Winning the Oil Endgame: Innovation for Profits, Jobs and Security*; Rocky Mountian Institute, 2004.

3. Foster, R.; Ghassemi, M.; Cota, A. *Solar Energy: Renewable Energy and the Environment*; CRC Press, 2009; p. 382.

4. Becquerel, A. Recherche Sur Les Effets de La Radiation Chimique de La Lumière Solaire Au Moyen de Courant Électrique. *Comptes rendus l'Académie des Sci.* **1839**, *9*, 145–149.

5. Golbeck, J. *Photosystem I: The Light-Driven Plastocyanin: Ferredoxin Oxidoreductase*; Springer: Urbana, 2006; Vol. 24, p. 764.

6. Hogewoning, S. W.; Wientjes, E.; Douwstra, P.; Trouwborst, G.; van, I. W.; Croce, R.; Harbinson, J. Photosynthetic Quantum Yield Dynamics: From Photosystems to Leaves. *Plant Cell* **2012**, *24*, 1921–1935.

7. Amunts, A.; Drory, O.; Nelson, N. The Structure of a Plant Photosystem I Supercomplex at 3.4Å Resolution. *Nature* **2007**, *447*, 58–63.

8. Ciesielski, P. Photosystem I–Based Systems for Photoelectrochemical Energy Conversion, Vanderbilt University, 2010.

9. Badura, A.; Kothe, T.; Schuhmann, W.; Rogner, M. Wiring Photosynthetic Enzymes to Electrodes. *Energy Environ. Sci.* **2011**, *4*, 3263–3274.

10. Greenbaum, E. Platinized Chloroplasts: a Novel Photocatalytic Material. *Science.* **1985**, *230*, 1373–1375.

11. Greenbaum, E. Photobioelectronic Studies with Thylakoid Membranes. *Appl. Biochem. Biotechnol.* **1989**, *20-21*, 813–824.

12. Iwuchukwu, I. J.; Vaughn, M.; Myers, N.; O'Neill, H.; Frymier, P.; Bruce, B. D. Self-Organized Photosynthetic Nanoparticle for Cell-Free Hydrogen Production. *Nat. Nanotechnol.* **2010**, *5*, 73–9.

13. Evans, B. R.; O'Neill, H. M.; Hutchens, S. A.; Bruce, B. D.; Greenbaum, E. Enhanced Photocatalytic Hydrogen Evolution by Covalent Attachment of Plastocyanin to Photosystem I. *Nano Lett.* **2004**, *4*, 1815–1819.

14. Utschig, L. M.; Dimitrijevic, N. M.; Poluektov, O. G.; Chemerisov, S. D.; Mulfort, K. L.; Tiede, D. M. Photocatalytic Hydrogen Production from Noncovalent Biohybrid Photosystem I/Pt Nanoparticle Complexes. *J. Phys. Chem. Lett.* **2011**, *2*, 236–241.

15. Krassen, H.; Schwarze, A.; Friedrich, B.; Ataka, K. Photosynthetic Hydrogen Production by a Hybrid Complex of Photosystem I and Hydrogenase. *ACS Nano* **2009**, *3*, 4055–4061.

16. Lee, J. W.; Lee, I.; Greenbaum, E. Platinization: a Novel Technique to Anchor Photosystem I Reaction Centers onto a Metal Surface at Biological Temperature and pH. *Biosens. Bioelectron.* **1996**, *11*, 375–387.

17. Frolov, L.; Wilner, O.; Carmeli, C.; Carmeli, I. Fabrication of Oriented Multilayers of Photosystem I Proteins on Solid Surfaces by Auto-Metallization. *Adv. Mater.* **2008**, *20*, 263–266.

18. Lee, I.; Lee, J. W.; Greenbaum, E. Biomolecular Electronics: Vectorial Arrays of Photosynthetic Reaction Centers. *Phys. Rev. Lett.* **1997**, *79*, 3294–3297.

19. Munge, B.; Das, S.; Ilagan, R.; Pendon, Z.; Yang, J.; Frank, H. A.; Rusling, J. F. Electron Transfer Reactions of Redox Cofactors in Spinach Photosystem I Reaction Center Protein in Lipid Films on Electrodes. *J. Am. Chem. Soc.* **2003**, *125*, 12457–12463.

20. Kievit, O.; Brudvig, G. W. Direct Electrochemistry of Photosystem I. *J. Electroanal. Chem.* **2001**, *497*, 139–149.

21. Das, R.; Kiley, P. J.; Segal, M.; Norville, J.; Yu, A. A.; Wang, L. Y.; Trammell, S. A.; Reddick, L. E.; Kumar, R.; Stellacci, F.; *et al.* Integration of Photosynthetic Protein Molecular Complexes in Solid-State Electronic Devices. *Nano Lett.* **2004**, *4*, 1079–1083.

22. Ciobanu, M.; Kincaid, H. A.; Lo, V.; Dukes, A. D.; Jennings, G. K.; Cliffel, D. E. Electrochemistry and Photoelectrochemistry of Photosystem I Adsorbed on Hydroxyl-Terminated Monolayers. *J. Electroanal. Chem.* **2007**, *599*, 72–78.

23. Faulkner, C. J.; Lees, S.; Ciesielski, P. N.; Cliffel, D. E.; Jennings, G. K. Rapid Assembly of Photosystem I Monolayers on Gold Electrodes. *Langmuir* **2008**, *24*, 8409–8412.

24. Ciesielski, P. N.; Scott, A. M.; Faulkner, C. J.; Berron, B. J.; Cliffel, D. E.; Jennings, G. K. Functionalized Nanoporous Gold Leaf Electrode Films for the Immobilization of Photosystem I. *ACS Nano* **2008**, *2*, 2465–2472.

25. Ciesielski, P. N.; Hijazi, F. M.; Scott, A. M.; Faulkner, C. J.; Beard, L.; Emmett, K.; Rosenthal, S. J.; Cliffel, D.; Jennings, G. K. Photosystem I - Based Biohybrid Photoelectrochemical Cells. *Bioresour. Technol.* **2010**, *101*, 3047–3053.

26. Ciesielski, P. N.; Faulkner, C. J.; Irwin, M. T.; Gregory, J. M.; Tolk, N. H.; Cliffel, D. E.; Jennings, G. K. Enhanced Photocurrent Production by Photosystem I Multilayer Assemblies. *Adv. Funct. Mater.* **2010**, *20*, 4048–4054.

27. LeBlanc, G.; Chen, G.; Gizzie, E. A.; Jennings, G. K.; Cliffel, D. E. Enhanced Photocurrents of Photosystem I Films on p-Doped Silicon. *Adv. Mater.* **2012**, *24*, 5959–5962.

28. Yella, A.; Lee, H.-W.; Tsao, H. N.; Yi, C.; Chandiran, A. K.; Nazeeruddin, M. K.; Diau, E. W.-G.; Yeh, C.-Y.; Zakeeruddin, S. M.; Grätzel, M. Porphyrin-Sensitized Solar Cells with Cobalt (II/III)–based Redox Electrolyte Exceed 12 Percent Efficiency. *Science.* **2011**, *334*, 629–634.

29. Chen, G.; LeBlanc, G.; Jennings, G. K.; Cliffel, D. E. Effect of Redox Mediator on the Photo-Induced Current of a Photosystem I Modified Electrode. *J. Electrochem. Soc.* **2013**, *160*, H315–H320.

30. Gunther, D.; LeBlanc, G.; Prasai, D.; Zhang, J. R.; Cliffel, D. E.; Bolotin, K. I.; Jennings, G. K. Photosystem I on Graphene as a Highly Transparent Photoactive Electrode. *Langmuir* **2013**, *29*, 4177–4180.

31. LeBlanc, G.; Winter, K. M.; Crosby, W. B.; Jennings, G. K.; Cliffel, D. E. Integration of Photosystem I with Graphene Oxide for Photocurrent Enhancement. *Adv. Energy Mater.* **2014**.

32. LeBlanc, G.; Chen, G.; Jennings, G. K.; Cliffel, D. E. Photoreduction of Catalytic Platinum Particles Using Immobilized Multilayers of Photosystem I. *Langmuir* **2012**, *28*, 7952–7956.

33. LeBlanc, G.; Gizzie, E. A.; Yang, S.; Cliffel, D. E.; Jennings, G. K. Photosystem I Protein Films at Electrode Surfaces for Solar Energy Conversion. *Langmuir* **2014**.

34. Reeves, S. G.; Hall, D. O. [8] Higher plant chloroplasts and grana: General preparative procedures (excluding high carbon dioxide fixation ability chloroplasts). In *Methods in enzymology*; Academic Press: New York, 1980; Vol. 69, pp. 85–94.

35.   Fromme, P.; Witt, H. T. Improved Isolation and Crystallization of Photosystem I for Structural Analysis. *Biochim. Biophys. Acta (BBA)-Bioenergetics* **1998**, *1365*, 175–184.

36.   Baba, K.; Itoh, S.; Hastings, G.; Hoshina, S. Photoinhibition of Photosystem I Electron Transfer Activity in Isolated Photosystem I Preparations with Different Chlorophyll Contents. *Photosynth. Res.* **1996**, *47*, 121–130.

37.   Shiozawa, J. A.; Alberte, R. S.; Thornber, J. P. The P700-Chlorophyll a-Protein: Isolation and Some Characteristics of the Complex in Higher Plants. *Arch. Biochem. Biophys.* **1974**, *165*, 388–397.

38.   Scheller, H. V.; Jensen, P. E.; Haldrup, A.; Lunde, C.; Knoetzel, J. Role of Subunits in Eukaryotic Photosystem I. *Biochim. Biophys. Acta (BBA)-Bioenergetics* **2001**, *1507*, 41–60.

39.   Gunther, D.; LeBlanc, G.; Cliffel, D. E.; Jennings, G. K. Pueraria Lobata (Kudzu) Photosystem I Improves the Photoelectrochemical Performance of Silicon. *Ind. Biotechnol.* **2013**, *9*, 37–41.

40.   Forseth, I. N.; Innis, A. F. Kudzu (Pueraria Montana): History, Physiology, and Ecology Combine to Make a Major Ecosystem Threat. *CRC. Crit. Rev. Plant Sci.* **2004**, *23*, 401–413.

41.   Lee, J. W.; Lee, I.; Laible, P. D.; Owens, T. G.; Greenbaum, E. Chemical Platinization and Its Effect on Excitation Transfer Dynamics and P700 Photooxidation Kinetics in Isolated Photosystem I. *Biophys. J.* **1995**, *69*, 652–659.

42.   Ko, B. S.; Babcock, B.; Jennings, G. K.; Tilden, S. G.; Peterson, R. R.; Cliffel, D.; Greenbaum, E. Effect of Surface Composition on the Adsorption of Photosystem I onto Alkanethiolate Self-Assembled Monolayers on Gold. *Langmuir* **2004**, *20*, 4033–4038.

43.   Kincaid, H. A.; Niedringhaus, T.; Ciobanu, M.; Cliffel, D. E.; Jennings, G. K. Entrapment of Photosystem I Within Self-Assembled Films. *Langmuir* **2006**, *22*, 8114–8120.

44.   Mukherjee, D.; May, M.; Vaughn, M.; Bruce, B. D.; Khomami, B. Controlling the Morphology of Photosystem I Assembly on Thiol-Activated Au Substrates. *Langmuir* **2010**, *26*, 16048–16054.

45.   Lee, I.; Lee, J. W.; Stubna, A.; Greenbaum, E. Measurement of Electrostatic Potentials Above Oriented Single Photosynthetic Reaction Centers. *J. Phys. Chem. B* **2000**, *104*, 2439–2443.

46.	Carmeli, I.; Frolov, L.; Carmeli, C.; Richter, S. Photovoltaic Activity of Photosystem I-Based Self-Assembled Monolayer. *J. Am. Chem. Soc.* **2007**, *129*, 12352–12353.

47.	Hollander, M.-J. den; Magis, J. G.; Fuchsenberger, P.; Aartsma, T. J.; Jones, M. R.; Frese, R. N. Enhanced Photocurrent Generation by Photosynthetic Bacterial Reaction Centers through Molecular Relays, Light-Harvesting Complexes, and Direct Protein–Gold Interactions. *Langmuir* **2011**, *27*, 10282–10294.

48.	Kondo, M.; Nakamura, Y.; Fujii, K.; Nagata, M.; Suemori, Y.; Dewa, T.; Iida, K.; Gardiner, A. T.; Cogdell, R. J.; Nango, M. Self-Assembled Monolayer of Light-Harvesting Core Complexes from Photosynthetic Bacteria on a Gold Electrode Modified with Alkanethiols. *Biomacromolecules* **2007**, *8*, 2457–2463.

49.	Terasaki, N.; Yamamoto, N.; Hiraga, T.; Yamanoi, Y.; Yonezawa, T.; Nishihara, H.; Ohmori, T.; Sakai, M.; Fujii, M.; Tohri, A.; *et al.* Plugging a Molecular Wire into Photosystem I: Reconstitution of the Photoelectric Conversion System on a Gold Electrode. *Angew. Chemie Int. Ed.* **2009**, *48*, 1585–1587.

50.	Lee, I.; Lee, J. W.; Warmack, R. J.; Allison, D. P.; Greenbaum, E. Molecular Electronics of a Single Photosystem I Reaction Center: Studies with Scanning Tunneling Microscopy and Spectroscopy. *Proc. Natl. Acad. Sci.* **1995**, *92*, 1965–1969.

51.	Frolov, L.; Rosenwaks, Y.; Carmeli, C.; Carmeli, I. Fabrication of a Photoelectronic Device by Direct Chemical Binding of the Photosynthetic Reaction Center Protein to Metal Surfaces. *Adv. Mater.* **2005**, *17*, 2434–2437.

52.	Mukherjee, D.; Vaughn, M.; Khomami, B.; Bruce, B. D. Modulation of Cyanobacterial Photosystem I Deposition Properties on Alkanethiolate Au Substrate by Various Experimental Conditions. *Colloids Surfaces B Biointerfaces* **2011**, *88*, 181–190.

53.	Manocchi, A. K.; Baker, D. R.; Pendley, S. S.; Nguyen, K.; Hurley, M. M.; Bruce, B. D.; Sumner, J. J.; Lundgren, C. A. Photocurrent Generation from Surface Assembled Photosystem I on Alkanethiol Modified Electrodes. *Langmuir* **2013**, *29*, 2412–2419.

54.	Yan, X.; Faulkner, C. J.; Jennings, G. K.; Cliffel, D. E. Photosystem I in Langmuir–Blodgett and Langmuir–Schaefer Monolayers. *Langmuir* **2012**, *28*, 15080–15086.

55.	Lee, I.; Justus, B. L.; Lee, J. W.; Greenbaum, E. Molecular Photovoltaics and Surface Potentials at the Air-Water Interface. *J. Phys. Chem. B* **2003**, *107*, 14225–14230.

56. Bard, A. J.; Faulkner, L. R. *Electrochemical Methods: Fundamentals and Applications*; 2nd Editio.; John Wiley & Sons: New York, 2000; p. 864.

57. He, W. Z.; Malkin, R. Photosystems I and II. In *Photosynthesis: A Comprehensive Treatise*; Cambridge: University Press, 1998; pp. 29–43.

58. Chen, G.; Hijazi, F. M.; LeBlanc, G.; Jennings, G. K.; Cliffel, D. E. Scanning Electrochemical Microscopy of Multilayer Photosystem I Photoelectrochemistry. *ECS Electrochem. Lett.* **2013**, *2*, H59–H62.

59. Gizzie, E. A.; LeBlanc, G.; Jennings, G. K.; Cliffel, D. E. Electrochemical Preparation of Photosystem I - Polyaniline Films Composite Films for Biohybrid Solar Energy Conversion. *Prep.*

60. Andreeva, A.; Velitchkova, M. Resonance Raman Spectroscopy of Carotenoids in Photosystem I Particles. *Biophys. Chem.* **2005**, *114*, 129–135.

61. Frolov, L.; Rosenwaks, Y.; Richter, S.; Carmeli, C.; Carmeli, I. Photoelectric Junctions Between GaAs and Photosynthetic Reaction Center Protein. *J. Phys. Chem. C* **2008**, *112*, 13426–13430.

62. Mershin, A.; Matsumoto, K.; Kaiser, L.; Yu, D.; Vaughn, M.; Nazeeruddin, M. K.; Bruce, B. D.; Graetzel, M.; Zhang, S. Self-Assembled Photosystem-I Biophotovoltaics on Nanostructured TiO2 and ZnO. *Sci. Rep.* **2012**, *2*.

63. Tan, S. C.; Crouch, L. I.; Jones, M. R.; Welland, M. Generation of Alternating Current in Response to Discontinuous Illumination by Photoelectrochemical Cells Based on Photosynthetic Proteins. *Angew. Chemie Int. Ed.* **2012**, *51*, 6667–6671.

64. Gerischer, H. Electrochemistry of the Excited Electronic State. *J. Electrochem. Soc.* **1978**, *125*, 218C–226C.

65. Green, M. A. *Solar Cells: Operating Principles, Technology, and System Applications*; Prentice-Hall: Englewood Cliffs, 1982; Vol. 1, p. 288.

66. Ciesielski, P. N.; Cliffel, D. E.; Jennings, G. K. Kinetic Model of the Photocatalytic Effect of a Photosystem I Monolayer on a Planar Electrode Surface. *J. Phys. Chem. A* **2011**, *115*, 3326–3334.

67. Ciobanu, M.; Kincaid, H. A.; Jennings, G. K.; Cliffel, D. E. Photosystem I Patterning Imaged by Scanning Electrochemical Microscopy. *Langmuir* **2005**, *21*, 692–698.

68.   Porra, R. J. The Chequered History of the Development and Use of Simultaneous Equations for the Accurate Determination of Chlorophylls a and B. *Photosynth. Res.* **2002**, *73*, 149–56.

69.   Salmon, R. T.; Hawkridge, F. M. The Electrochemical Properties of Three Dipyridinium Salts as Mediators. *J. Electroanal. Chem. Interfacial Electrochem.* **1980**, *112*, 253–264.

70.   Sassoon, R. E.; Gershuni, S.; Rabani, J. Charge Separation in Photoinitiated Electron-Transfer Systems with Polyviologen Polyelectrolytes as Quenchers. *J. Phys. Chem.* **1985**, *89*, 1937–1945.

71.   Topoglidis, E.; Cass, A. E. G.; O'Regan, B.; Durrant, J. R. Immobilisation and Bioelectrochemistry of Proteins on Nanoporous TiO2 and ZnO Films. *J. Electroanal. Chem.* **2001**, *517*, 20–27.

72.   Hilgendorff, M.; Spanhel, L.; Rothenhäusler, C.; Müller, G. From ZnO Colloids to Nanocrystalline Highly Conductive Films. *J. Electrochem. Soc.* **1998**, *145*, 3632–3637.

73.   Lujala, V.; Skarp, J.; Tammenmaa, M.; Suntola, T. Atomic Layer Epitaxy Growth of Doped Zinc Oxide Thin Films from Organometals. *Appl. Surf. Sci.* **1994**, *82/83*, 34–40.

74.   Yang, T. L.; Zhang, D. H.; Ma, J.; Ma, H. L.; Chen, Y. Transparent Conducting ZnO: Al Films Deposited on Organic Substrates Deposited by Rf Magnetron-Sputtering. *Thin Solid Films* **1998**, *326*, 60–62.

75.   Fay, S.; Kroll, U.; Bucher, C.; Vallat-Sauvain, E.; Shah, A. Low Pressure Chemical Vapour Deposition of ZnO Layers for Thin-Film Solar Cells: Temperature-Induced Morphological Changes. *Sol. Energy Mater. Sol. Cells* **2005**, *86*, 385–397.

76.   Sun, Y.; Fuge, G. M.; Ashfold, M. N. R. Growth of Aligned ZnO Nanorod Arrays by Catalyst-Free Pulsed Laser Deposition Methods. *Chem. Phys. Lett.* **2004**, *396*, 21–26.

77.   Hong, S.-K.; Hanada, T.; Ko, H.-J.; Chen, Y.; Yao, T.; Imai, D.; Araki, K.; Shinohara, M.; Saitoh, K.; Terauchi, M. Control of Crystal Polarity in a Wurtzite Crystal: ZnO Films Grown by Plasma-Assisted Molecular-Beam Epitaxy on GaN. *Phys. Rev. B* **2002**, *65*, 115331.

78.   Peulon, S.; Lincot, D. Cathodic Electrodeposition from Aqueous Solution of Dense or Open-structured Zinc Oxide Films. *Adv. Mater.* **1996**, *8*, 166–170.

79. Ivanov, B. L.; Wellons, M. S.; Lukehart, C. M. Confined-Plume Chemical Deposition: Rapid Synthesis of Crystalline Coatings of Known Hard or Superhard Materials on Inorganic or Organic Supports by Resonant IR Decomposition of Molecular Precursors. *J. Am. Chem. Soc.* **2009**, *131*, 11744–11750.

80. Goux, A.; Pauporté, T.; Chivot, J.; Lincot, D. Temperature Effects on ZnO Electrodeposition. *Electrochim. Acta* **2005**, *50*, 2239–2248.

81. Du, Y.; Zhang, M.-S.; Hong, J.; Shen, Y.; Chen, Q.; Yin, Z. Structural and Optical Properties of Nanophase Zinc Oxide. *Appl. Phys. A* **2003**, *76*, 171–176.

82. Arguello, C. A.; Rousseau, D. L.; Porto, S. P. da S. First-Order Raman Effect in Wurtzite-Type Crystals. *Phys. Rev.* **1969**, *181*, 1351.

83. Kimmel, D. W.; LeBlanc, G.; Meschievitz, M. E.; Cliffel, D. E. Electrochemical Sensors and Biosensors. *Anal. Chem.* **2011**, *84*, 685–707.

84. Carmeli, I.; Mangold, M.; Frolov, L.; Zebli, B.; Carmeli, C.; Richter, S.; Holleitner, A. W. A Photosynthetic Reaction Center Covalently Bound to Carbon Nanotubes. *Adv. Mater.* **2007**, *19*, 3901–3905.

85. Novoselov, K. S.; Geim, A. K.; Morozov, S. V; Jiang, D.; Zhang, Y.; Dubonos, S. V; Grigorieva, I. V; Firsov, A. A. Electric Field Effect in Atomically Thin Carbon Films. *Science.* **2004**, *306*, 666–669.

86. Zhang, Y.; Tang, T.-T.; Girit, C.; Hao, Z.; Martin, M. C.; Zettl, A.; Crommie, M. F.; Shen, Y. R.; Wang, F. Direct Observation of a Widely Tunable Bandgap in Bilayer Graphene. *Nature* **2009**, *459*, 820–823.

87. Bolotin, K. I.; Sikes, K. J.; Jiang, Z.; Klima, M.; Fudenberg, G.; Hone, J.; Kim, P.; Stormer, H. L. Ultrahigh Electron Mobility in Suspended Graphene. *Solid State Commun.* **2008**, *146*, 351–355.

88. Novoselov, K. S.; Jiang, Z.; Zhang, Y.; Morozov, S. V; Stormer, H. L.; Zeitler, U.; Maan, J. C.; Boebinger, G. S.; Kim, P.; Geim, A. K. Room-Temperature Quantum Hall Effect in Graphene. *Science.* **2007**, *315*, 1379.

89. Lee, C.; Wei, X.; Kysar, J. W.; Hone, J. Measurement of the Elastic Properties and Intrinsic Strength of Monolayer Graphene. *Science.* **2008**, *321*, 385–388.

90. Seol, J. H.; Jo, I.; Moore, A. L.; Lindsay, L.; Aitken, Z. H.; Pettes, M. T.; Li, X.; Yao, Z.; Huang, R.; Broido, D. Two-Dimensional Phonon Transport in Supported Graphene. *Science.* **2010**, *328*, 213–216.

91. Nair, R. R.; Blake, P.; Grigorenko, A. N.; Novoselov, K. S.; Booth, T. J.; Stauber, T.; Peres, N. M. R.; Geim, A. K. Fine Structure Constant Defines Visual Transparency of Graphene. *Science.* **2008**, *320*, 1308.

92. Geim, A. K. Graphene: Status and Prospects. *Science.* **2009**, *324*, 1530–1534.

93. Reina, A.; Jia, X.; Ho, J.; Nezich, D.; Son, H.; Bulovic, V.; Dresselhaus, M. S.; Kong, J. Large Area, Few-Layer Graphene Films on Arbitrary Substrates by Chemical Vapor Deposition. *Nano Lett.* **2008**, *9*, 30–35.

94. Li, X.; Cai, W.; An, J.; Kim, S.; Nah, J.; Yang, D.; Piner, R.; Velamakanni, A.; Jung, I.; Tutuc, E. Large-Area Synthesis of High-Quality and Uniform Graphene Films on Copper Foils. *Science.* **2009**, *324*, 1312–1314.

95. Zhu, Y.; Murali, S.; Cai, W.; Li, X.; Suk, J. W.; Potts, J. R.; Ruoff, R. S. Graphene and Graphene Oxide: Synthesis, Properties, and Applications. *Adv. Mater.* **2010**, *22*, 3906–3924.

96. Dikin, D. A.; Stankovich, S.; Zimney, E. J.; Piner, R. D.; Dommett, G. H. B.; Evmenenko, G.; Nguyen, S. T.; Ruoff, R. S. Preparation and Characterization of Graphene Oxide Paper. *Nature* **2007**, *448*, 457–460.

97. Becerril, H. A.; Mao, J.; Liu, Z.; Stoltenberg, R. M.; Bao, Z.; Chen, Y. Evaluation of Solution-Processed Reduced Graphene Oxide Films as Transparent Conductors. *ACS Nano* **2008**, *2*, 463–470.

98. Mueller, T.; Xia, F.; Freitag, M.; Tsang, J.; Avouris, P. Role of Contacts in Graphene Transistors: A Scanning Photocurrent Study. *Phys. Rev. B* **2009**, *79*, 245430.

99. Eda, G.; Chhowalla, M. Graphene-Based Composite Thin Films for Electronics. *Nano Lett.* **2009**, *9*, 814–818.

100. Xu, Y.; Hong, W.; Bai, H.; Li, C.; Shi, G. Strong and Ductile Poly (vinyl Alcohol)/graphene Oxide Composite Films with a Layered Structure. *Carbon N. Y.* **2009**, *47*, 3538–3543.

101. Li, C.; Adamcik, J.; Mezzenga, R. Biodegradable Nanocomposites of Amyloid Fibrils and Graphene with Shape-Memory and Enzyme-Sensing Properties. *Nat. Nanotechnol.* **2012**, *7*, 421–427.

102. Li, X.; Zhu, Y.; Cai, W.; Borysiak, M.; Han, B.; Chen, D.; Piner, R. D.; Colombo, L.; Ruoff, R. S. Transfer of Large-Area Graphene Films for High-Performance Transparent Conductive Electrodes. *Nano Lett.* **2009**, *9*, 4359–4363.

103. Gómez-Navarro, C.; Weitz, R. T.; Bittner, A. M.; Scolari, M.; Mews, A.; Burghard, M.; Kern, K. Electronic Transport Properties of Individual Chemically Reduced Graphene Oxide Sheets. *Nano Lett.* **2007**, *7*, 3499–3503.

104. Paredes, J. I.; Villar-Rodil, S.; Martinez-Alonso, A.; Tascon, J. M. D. Graphene Oxide Dispersions in Organic Solvents. *Langmuir* **2008**, *24*, 10560–10564.

105. Cuong, T. V.; Pham, V. H.; Tran, Q. T.; Hahn, S. H.; Chung, J. S.; Shin, E. W.; Kim, E. J. Photoluminescence and Raman Studies of Graphene Thin Films Prepared by Reduction of Graphene Oxide. *Mater. Lett.* **2010**, *64*, 399–401.

106. Zhang, J.; Yang, H.; Shen, G.; Cheng, P.; Zhang, J.; Guo, S. Reduction of Graphene Oxide via l-Ascorbic Acid. *Chem. Commun.* **2010**, *46*, 1112–1114.

107. Lee, J.; Greenbaum, E. Bioelectronics and Biometallocatalysis for Production of Fuels and Chemicals by Photosynthetic Water Splitting. *Appl. Biochem. Biotechnol.* **1995**, *51/52*, 293–324.

108. Golbeck, J. Structure and Function of Photosystem I. *Annu. Rev. Plant Biol.* **1992**, *43*, 293–324.

109. Blankenship, R. E.; Tiede, D. M.; Barber, J.; Brudvig, G. W.; Fleming, G.; Ghirardi, M.; Gunner, M. R.; Junge, W.; Kramer, D. M.; Melis, A. Comparing Photosynthetic and Photovoltaic Efficiencies and Recognizing the Potential for Improvement. *Science.* **2011**, *332*, 805–809.

110. Grimme, R. A.; Lubner, C. E.; Bryant, D. A.; Golbeck, J. H. Photosystem I/molecular Wire/metal Nanoparticle Bioconjugates for the Photocatalytic Production of H2. *J. Am. Chem. Soc.* **2008**, *130*, 6308–6309.

111. Yehezkeli, O.; Wilner, O. I.; Tel-Vered, R.; Roizman-Sade, D.; Nechushtai, R.; Willner, I. Generation of Photocurrents by Bis-Aniline-Cross-Linked Pt Nanoparticle/Photosystem I Composites on Electrodes. *J. Phys. Chem. B* **2010**, *114*, 14383–14388.

112. Terasaki, N.; Yamamoto, N.; Hiraga, T.; Sato, I.; Inoue, Y.; Yamada, S. Fabrication of Novel Photosystem I–gold Nanoparticle Hybrids and Their Photocurrent Enhancement. *Thin Solid Films* **2006**, *499*, 153–156.

113. Jung, C.; Sánchez-Sánchez, C. M.; Lin, C.-L.; Rodríguez-López, J.; Bard, A. J. Electrocatalytic Activity of Pd− Co Bimetallic Mixtures for Formic Acid Oxidation Studied by Scanning Electrochemical Microscopy. *Anal. Chem.* **2009**, *81*, 7003–7008.

114. Cannan, S.; Cervera, J.; Steliaros, R. J.; Bitziou, E.; Whitworth, A. L.; Unwin, P. R. Scanning Electrochemical Microscopy (SECM) Studies of Catalytic EC′ Processes: Theory and Experiment for Feedback, Generation/collection and Imaging Measurements. *Phys. Chem. Chem. Phys.* **2011**, *13*, 5403–5412.

115. Casella, I. G.; Desimoni, E. XPS, SEM and Electrochemical Characterization of a Platinum-based Glassy Carbon Modified Electrode. Electrocatalytic Oxidation of Ethanol in Acidic Medium. *Electroanalysis* **1996**, *8*, 447–453.

116. Lee, C.; Kwak, J.; Anson, F. C. Application of Scanning Electrochemical Microscopy to Generation/collection Experiments with High Collection Efficiency. *Anal. Chem.* **1991**, *63*, 1501–1504.

117. Smith, R. L.; Collins, S. D. Porous Silicon Formation Mechanisms. *J. Appl. Phys.* **1992**, *71*, R1–R22.

118. Lehmann, V.; Gösele, U. Porous Silicon Formation: A Quantum Wire Effect. *Appl. Phys. Lett.* **1991**, *58*, 856.

119. Toporik, H.; Carmeli, I.; Volotsenko, I.; Molotskii, M.; Rosenwaks, Y.; Carmeli, C.; Nelson, N. Large Photovoltages Generated by Plant Photosystem I Crystals. *Adv. Mater.* **2012**, *24*, 2988–91.

ORIENTING PHOTOSYSTEM I USING LANGMUIR-BLODGETT[*]

Introduction

One of the key areas of research in the field of biohybrid electrodes based on Photosystem I (PSI) concerns the orientation of the protein complex on the surface of the electrode, as described in Chapters I, II, and VII of this dissertation. Previous studies have demonstrated how self-assembled monolayer (SAM) modified electrodes can enable PSI monolayers to form,[1] however a specific orientation was typically not observed. To favor specific protein orientations several methods of protein attachment have been attempted including genetic modification of the PSI complex,[2] the use of molecular wires,[3] or using cytochrome-c to anchor PSI.[4]

In this study we propose a modified Langmuir-Blodgett (L-B) deposition strategy to favor the orientation of PSI on the surface of a SAM modified gold electrode (**Figure A.1**). Previous experiments in our research group have demonstrated that L-B or Langmuir-Schaefer (L-S) deposition could be used to deposit a monolayer of PSI onto the surface of SAM modified gold electrodes.[5] For these deposition strategies, a small volume of PSI extract is spread over the surface of an aqueous subphase. Because PSI is a membrane protein, it is hydrophilic on the top and bottom but hydrophobic at the center

---

[*] Some of the experiments described in this appendix were performed by Yiliang Zhao.

membrane region. Thus it will remain at the air-water interface with roughly half of the proteins oriented in an "up" configuration, with the other proteins oriented in the "down" configuration. Barriers can then be used to reduce the surface area of the aqueous subphase. This brings the PSI complexes closer to one another, generating a dense film of PSI at the air-water interface. By raising a hydrophilic electrode through the air-water interface, the dense PSI monolayer can be transfer to generate a biohybrid electrode. Using this traditional L-B method, it was found that $57 \pm 6\%$ of the PSI was oriented in the "up" configuration.[5] Here, we hypothesized that this orientation could be improved by changing the pH environment of the subphase.
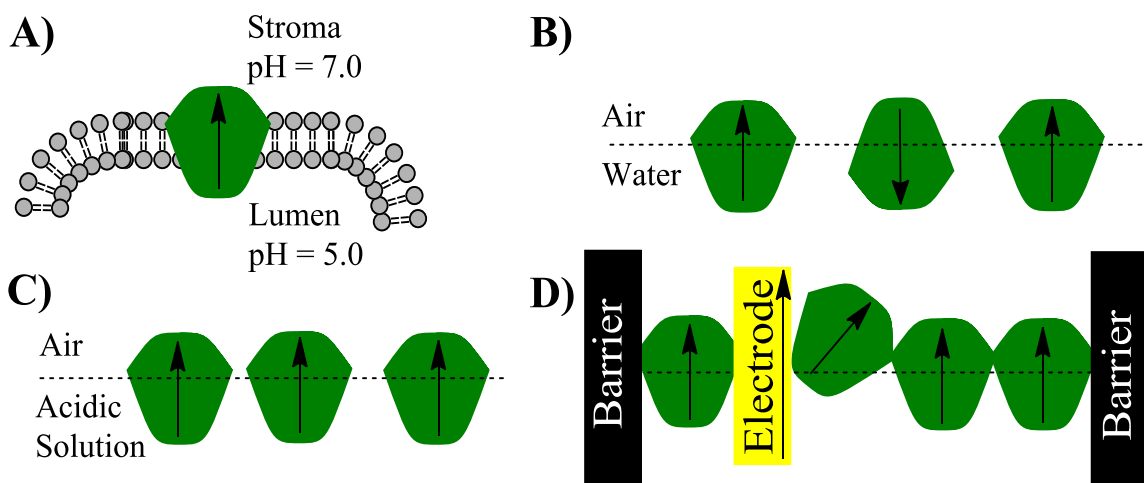
Figure A.1. Schematic for modified L-B deposition method. A) Oriented PSI complex in the thylakoid membrane. B) Random orientation of PSI at the air-water interface using a traditional L-B subphase. C) Proposed orientation of PSI using an acidic subphase. D) L-B deposition of PSI from the acidic subphase.

Studies of the thylakoid membrane in higher order plants have demonstrated that a significant pH gradient is present, with the interior of the thylakoid (lumen) possessing a much lower pH than the exterior of the thylakoid (stroma).[6] In higher order plants, this

pH gradient is used to trigger responses related to photodegradation protection[7] and carbon dioxide assimilation.[8] The lumen is capable of pH values below 5,[8] with even lower values possible at specific regions. We therefore hypothesized that the orientation of the PSI complex could be significantly influenced by the pH of the subphase at an air-water interface. Thus the resulting L-B deposition would provide a biohybrid electrode with improved PSI orientation.

Results and Discussion

Following our hypothesis, we anticipated significant photocurrent increases by using a acidic subphase during L-B deposition onto a SAM modified gold electrode. Therefore our initial experiments utilized a subphase with a pH of 2.0. Adding 15 μL of PSI extract to the surface of the subphase allowed the PSI complexes to spread across the surface and, presumably, orient at the air-water interface. A gold substrate electrode was then lowered into the subphase before closing the barriers. The gold electrode was modified with 6-mercapto-1-hexanol to make the substrate more hydrophilic, which was confirmed using contact angle measurements and ellipsometry. The barriers of the L-B trough were then closed to increase the surface pressure of the PSI complexes (**Figure A.2**). From the surface pressure – area isotherm it is apparent that the PSI protein increases the surface pressure of the system even before the barriers are closed. As the barriers close, the surface pressure quickly increases as the PSI complexes interact with each other more. At approximately 75 cm^2, the surface pressure begins increasing at a higher rate, indicating that the PSI complexes are beginning to pack together in the form

of a dense monolayer on the surface of the subphase. In order to prevent multilayer formation, we utilized a pressure of 20 mN/m during the L-B deposition process.
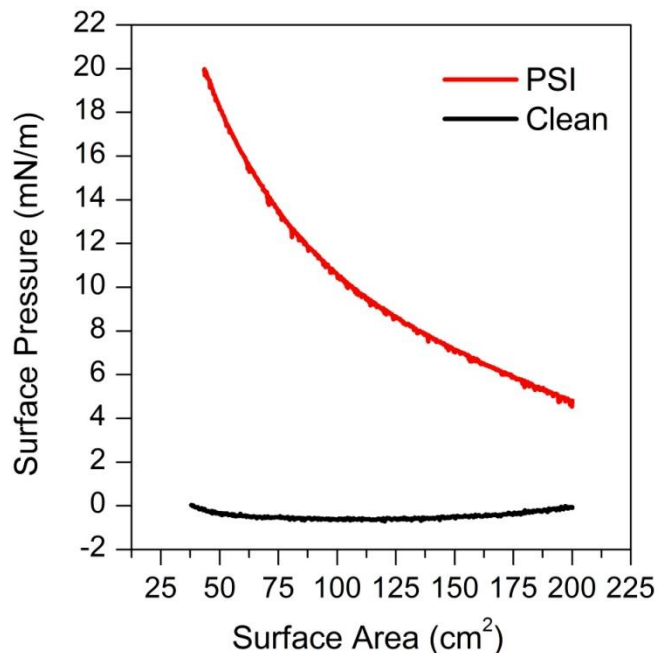
Figure A.2. Surface pressure – area isotherm of PSI. The surface pressure – area isotherm of a clean pH = 2.0 subphase (black) and the isotherm of the same subphase with PSI (red) at the air-water interface.

After allowing the system to equilibrate at 20 mN/m, the SAM modified gold electrode was removed using a traditional L-B technique. Using ellipsometry, the average thickness of the PSI layer was determined to be 31.8 ± 3.9 Å. This represents roughly 44% coverage compared with a complete dense monolayer of PSI (70 Å).[9] To test to photoactivity of the biohybrid electrode, photochronoamperometry was employed (**Figure A.3**). Incredibly, the photocurrent for one of these electrodes exceeded any previous report from our research group for a monolayer film of PSI on a metal electrode.[9] While the photocurrent production from this single biohybrid electrode was

reproducible over a period of several days, efforts to reproduce these extremely high photocurrent values with different electrodes proved unsuccessful. The interesting result, however, led us to perform a more systematic evaluation of the subphase pH on the photocurrent production.
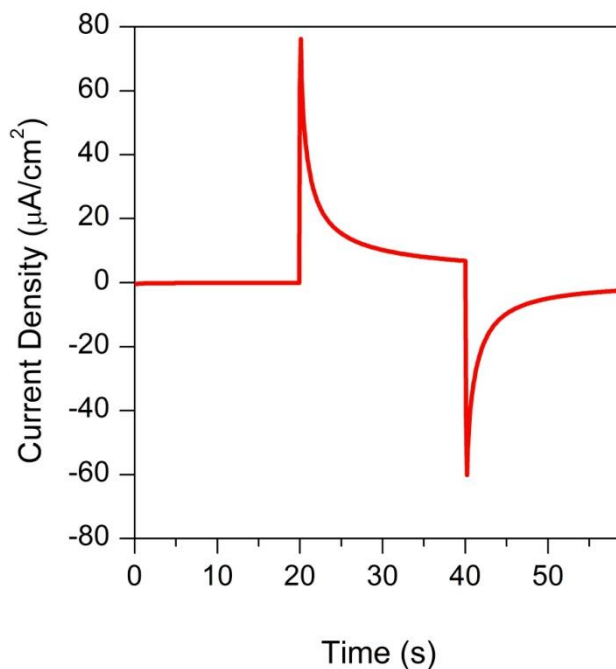
Figure A.3. Photochronoamperometry of L-B PSI film on gold. PSI monolayer was deposited onto a SAM modified gold electrode using L-B using an aqueous subphase at pH 2.0. Photochronoamperometry was performed using 0.2 mM Ferricyanide, 100 mM KCl, a Ag/AgCl reference electrode, and a Pt mesh counter electrode. The working electrode was held at the dark open circuit potential and illuminated with red light from the time points of 20 - 40 s.

As seen in **Figure A.4**, changing the pH of the subphase during the L-B deposition process had a significant impact on the resulting photocurrent of the biohybrid electrode. Unfortunately the photocurrent and photovoltage values were significantly lower than our original measurement. While no obvious trends emerged by changing the

131

pH of the subphase, it is worth noting that the photocurrent values reported for L-B depositions performed at a pH of 2 gave significantly higher photocurrent and photovoltage values. This could indicate that the subphase acidity must be very high to improve the orientation of PSI at the air-water interface.
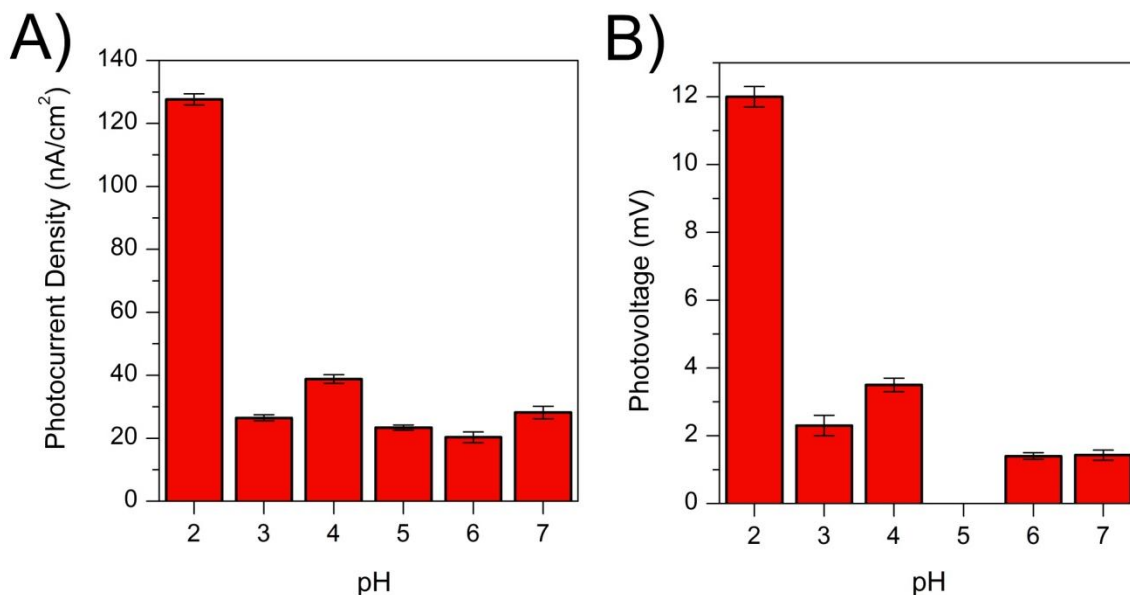
Figure A.4. Photocurrent and Photovoltage as a function of subphase pH. A) Photocurrent values for PSI modified gold electrodes prepared by L-B deposition at various subphase pH values (4 measurements per sample). B) Photovoltage values for PSI modified gold electrodes prepared by L-B deposition at various subphase pH values (3 measurements per sample). The electrochemical mediator consisted of 5 mM sodium ascorbate, 0.25 mM dichloroindophenol (DCPIP), 5 mM phosphate buffer, and 100 mM KCl. Ag/AgCl and Pt mesh were used as the reference and counter electrode respectively.

These preliminary results suggest that changing the pH of the subphase during L-B deposition could significantly improve photocurrent performance of biohybrid electrodes based on monolayers of PSI. We believe that this is the result of improved orientation of PSI at the air-water interface during L-B deposition when an acidic subphase is used. The acidic subphase helps mimic the natural pH gradient present across

the thylakoid membrane. In order to support these claims, additional experiments will be necessary. Specifically, replication of the initial photocurrent production (on the order of $\mu A/cm^2$) will be necessary. Additionally, L-B depositions using a subphase with a wider pH range, including more acidic pH values, should be performed. The results described here provide a promising avenue for generating oriented PSI monolayers on the surface of hydrophilic electrodes.

Experimental

Preparation of gold substrates

Gold substrates were prepared by thermally depositing ~125 nm of gold onto a silicon support (Montico Silicon, <100> orientation). Gold substrates were then made hydrophilic using a hydroxyl-terminated SAM. This modification was performed by immersing the gold substrate in an ethanolic solution of 6-mercapto-1-hexanol for at least 24 hours. After modification, the substrate was removed and rinsed with ethanol followed by water and dried prior to further modification.

L-B technique

PSI was deposited onto the gold substrates using a modified L-B technique. Similar to a traditional L-B technique, a L-B trough (Nima 611D), with an effective surface area of 260 cm^2, was filled with an aqueous subphase.[5] In this case, however, the pH of the subphase was modified. The subphase was then cleaned by closing the barriers and removing any unwanted material from the surface using suction. The barriers were then reopened and the gold electrode was submerged in the subphase. 15 μL of PSI extract (10^{-7} M) was then added to the surface. The barriers were then closed at a constant

speed of 10 cm^2/s until the surface pressure reached 20 mN/m. The substrate was removed from the subphase at a speed of 2 mm/min which deposited a submonolayer of PSI on the surface of the gold.

Instruments and Equipment

Electrochemical measurements were performed using a CH Instruments CHI 660a electrochemical workstation equipped with a Faraday cage. A custom built, three electrode cell was used where the modified gold sample was set as the working electrode, platinum mesh as the counter electrode, and Ag/AgCl as the reference electrode. The electrochemical mediator used varied for these experiments and is listed in the figure captions.

Spectroscopic ellipsometry measurements were obtained on a J.A. Woolham Co. M-2000DI variable angle spectroscopic ellipsometer with CompleteEase^{TM} software for modeling. Measurements were made at three locations on each sample and the thickness was determined using a Cauchy film as the starting material.

References

1. LeBlanc, G.; Gizzie, E. A.; Yang, S.; Cliffel, D. E.; Jennings, G. K. Photosystem I Protein Films at Electrode Surfaces for Solar Energy Conversion. *Langmuir* **2014**.

2. Frolov, L.; Wilner, O.; Carmeli, C.; Carmeli, I. Fabrication of Oriented Multilayers of Photosystem I Proteins on Solid Surfaces by Auto-Metallization. *Adv. Mater.* **2008**, *20*, 263–266.

3. Terasaki, N.; Yamamoto, N.; Hiraga, T.; Yamanoi, Y.; Yonezawa, T.; Nishihara, H.; Ohmori, T.; Sakai, M.; Fujii, M.; Tohri, A.; *et al.* Plugging a Molecular Wire into Photosystem I: Reconstitution of the Photoelectric Conversion System on a Gold Electrode. *Angew. Chemie Int. Ed.* **2009**, *48*, 1585–1587.

4. Hollander, M.-J. den; Magis, J. G.; Fuchsenberger, P.; Aartsma, T. J.; Jones, M. R.; Frese, R. N. Enhanced Photocurrent Generation by Photosynthetic Bacterial

Reaction Centers through Molecular Relays, Light-Harvesting Complexes, and Direct Protein–Gold Interactions. *Langmuir* **2011**, *27*, 10282–10294.

5. Yan, X.; Faulkner, C. J.; Jennings, G. K.; Cliffel, D. E. Photosystem I in Langmuir–Blodgett and Langmuir–Schaefer Monolayers. *Langmuir* **2012**, *28*, 15080–15086.

6. Demmig-Adams, B.; Adams Iii, W. W. Photoprotection and Other Responses of Plants to High Light Stress. *Annu. Rev. Plant Biol.* **1992**, *43*, 599–626.

7. Noctor, G.; Rees, D.; Young, A.; Horton, P. The Relationship Between Zeaxanthin, Energy-Dependent Quenching of Chlorophyll Fluorescence, and Trans-Thylakoid pH Gradient in Isolated Chloroplasts. *Biochim. Biophys. Acta (BBA)-Bioenergetics* **1991**, *1057*, 320–330.

8. Raven, J. A. CO2-Concentrating Mechanisms: a Direct Role for Thylakoid Lumen Acidification? *Plant. Cell Environ.* **1997**, *20*, 147–154.

9. Faulkner, C. J.; Lees, S.; Ciesielski, P. N.; Cliffel, D. E.; Jennings, G. K. Rapid Assembly of Photosystem I Monolayers on Gold Electrodes. *Langmuir* **2008**, *24*, 8409–8412.

APPENDIX B

SOLID-STATE PHOTOVOLTAIC USING A GRAPHENE COUNTER ELECTRODE

Introduction

The results of integrating Photosystem I (PSI) with graphene electrodes to generate FET or photoelectrochemical cells was presented in Chapter V. Our interest in using graphene, a single layer of carbon atoms, stems from its remarkable properties as a transparent and conductive electrode.[1] This has allowed our research team to generate the thinnest photoactive electrode based on PSI (10 nm).[2] This thin photoelectode required an electrochemical mediator, however, to replace the electrons to the P700 reaction center in PSI. While the use of an electrochemical mediator allows for a straightforward connection method to complete an electrochemical circuit, the application of these systems in the environment presents several problems, such as leaking.[3]

The use of a solid-state photovoltaic device presents several advantages over a photoelectrochemical cell. In particular, the effects of mediator diffusion can be eliminated. In 2004, Das and co-workers described the first solid-state photovoltaic using PSI and reaction centers.[4] While the efficiencies were quite low and the materials used were relatively expensive, this important study demonstrated the feasibility of developing a solid-state system that took advantage of the unique properties of PSI. In Chapter IV we described some of our preliminary efforts to generate a solid-state photovoltaic using p-

doped silicon and zinc oxide electrodes. In this appendix we describe efforts to use a transparent graphene electrode in direct contact with a PSI film to generate a solid-state photovoltaic (**Figure B.1**) We hypothesized that the high elasticity of graphene, with a breaking strength of 42 N/m,[5] would enable the electrode to form around the contours of a monolayer or multilayer film of PSI.
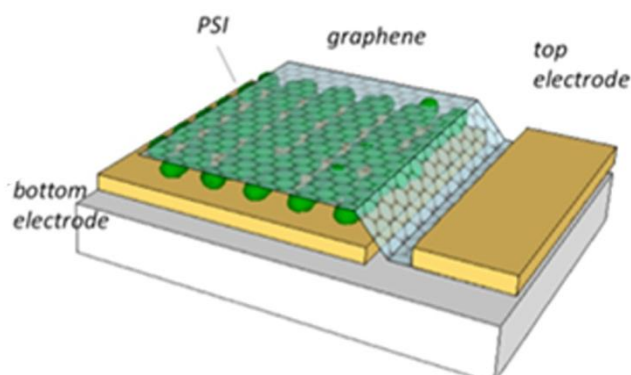
Figure B.1. Cartoon depiction of PSI-graphene solid-state photovoltaic.

Results and Discussion

PSI biohybrid electrodes were prepared on gold electrodes as either monolayer[6] or multilayer[7] films according to previously reported methods. Monolayer graphene electrodes were prepared using CVD on copper substrates.[8] After spin-coating a supporting polymer onto the graphene, the copper was etched away leaving a transparent and conductive electrode that could be transferred on top of the biohybrid electrode. While the deposition of PSI monolayers was confirmed using ellipsometry and contact angle measurements, all of these systems demonstrated short-circuit behavior after the graphene electrode was applied. The multilayer films, however, showed more interesting properties.

The I-V analysis of our best performing device can be seen in **Figure B.2**. There are several interesting attributes that can be observed in this data. The first is the high short-circuit current (-21 μA/cm^2). This is twice the photocurrent we observe for multilayer films on gold electrodes.[7] The second is the low fill factor (0.45) and open circuit potential (0.1 V), which has a significant impact on the external efficiency of the device (1.64x10^{-4}%). This device was tested multiple times on different days and demonstrated similar efficiencies (10^{-4}%) up to two weeks later. After one month, the efficiency of the device began to decrease (10^{-6} %), but was still photoactive until the device broke due to poor handling. This demonstrates the stability of these solid-state devices.
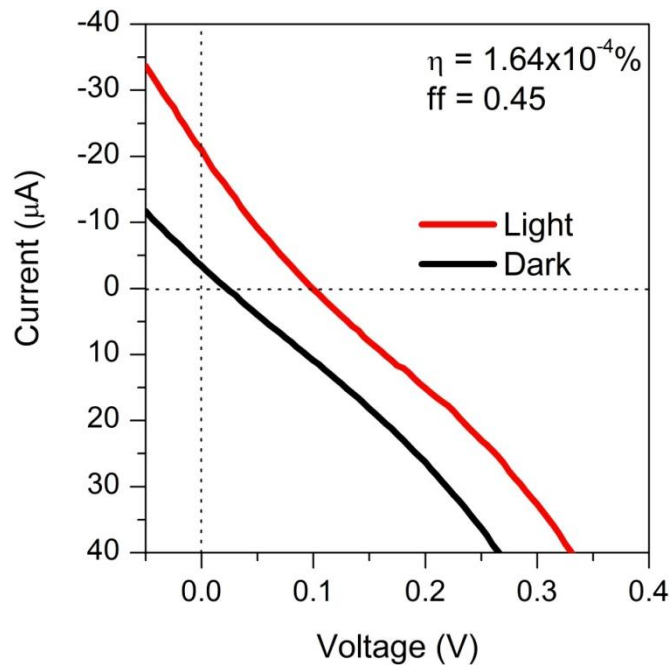
Figure B.2. I-V analysis of a PSI-graphene solid state photovoltaic. The device, comprised of a PSI multilayer film deposited on a gold substrate with a graphene counter electrode, was analyzed under dark (black) and 1 sun illumination (red).

Efforts to generate more of these devices proved very challenging. Typical device efficiencies ranged from 10^{-6} to 10^{-8} % if the device did not short-circuit. After preparing over 50 solid-state devices, we determined that the surface roughness of the PSI film was playing a significant role in the efficiency of the devices. As seen in **Figure B.3**, the PSI multilayer film is very rough, with portions of the film nearly 6 μm higher than the lowest areas. This means that even under the best circumstances the graphene electrode is only in direct contact with a portion of the PSI film.
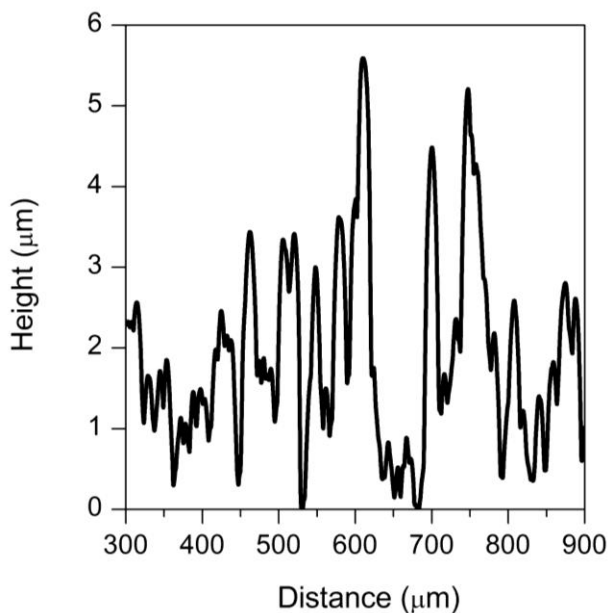
Figure B.3. Profilometry of a PSI multilayer film. The profilometry scan was performed at a scan rate of 2.5 μm/s.

Efforts to decrease this roughness using the same deposition method were unsuccessful, however an electropolymerization technique has recently been developed that generates films with a peak-to-valley ratios of less than 0.1 μm.[9] These films may provide greater electrode contact and thus improve both the efficiency and reproducibility

of these solid-state photovoltaic devices. Another strategy is to incorporate several PSI monolayer films in a stacked solid-state device (**Figure B.4**). This concept would require the PSI monolayer to be oriented and the graphene electrode to be either p- or n-doped.[10] The promising results observed for the simple solid-state device described in this appendix demonstrate the feasibility of using graphene as an electrode for PSI-based photovoltaic devices.
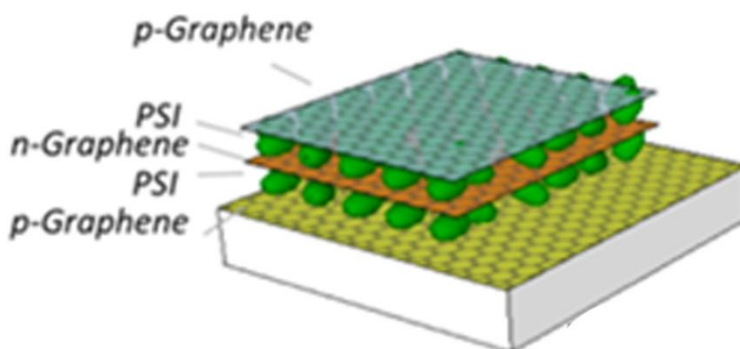
Figure B.4. Proposed stacked solid-state device. The device would utilized oriented PSI monolayers separated by doped graphene electrodes to efficiently shuttle photogenerated electrons and holes through the circuit.

Experimental

Preparation of gold substrates

Gold substrates were prepared by thermally depositing ~125 nm of gold onto a silicon support (Montico Silicon, <100> orientation).

Deposition of PSI films

PSI multilayer films were deposited onto electrodes using previously published methods.[6,7] Briefly, 50 µL of PSI solution (10^{-6} M) was placed on the surface of the

electrode. The system was then placed under vacuum until the film was dried. For monolayer film formation the PSI solution was left undialyzed,[6] while multilayer film formation required the PSI solution to be dialyzed prior to exposing the system to vacuum.[7]

CVD of graphene and transfer methods

CVD graphene was prepared and transferred to various substrates following previously published methods.[11] Briefly, following CVD deposition onto 25-μm thick Cu foils (Alfa Aesar), poly(methyl methacrylate) (PMMA) was spun onto the graphene surface, and the copper was etched away using copper etchant type CE 100 (Transene Company). The PMMA-graphene substrate was then floated on deionized water to remove copper etchant before transfer onto the solid-state device.

Instruments and Equipment

Profilometry was performed on all samples using a Dektak 150 surface profiler from Veeco Instruments Incorporated. The profilometry scan was performed at a scan rate of 2.5 μm/s.

Evaluation of the solid-state solar cell device was obtained by way of a Sciencetech SF150B solar simulator with AM1.5G filter (class A spectral match, class B non-uniformity) connected to a Keithley 2400 sourcemeter controlled by Labview software. The lamp was calibrated to 1.00 full sun with an NREL certified silicon reference diode.

References

1.	Eda, G.; Fanchini, G.; Chhowalla, M. Large-Area Ultrathin Films of Reduced Graphene Oxide as a Transparent and Flexible Electronic Material. *Nat. Nanotechnol.* **2008**, *3*, 270–274.

2.	Gunther, D.; LeBlanc, G.; Prasai, D.; Zhang, J. R.; Cliffel, D. E.; Bolotin, K. I.; Jennings, G. K. Photosystem I on Graphene as a Highly Transparent Photoactive Electrode. *Langmuir* **2013**, *29*, 4177–4180.

3.	Ciesielski, P. N.; Hijazi, F. M.; Scott, A. M.; Faulkner, C. J.; Beard, L.; Emmett, K.; Rosenthal, S. J.; Cliffel, D.; Jennings, G. K. Photosystem I - Based Biohybrid Photoelectrochemical Cells. *Bioresour. Technol.* **2010**, *101*, 3047–3053.

4.	Das, R.; Kiley, P.; Segal, M.; Norville, J.; Yu, A. Integration of Photosynthetic Protein Molecular Complexes in Solid-State Electronic Devices. *Nano Lett.* **2004**, *4*, 1079–1083.

5.	Lee, C.; Wei, X.; Kysar, J. W.; Hone, J. Measurement of the Elastic Properties and Intrinsic Strength of Monolayer Graphene. *Science.* **2008**, *321*, 385–388.

6.	Faulkner, C. J.; Lees, S.; Ciesielski, P. N.; Cliffel, D. E.; Jennings, G. K. Rapid Assembly of Photosystem I Monolayers on Gold Electrodes. *Langmuir* **2008**, *24*, 8409–8412.

7.	Ciesielski, P. N.; Faulkner, C. J.; Irwin, M. T.; Gregory, J. M.; Tolk, N. H.; Cliffel, D. E.; Jennings, G. K. Enhanced Photocurrent Production by Photosystem I Multilayer Assemblies. *Adv. Funct. Mater.* **2010**, *20*, 4048–4054.

8.	Li, X.; Cai, W.; An, J.; Kim, S.; Nah, J.; Yang, D.; Piner, R.; Velamakanni, A.; Jung, I.; Tutuc, E. Large-Area Synthesis of High-Quality and Uniform Graphene Films on Copper Foils. *Science.* **2009**, *324*, 1312–1314.

9.	Gizzie, E. A.; LeBlanc, G.; Jennings, G. K.; Cliffel, D. E. Electrochemical Preparation of Photosystem I - Polyaniline Films Composite Films for Biohybrid Solar Energy Conversion. *Prep. Biomacromolecules*.

10.	Panchakarla, L. S.; Subrahmanyam, K. S.; Saha, S. K.; Govindaraj, A.; Krishnamurthy, H. R.; Waghmare, U. V; Rao, C. N. R. Synthesis, Structure, and Properties of Boron-and Nitrogen-Doped Graphene. *Adv. Mater.* **2009**, *21*, 4726–4730.

11. Li, X.; Zhu, Y.; Cai, W.; Borysiak, M.; Han, B.; Chen, D.; Piner, R. D.; Colombo, L.; Ruoff, R. S. Transfer of Large-Area Graphene Films for High-Performance Transparent Conductive Electrodes. *Nano Lett.* **2009**, *9*, 4359–4363.

Gabriel LeBlanc

Curriculum Vitae

Vanderbilt University │ 2002 Convent Place, Apt. 8 │ Nashville, TN 37212
E-mail: gabriel.leblanc@vanderbilt.edu; gabriel.leblanc9@gmail.com

Education

PhD. Chemistry, Vanderbilt University, May 2014   GPA: 3.930
    Dissertation Title: *Biohybrid Electrodes Based on*
                Photosystem I for Solar Energy Conversion
B.S. Chemistry, Lyon College, May 2010   GPA: 3.865

Research Experience

Graduate Research   Summer 2010 - Present
    Vanderbilt University, Nashville, TN
    Incorporated Photosystem I into electrode and solar cell devices for the capture and storage of solar energy. Analyzed such systems using electrochemical methods, X-ray spectroscopy, profilometry, ellipsometry, reflection-absorption infrared spectroscopy, UV-vis spectroscopy, electron microscopy, and dynamic light scattering.
        Advisor: Professor David E. Cliffel

Research Internship   Fall 2009
    Future Fuel Chemical Company, Batesville, AR
    Demonstrated the ability for diethoxymethane to be used as a recyclable solvent in phase transfer reactions. This "green-chemistry" solvent has shown the ability to aid in the recovery of phase transfer catalysts.
        Advisor: Dr. Todd Coleman

Summer Undergraduate Research   Summer 2009
    Vanderbilt University, Nashville, TN
    Synthesized and identified dendritic molecular transporters and multifunctional nanoparticle scaffolds. These molecules have shown promise in the development of a novel drug delivery system.
        Advisor: Professor Eva Harth

Directed Undergraduate Research   Spring 2008
    Lyon College, Batesville, AR
    Synthesized novel thiosemicarbazones and their metal complexes, and identified these compounds using infrared spectroscopy. Some of these compounds have shown good cytotoxic profiles against certain cell lines.
        Advisor: Professor Floyd Beckford

Gabriel LeBlanc

Curriculum Vitae

Awards and Honors

SciFinder® Future Leaders in Chemistry   2013
Materials Research Society Grassroots Outreach Grant   2013
American Chemical Society Division of Analytical Chemistry
      Summer Fellowship   2013
Physical and Analytical Electrochemistry Division Travel Award   2013
Society for Electroanalytical Chemistry Travel Award   2013
Materials Research Society Travel Award   2012
Top poster award (TN-Score annual conference)   2012
National Association of Intercollegiate Athletics Scholar Athlete All-American 2009

Teaching Experience

Leader and Co-coordinator for Materials Outreach for
    Rural Education Program   2013 – Present
    After co-authoring a successful grassroots outreach grant with the Materials
Research Society, I am currently involved with the implementation of this new
outreach program. This includes the development of hands-on lessons,
coordinating dates with rural teachers, and leading hands-on science lessons for
middle school students in Tennessee.

Teacher for Science Lessons for the Aspirnaut Program   2010 – Present
    The Aspirnaut program is an innovative concept in science education that
enables the presentation of hands-on science lessons by collegiate and graduate
scientists to elementary and middle school students in rural schools using
internet based video chat (http://www.aspirnaut.org/).

Teacher for Vanderbilt Student Volunteers for Science   2010 – Present
    The Vanderbilt student volunteers for science program is a student run
organization that brings science lessons to elementary and middle school
students in the Nashville area (http://studentorgs.vanderbilt.edu/vsvs/).

Research Mentor for Undergraduate and first-year Graduate Students   2011-Present
    Tailored research projects for undergraduate students (8) and first-year
graduate students (8) that fit their particular skills and taught them new
research techniques and tools.

Teaching Aid for the Vanderbilt Science Academy   Summer 2011, 2012, 2013
    Teaching assistant for a nano-chemistry lab for high school students

Chemistry Tutor for Undergraduates   2007-2010
    Facilitated undergraduate students in the understanding of fundamental
chemistry concepts.

Gabriel LeBlanc
Curriculum Vitae

Professional Societies
American Chemical Society
Electrochemical Society
Materials Research Society

Publications

(13) LeBlanc, G.; Gizzie, E. A.; Yang, S.; Cliffel, D. E.; Jennings, G. K. Photosystem I Protein Films at Electrode Surfaces for Solar Energy Conversion. *Langmuir* **2014**, *In Press.*

(12) LeBlanc, G., Winter, K. M., Crosby, W. B., Jennings, G. K., Cliffel, D. E. Integration of Photosystem I with Graphene Oxide for Photocurrent Enhancement. *Adv. Energy Mater. In Press.*

(11) Chen, C., Hijazi, F. M., LeBlanc, G., Jennings, G. K., Cliffel, D. E. Scanning Electrochemical Microscopy of Multilayer Photosystem I Photoelectrochemistry. *ECS Electrochem. Lett.* **2013**, *2*, H59-H62.

(10) Gunther, D., LeBlanc, G., Prasai, D., Zhang, J. R., Cliffel, D. E., Bolotin, K. I., Jennings, G. K. Photosystem I on Graphene as a Highly Transparent, Photoactive Electrode. *Langmuir* **2013**, *29*, 4177-4180.

(9) Chen, G., LeBlanc, G., Jennings, G. K., Cliffel, D. E. Effect of Redox Mediator on the Photo-Induced Current of a Photosystem I Modified Electrode. *J. Electrochem. Soc*. **2013**, *160*, H315-H320.

(8) Gunther, D., LeBlanc, G., Cliffel, D. E., Jennings, G. K. *Pueraria lobata* (Kudzu) Photosystem I Improves the Photoelectrochemical Performance of Silicon. *Ind. Biotech*. **2013**. *9*, 37-41.

(7) LeBlanc, G., Chen, G., Gizzie, E. A., Jennings, G. K., Cliffel, D. E. Enhanced Photocurrents of Photosystem I Films on p-doped Silicon. *Adv. Mat*. **2012**, *24*, 5959-5962.

(6) LeBlanc, G., Chen, G., Jennings, G. K., Cliffel, D. E. Photoreduction of Catalytic Platinum Particles Using Immobilized Multilayers of Photosystem I. *Langmuir* **2012**, *28*, 7952-7956.

(5) Kimmel, D. W., LeBlanc, G., Meschievitz, M. E., Cliffel, D. E. Electrochemical Sensors and Biosensors. *Anal. Chem.* **2011**, *84*, 685-707.

(4) LeBlanc, G. An undergraduate perspective on scientific research. *Alpha Chi Recorder: Undergraduate Issue*. **2011**, *54*, 3-10.

(3) Coleman, M.T., LeBlanc, G. Use of diethoxymethane as a solvent for phase transfer catalyzed reactions. *Org. Proc. Res. Dev.* **2010**, *14*, 732-736.

(2) Beckford, F.A., Shaloski, M. Jr., LeBlanc, G., Thessing, J., Lewis-Alleyne, L.C., Holder, A. A., Li, L., Seeram, N.P. Microwave synthesis of mixed ligand diimine-thiosemicarbazone complexes of ruthenium(II): biophysical reactivity and cytotoxicity. *Dalton Trans*., **2009,** *48*, 10757-10764.

(1) Beckford, F.A., LeBlanc, G., Thessing, J., Shaloski, M. Jr., Frost, B. J., Li, L., Seeram, N. P. Organometallic ruthenium complexes with thiosemicarbazone ligands:Synthesis, structure and cytotoxicity of $[(\eta^6\text{-}p\text{-cymene})Ru(NS)Cl]^+$ (NS = 9-anthraldehyde thiosemicarbazones). *Inorg. Chem. Comm*. **2009**, *12*, 1094-1098.

Gabriel LeBlanc
Curriculum Vitae

Publications in Preparation

(14) Darby, E., <u>LeBlanc, G.</u>, Gizzie, E. A., Jennings, G. K., Cliffel, D. E. Photoactive Films of Photosystem I on Transparent Reduced Graphene Oxide Electrodes. *Langmuir* Submitted.

(15) Gizzie, E. A., <u>LeBlanc, G.</u>, Jennings, G. K., Cliffel, D. E. Electrochemical Preparation of Ohotosystem I-Polyaniline Composite Films for Biohybrid Solar Energy Conversion. In preparation for *Biomacromolecules*.

Patents

Cliffel, D. E., <u>LeBlanc, G.</u>, Jennings, G. K., and Chen, G. "Biohybrid Photoelectrochemical Energy Conversion Device" U.S. Provisional Patent Application No. 61/680,875

Presentations

(19)   <u>LeBlanc, G.</u> *"Powered by Plants! Biohybrid Electrodes Based on Photosystem I for Solar Energy Conversion"* Invited Lecture at King University. Bristol, TN.   February 2014

(18)   <u>LeBlanc, G.</u>, Wrenn, T. *"Science Outreach: Importance, Programs, and Opportunities"* 14th Annual Nanoscience and Nanotechnology Forum, Nashville, TN, Oral Presentation.   November 2013

(17)   <u>LeBlanc, G.</u>, Wrenn, T., Satterwhite, S., Tellinghuisen, P. *"Keys to Scientific Outreach: Proposals, Preparing, and Performing"* Science Outreach and Communication Symposium, Columbia, MO, Poster Presentation.   September 2013

(16)   <u>LeBlanc, G.</u>, Jennings, G. K., and Cliffel, D.E. *"Biohybrid Electrodes Based on Photosystem I for Solar Energy Conversion"* 246th ACS National Meeting, Indianapolis, IN, Oral and Poster Presentation. September 2013

(15)   <u>LeBlanc, G.</u>, Jennings, G. K., and Cliffel, D.E. *"Integration of Photosystem I with Semi-Conducting and Carbon-Based Materials for Solar Energy Conversion"* 3rd Annual TN-SCORE Conference, Nashville, TN, Oral and Poster Presentation.   June 2013

(14)   <u>LeBlanc, G.</u>, Jennings, G. K., and Cliffel, D.E. *"The Effect of Electrochemical Mediator and Electrode Materials on the Photocurrent Production of Photosystem I Films"* 2nd Annual TN-SCORE Thrust 1 Retreat, Burns, TN, Oral Presentation.   May 2013

(13)   <u>LeBlanc, G.</u>, Chen, G., Jennings, G. K., and Cliffel, D. E. *"Electrochemical Analysis of Photosystem I Films Deposited on Various Electrode Materials"* 223rd Electrochemical Society Meeting, Toronto, ON, Canada, Oral Presentation.   May 2013

(12)   <u>LeBlanc, G.</u>, Chen, G., Gizzie, E. A., Jennings, G. K., and Cliffel, D. E. "*Interfacing Photosystem I with Semiconducting Materials for Enhanced Photocurrents*" Materials Research Society Spring Meeting, San Francisco, CA, Oral Presentation.   April 2013

Gabriel LeBlanc
Curriculum Vitae

(11) <u>LeBlanc, G.</u>, Chen, G., Gizzie, E. A., Jennings, G. K., and
Cliffel, D. E. "*Electrochemical Analysis of a Semiconductor/Protein
Interface*" PittCon. Philadelphia, PA, Oral Presentation.　　March 2013

(10) <u>LeBlanc, G.</u>, Chen, G., Gizzie, E. A., Jennings, G. K., and
Cliffel, D. E. *"Scanning Electrochemical Microscopy (SECM) of
Hydrogen Photogenerated from Platinized Photosystem I
Modified Electrodes"* Inaugural SEC Symposium. Atlanta, GA,
Poster Presentation.　　February 2013

(9) <u>LeBlanc, G.</u> *"Powered by Plants! Using Photosystem I for Next
Generation Solar Energy Conversion Devices"* Guest Lecture
at Hendrix College. Conway, AR.　　October 2012

(8) <u>LeBlanc, G.</u> *"Powered by Plants! Using Photosystem I for Next
Generation Solar Energy Conversion Devices"* Invited Lecture
at Lyon College. Batesville, AR.　　October 2012

(7) <u>LeBlanc, G.</u> *"Interfacing Photosystem I with Semiconducting
Materials for Enhanced Photocurrents"* 1st Annual Conference
Contest for the Vanderbilt/Fisk Materials Research Society Chapter.
Nashville, TN, Oral Presentation.　　October 2012

(6) <u>LeBlanc, G.</u>, Chen, G. Jennings, G.K., and Cliffel, D. E. "*Analyzing
the Effect of Electrode Material on Photoactive Films of Photosystem I*"
2nd Annual TN-SCORE Conference, Nashville, TN,
Poster Presentation.　　June 2012

(5) <u>LeBlanc, G.</u>, Chen, G. Jennings, G.K., and Cliffel, D. E. "*Analyzing
the Effect of Electrode Material on Photoactive Films of Photosystem I*"
243rd ACS National Meeting, San Diego, CA, Oral Presentation and
Poster Presentation.　　March 2012

(4) <u>LeBlanc, G.</u>, Chen, G., Jenning, G. K., and Cliffel, D. E.
"*Photoreduction of Platinum Particles onto Multilayer Films
of Photosystem I"* Tennessee Valley Solar Solutions Conference,
Nashville, TN, Poster Presentation.　　August 2011

(3) <u>LeBlanc, G.</u> "*An Undergraduate Perspective on Scientific Research*"
Alpha Chi National College Honor Society Super-Regional
Convention, Little Rock, AR, Oral Presentation.　　April 2010

(2) <u>LeBlanc, G.</u>, Sims, A., and Harth, E. "*Building Molecular Transporters*"
Summer Academy Research Symposium, Vanderbilt University,
Nashville, TN, Poster Presentation.　　July 2009

(1) <u>LeBlanc, G.</u> and Beckford, F.A. "*Novel thiosemicarbazones from
9-anthraldehyde and their copper and ruthenium complexes*"
92nd Annual Meeting of the Arkansas Academy of Science,
Henderson State University, Arkadelphia, AR,
Poster Presentation.　　April 2008